Cruise Report:
RV *Araon* ARA03B, August 1-Septmeber 10, 2012
Chukchi Borderland and Mendeleyev Ridge

Sung-Ho Kang, Chief Scientist
Korea Polar Research Institute (KOPRI)

Korea Polar Research Institute

Report Editors:
Sung-Ho Kang*, Seung Il Nam, Jung Han Yim,
Kyung Ho Chung, Jong Kuk Hong
Korea Polar Research Institute (KOPRI)
Get-Pearl Tower, 12 Gaetbeol-ro, Yeonsu-Gu
Incheon, 406-840, Korea

*e-mail: shkang@kopri.re.kr
Telephone: +82 32.260.6251

Contents

RV *Araon* Arctic Cruise ARA03B
August 1 - September 10, 2012

Summary:

Araon Cruise (ARA03B) departed Nome, Alaska on August 1, 2012 and returned to Nome on September 10, 2012. With funding provided by the Ministry of Land, Transport and Maritime Affairs (MLTM) and by Korea Polar Research Institute (KOPRI), the aim of the cruise was to investigate the structure and processes in the water column and subsurface (sediment) around the Chukchi Borderland and Mendeleyev Ridge in rapid transition. The research effort was the first jointly sponsored research cruise of the Korea-Polar Ocean in Rapid Transition (K-PORT) Program, the Arctic Paleoceanography (K-POLAR) Program, and the Korea-Polar Ocean Discovery (K-POD) Program, with support from the MLTM and the KOPRI, respectively. Because of high demand for berth space and ship time on the Arctic cruise aboard Araon in 2012, special efforts were made to accommodate three main projects compatible with the use of the ship during the K-PORT study, and these individual projects are outlined below. In addition to science programs, additional efforts were made to communicate scientific efforts and research issues by providing berth space for a writer that undertook interviews during the scientific work.

Acknowledgements:

Core Projects:

K-PORT (Korea-Polar Ocean in Rapid Transition) Program: Ministry of Land, Transport and Maritime Affairs (MLTM), KOPRI Project No. PM11080, PI: Sung-Ho Kang, KOPRI

K-POLAR (Arctic Paleoceanography) Program: Korea Polar Research Institute, PI: Seung Il Nam, KOPRI

K-POD (Korea-Polar Ocean Discovery) Program: Ministry of Land, Transport and Maritime Affairs (MLTM), PI: Jung Han Yim, KOPRI

Cruise Participants:

1. Dr. Sung-Ho KANG, Korea Polar Research Institute (KOPRI) (shkang@kopri.re.kr)
2. Dr. Seung Il NAM, Korea Polar Research Institute (KOPRI) (sinam@kopri.re.kr)
3. Dr. Jung Han YIM, Korea Polar Research Institute (KOPRI) (jhyim@kopri.re.kr)
4. Dr. Kyung Ho CHUNG, Korea Polar Research Institute (KOPRI) (khchung@kopri.re.kr)
5. Dr. Jong Kuk HONG, Korea Polar Research Institute (KOPRI) (jkhong@kopri.re.kr)
6. Dr. Koji SHIMADA, Tokyo University of Marine Science and Technology (TUMSAT), Japan (koji@kaiyodai.ac.jp)
7. Dr. Ho Jin LEE, Korea Maritime University (KMU) (hjlee@hhu.ac.kr)
8. Dr. Eun Jin YANG, Korea Polar Research Institute (KOPRI) (ejyang@kopri.re.kr)
9. Dr. Jinping ZHAO, Ocean University of China (OUC), China (jpzhao@ouc.edu.cn)
10. Mr. Chanu LEE, Korea Polar Research Institute (KOPRI) (ejyang@kopri.re.kr)
11. Dr. Frank NIESSEN, Alfred Wegener Institute for Polar and Marine Research (AWI), Germany (frank.niessen@awi.de)
12. Dr. Il Chang KIM, Korea Polar Research Institute (KOPRI) (ickim@kopri.re.kr)
13. Dr. Tae Wan KIM, Korea Polar Research Institute (KOPRI) (twkim@kopri.re.kr)
14. Dr. Masanobu YAMAMOTO, Hokkaido University (HU), Japan (myama@ees.hokudai.ac.jp)
15. Dr. Puneeta NAIK, Louisiana State University (LSU), USA (puneeta123@gmail.com)
16. Dr. Phil HWANG, The Scottish Association for Marine Science (SAMS), Scottish Marine Institute, UK (phil.hwang@sams.ac.uk)
17. Dr. Chung Yeon HWANG, Korea Polar Research Institute (KOPRI) (cyhwang@kopri.re.kr)
18. Dr. Hari Datta BHATTARAI, Korea Polar Research Institute (KOPRI) (hari@kopri.re.kr)
19. Ms. Inka SCHADE, Alfred Wegener Institute for Polar and Marine Research (AWI), Germany (inkaschade14@hotmail.com)
20. Ms. Saskia WASSMUTH, Alfred Wegener Institute for Polar and Marine Research (AWI), Germany (saskia.wassmuth@gmail.com)
21. Mr. Weibo WANG, Ocean University of China (OUS), China (bobolufei@126.com)
22. Ms. Hyun Jung LEE, Korea Polar Research Institute (KOPRI) (hyunjung@kopri.re.kr)
23. Ms. Eri YOSHIZAWA, Tokyo University of Marine Science and Technology (TUMSAT), Japan (eri.yoshizawa075@gmail.com)
24. Ms. Seung Kyeom LEE, Korea Polar Research Institute (KOPRI) (keomnara86@kopri.re.kr)
25. Mr. Bernard G. HAGAN, The Scottish Association for Marine Science (SAMS), Scottish Marine Institute, UK (bernardhagan@aol.com)
26. Mr. Vladimir PISAREV, Ice Navigator, Russia (irishka-4ever@mail.ru)
27. Mr. Travis GODWIN, Polar Bear Watcher, USA (tgodwin06@gmail.com)
28. Ms. Yeong Ju SON, Korea Polar Research Institute (KOPRI) (yj0331@kopri.re.kr)
29. Ms. Hyo Seon JI, Korea Polar Research Institute (KOPRI) (jhs07@kopri.re.kr)
30. Mr. In Seok CHUN, Surgeon, Medical Doctor, Korea (c811k905@yahoo.co.kr)
31. Mr. Dong Seob SHIN, Korea Polar Research Institute (KOPRI) (dsshin@kopri.re.kr)
32. Mr. Heung Soo MOON, Korea Polar Research Institute (KOPRI) (jepy@kopri.re.kr)
33. Ms. Jeonke HAN, Writer, Korea (jgh6012@hanmail.net)
34. Mr. Howard REED, Helicopter Pilot, USA (reedhoward03@gmail.com)

35. Mr. Jon COMBS, Helicopter Pilot, USA (flying.eth@gmail.com)
36. Mr. Chris COX, Helicopter Engineer, USA (coxcox2u69@yahoo.com)
37. Mr. Hyoung Jun KIM, Korea Polar Research Institute (KOPRI) (jun7100@kopri.re.kr)
38. Mr. Sookwan KIM, Korea Polar Research Institute (KOPRI) (skwan@kopri.re.kr)
39. Ms. Nari SEO, Korea Polar Research Institute (KOPRI) (snari@kopri.re.kr)
40. Mr. Yeongsam SIM, Korea Polar Research Institute (KOPRI) (sys@kopri.re.kr)
41. Mr. Dukki HAN, Gwangju Institute of Science and Technology (GIST) (dukkihan@gist.ac.kr)
42. Mr. Youngjin JOE, Jeju National University (JNU) (yjjoe011@naver.com)
43. Mr. Tai Kyoung KIM, Korea Polar Research Institute (KOPRI) (tkkim@kopri.re.kr)
44. Mr. Daesik HWANG, Hanyang University (HANYANG) (dshwang@hanyang.ac.kr)
45. Mr. Hyoung Min JOO, Korea Polar Research Institute (KOPRI) (hmjoo77@gmail.com)
46. Ms. Bo Kyung KIM, Pusan National University (PNU) (bokyung85@naver.com)
47. Mr. Jae Joong KANG, Pusan National University (PNU) (jaejung@pusan.ac.kr)
48. Mr. Jun Oh MIN, Korea Polar Research Institute (KOPRI) (jomin@kopri.re.kr)
49. Mr. Dong Jin LEE, Korea Polar Research Institute (KOPRI) (leedongjin@kopri.re.kr)
50. Mr. Jae Kwang LEE, Chungnam National University (CNU) (powermex@nate.com)
51. Mr. Jaeill YOO, Korea Polar Research Institute (KOPRI) (jiyoo@kopri.re.kr)
52. Mr. Kilsoo AHN, Korea Polar Research Institute (KOPRI) (ahnks@kopri.re.kr)
53. Mr. Yoon-Yong YANG, Korea Polar Research Institute (KOPRI) (tazmenia@kopri.re.kr)

2012 *ARAON* ARCTIC CRUISE

ARA03B (1ST AUG. – 10TH SEPT.)

KOPRI

Sung-Ho KANG *(K-PORT)*
강성호 KOPRI *(K-PORT)*
Chief Scientist
(Biological Oceanography)
shkang@kopri.re.kr

Seung Il NAM *(K-POLAR)*
남승일 KOPRI *(K-POLAR)*
Paleoceanography
sinam@kopri.re.kr

Jung Han YIM *(K-POD)*
임정한 KOPRI *(K-POD)*
Biotechnology
jhyim@kopri.re.kr

Kyung Ho CHUNG *(K-PORT)*
정경호 KOPRI *(K-PORT)*
Chemical Oceanography
khchung@kopri.re.kr

Jong Kuk HONG *(K-PORT)*
홍종국 KOPRI *(K-PORT)*
Geophysics
jkhong@kopri.re.kr

Koji SHIMADA
TUMSAT, Japan *(K-PORT)*
Physical Oceanography
koji@kaiyodai.ac.jp

Ho Jin LEE *(K-PORT)*
이호진 Korea Maritime Univ.
Physical Oceanography
hjlee@hhu.ac.kr

Eun Jin YANG *(K-PORT)*
양은진 KOPRI *(K-PORT)*
Biological Oceanography
ejyang@kopri.re.kr

Jinping ZHAO *(K-PORT)*
Ocean Unvi. of China
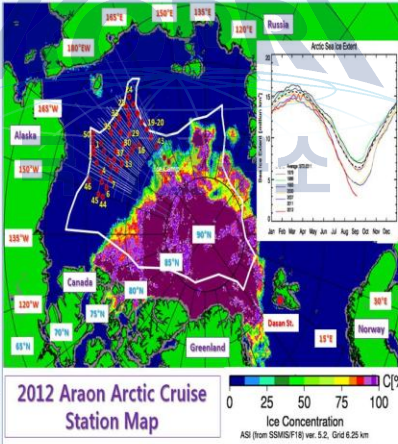Physical Oceanography
jpzhao@ouc.edu.cn

Chanu LEE
이찬우 KOPRI
Araon 해무감독
culee@kopri.re.kr

Frank NIESSEN *(K-POLAR)*
AWI, Germany *(K-POLAR)*
Paleoceanography
frank.niessen@awi.de

Il Chan KIM *(K-POD)*
김일찬 KOPRI *(K-POD)*
Biotechnology
ickim@kopri.re.kr

Tae Wan KIM *(K-PORT)*
김태완 KOPRI *(K-PORT)*
Physical Oceanography
twkim@kopri.re.kr

Masanobu YAMAMOTO
Hokkaido Univ., Japan
Geology *(K-POLAR)*
myama@ees.hokudai.ac.jp

Puneeta NAIK *(K-PORT)*
Louisiana Stat. Univ., USA
Remote Sensing
puneeta123@gmail.com

Phil HWANG *(K-PORT)*
SAMS, UK *(K-PORT)*
Sea Ice Physics
phil.hwang@sams.ac.uk

Chung Yeon HWANG
황청연 KOPRI *(K-POD &
K-PORT)* Microbiology
cyhwang@kopri.re.kr

Hari Datta BHATTARAI
바타라이 KOPRI *(K-POD)*
Biotechnology
hari@kopri.re.kr

Inka SCHADE
AWI, Germany *(K-POLAR)*
Paleoceanography
inkaschade@hotmail.com

Saskia WASSMUTH
AWI, Germany *(K-POLAR)*
Paleoceanography
saskia.wassmuth@gmail.com

Weibo WANG *(K-PORT)*
Ocean Unvi. of China
Physical Oceanography
bobolufei@126.com

Hyun Jung LEE *(K-PORT)*
이현정 KOPRI *(K-PORT)*
Physical Oceanography
hyunjung@kopri.re.kr

Eri YOSHIZAWA
TUMSAT, Japan *(K-PORT)*
Physical Oceanography
eri.yoshizawa075@gmail.com

Seung Kyeom LEE
이승겸 KOPRI *(K-PORT)*
Remote Sensing
keomnara86@gmail.com

Bernard G. HAGAN
SAMS, UK *(K-PORT)*
Sea Ice Physics
bernardhagan@aol.com

Vladimir PISAREV
Ice Navigator, Russia
irishka-4ever@mail.ru

Travis GODWIN
Polar Bear Watcher, USA
tgodwin06@gmail.com

Yeong Ju SON *(K-POLAR)*
손영주 KOPRI *(K-POLAR)*
Geology
yj0331@kopri.re.kr

Hyo Seon JI *(K-POLAR)*
지효선 KOPRI *(K-POLAR)*
Geology
jhs07@kopri.re.kr

In Seok CHUN
전인석 Surgeon
Medical Doctor
c811k905@yahoo.co.kr
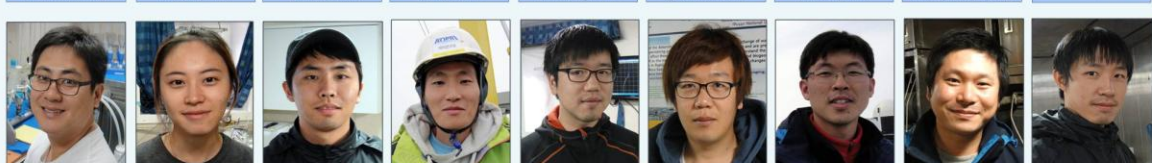
Dong Seob SHIN *(K-PORT)*
신동섭 KOPRI *(K-PORT)*
Geophysics
dsshin@kopri.re.kr

Heung Soo MOON *(K-POLAR)*
문흥수 KOPRI *(K-POLAR)*
Paleoceanography
jepy@kopri.re.kr

Jeonke HAN
한정기 Writer
jgh6012@hanmail.net

K-PORT

양극해 환경변화 이해 및 활용 연구

K-POLAR

K-POD

Howard REED
Helicopter Pilot
reedhoward03@gmail.com

Jon COMBS
Helicopter Pilot
flying.eth@gmail.com

2012 Araon Arctic Cruise
Station Map

Ice Concentration
ASI (from SSMIS/F18) ver. 5.2, Grid 6.25 km

Hyoung Jun KIM *(K-PORT)*
김형준 KOPRI *(K-PORT)*
Geophysics
jun7100@kopri.re.kr

Sookwan KIM *(K-PORT)*
김수관 KOPRI *(K-PORT)*
Geophysics
skwan@kopri.re.kr

Nari SEO *(K-PORT)*
서나리 KOPRI *(K-PORT)*
Geophysics
snari@kopri.re.kr

Yeongsam SIM *(K-PORT)*
심영삼 KOPRI *(K-PORT)*
Paleoceanography
sys@kopri.re.kr

Dulski HAN *(K-PORT)*
한덕기 GIST *(K-PORT)*
Paleocoeanography
dukkihan@gist.ac.kr

Youngjin JOE *(K-POLAR)*
조영진 Jeju Nat. Univ.
Paleocoeanography
yjjoe011@naver.com

Tai Kyoung KIM
김태경 KOPRI *(K-POD)*
Biotechnology
tkkim@kopri.re.kr

Daesik HWANG *(K-POD)*
황대식 Hanyang Univ.
Biotechnology
dshwang@hanyang.ac.kr

Chris COX
Helicopter Engineer
coxcox2u69@yahoo.com

Hyoung Min JOO *(K-PORT)*
주형민 KOPRI *(K-PORT)*
Phytoplankton Ecology
hmjoo77@kopri.re.kr

Bo Kyung KIM *(K-PORT)*
김보경 Pusan Nati. Univ.
Microalgal Ecology
bokyung85@naver.com

Jae Joong KANG *(K-PORT)*
강재중 Pusan Nati. Univ.
Microalgal Ecology
jaejung@pusan.ac.kr

Jun Oh MIN *(K-PORT)*
민준오 KOPRI *(K-PORT)*
Phytoplankton Ecology
jomin@kopri.re.kr

Dong Jin LEE *(K-PORT)*
이동진 KOPRI *(K-PORT)*
Protozoan Ecology
leedongjin@kopri.re.kr

Jae Kwang LEE *(K-PORT)*
이재광 Chungnam Nati. Univ.
Zooplankton Ecology
jwoermex@nate.com

Jaeill YOO *(K-PORT)*
유재일 KOPRI *(K-PORT)*
Atmospheric Science
jiyoo@kopri.re.kr

Kilsoo AHN
안길수 KOPRI *(K-POD &
K-PORT)* Chemistry
ahnks@kopri.re.kr

Yoon-Yong YANG
양윤용 KOPRI *(K-POD)*
Microbiology
tazmenia@kopri.re.kr

K-PORT (Korea-Polar Ocean in Rapid Transition) Project (PI, Dr. Sung-Ho Kang)
K-POLAR (Arctic Paleoceanography) Project (PI, Dr. Seung Il Nam)
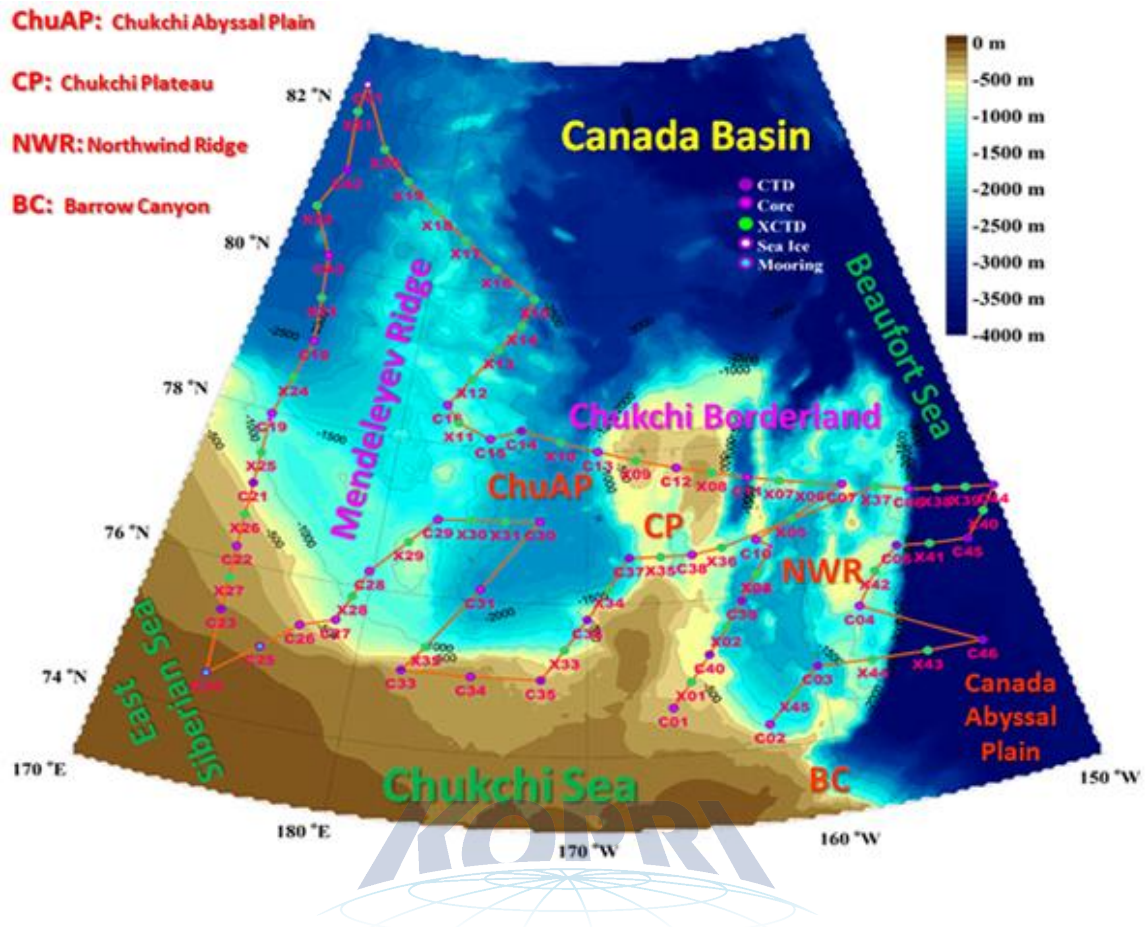*K-POD* (Korea-Polar Ocean Discovery) Project (PI, Dr. Jung Han Yim)

Figure : Map of 2012 Araon Arctic Cruise study area. CTD, XCTD, MOORING, Gravity Core, Box Core, Multi Core, Dredge, Deep-Sea Camera, SEA-ICE, Helicopter Survey stations.

2012 Araon Arctic Cruise

Araon Cruise (ARA03B) departed Nome, Alaska on August 1, 2012 and returned to Nome on September 10, 2012. With funding provided by the Ministry of Land, Transport and Maritime Affairs (MLTM) and by Korea Polar Research Institute (KOPRI), the aim of the cruise was to investigate the structure and processes in the water column and subsurface (sediment) around the Chukchi Borderland and Mendeleyev Ridge in rapid transition. The research effort was the first jointly sponsored research cruise of the Korea-Polar Ocean in Rapid Transition (K-PORT) Program, the Arctic Paleoceanography (K-POLAR) Program, and the Korea-Polar Ocean Discovery (K-POD) Program, with support from the MLTM and the KOPRI, respectively. Total of 53 scientists have participated from 10 countries (Korea, China, Japan, U.S., Canada, Russia, Germany, U.K., India, Nepal) representing 12 different universities and research organizations. Because of high demand for berth space and ship time on the Arctic cruise aboard Araon in 2012, special efforts were made to accommodate three main projects compatible with the use of the ship during the K-PORT study.

Araon data were collected on the physical, biological, geochemical, geological and geophysical properties of ocean waters and subsurfaces in the shelf, slope and deep-sea regions of the Chukchi Borderland and Mendeleyev Ridge. Profiles of water temperature and salinity were obtained with CTD, and an underway XCTD system. Additional sensors on the CTD profiler were collected in situ data on phytoplankton concentrations (fluorometer), optical clarity (transmissometer), dissolved oxygen and photoactive radiation. A rosette sampler was used with the CTD to obtain water samples from discrete depths for a broad suite of biological and geochemical parameters, some for onboard analysis, others to be stored for later analysis in shore-based laboratories. Subsurface sampling was conducted by using sediment corers and grabs. Both bio-acoustic backscatter data and depth-varying current information were collected using a Acoustic Doppler Current Profiler (ADCP) deployed under the ship at most of the science stations. Data were also collected from the ship-mounted transducer along the ship track to evaluate the possibility of using these data for bottom classification purposes. Plankton samples were obtained in vertical hauls by phyto and bongo-nets lowered to 200 m.

Survey components:

- • Water Column (WC) components
  - Water column observations of biota
  - Pelagic ecosystems observations
  - Plankton ecosystems
  - Nutrients and productivity
  - Bio-geochemical measurements
- • Underway collection of meteorological and near-surface seawater
- • Meteorological data from ship sensors
- • On-shore calibration of instrument compasses
- • XCTD (expendable temperature, salinity and depth profiler) casts
- • CTD/rosette casts for hydrograph and geochemistry (ecosystem, nutrients, salinity,

and barium)
• Deploy oceanographic moorings
• Sea-ice (ICE) observations through regular visual observations from bridge and automated fixed-camera photos.
  - Ice observations
  - Ice biology
• Geophysical and Paleoceongraphical components
  - Multiple corer sampling
  - Seabed Mapping: Seafloor mapping and paleoceanography
• Cryobiological components

Chapter 1. Atmospheric observation

Jaeill Yoo

[1]Korea Polar Research Institute, Incheon 406-840, Korea (jiyoo@kopri.re.kr)

1. Introduction

Kort *et al*.(2012) reported high methane concentrations are observed over open leads with frictional sea-ice cover through airborne observation of methane on Arctic Ocean. This observation suggested that significant decrease in ice area of Arctic sea may induce augmented emission of methane. Semiletov *et al*.(2007) also suggested sea-ice melting ponds and open channels may change the dynamics of carbon cycle between the atmosphere and the ocean in Artic ocean. As the Arctic sea ice shows the pronounced decreases in its area in summer season since 1997, its impact of arctic environmental change on global climate can be amplified. Despite such reports, most researches were supported by pCO_2 method or inverse model, not direct measurement. With a lack of direct observation on arctic sea, in-situ measurements in the Arctic Ocean are possible when ice-breaking research vessels are available. Since Arctic Expedition in 2011, test of on-board atmospheric instruments such as sonic anemometer and gas analyzer as components of direct flux measurement system, i.e., eddy covariance system, had been performed. Along with the purpose of the last cruise, it is aimed to measure methane and carbon dioxide fluxes using eddy covariance system with closed path analyzer, i.e., CRDS, and open-path analyzer during Arctic Expedition in 2012. And basic meteorological observations such as temperature, wind, and radiation are also served to the researchers in Araon.

2. Materials and methods

A wave-scanned cavity ring-down spectroscopy (CRDS) analyzer (figure 1.1), as a component of eddy covariance system, and an elastic LIDAR as well as meteorological instruments was operated during the cruise. It was primary purpose of operation of eddy covariance system with CRDS (G2301-f, Picarro Inc., USA) in the flux mode to quantify CH_4 and latent heat fluxes during the cruise. However, for the comparison of performance of CRDS and open-path gas analyzer, measuring CO_2 concentration was measured by the CRDS

at the beginning of the cruise (figure 1.2). CO_2 flux from CRDS was compared with that from open path gas analyzer during this period (e.g., Hong *et al*., 2000). And for the comparison of latent heat fluxes by both instruments, water vapor was not removed in operation of flux mode of CRDS through whole cruise. An eddy covariance system, consisting of 3D-Sonc anemometer (CSAT3, Campbell Scientific Inc., USA) and open-path CO_2/H_2O gas analyzer (LI-7500, Li-cor, USA) were operated during the cruise.

The LIDAR was operated to measure the profile of aerosol and atmospheric boundary layer height (figure 1.3). In addition, air temperature and relative humidity (HMP45D, Vaisala, the Netherlands), air pressure (PTB100, Vaisala) and downward shortwave (PSP, Eppley, USA) and long-wave radiation (PIR, Eppley) were measured (figure 1.4). Wind direction and speed was acquired from 2-D sonic anemometer used for the cruise of the Ice breaker, Araon. Apparent wind direction and speed by ship movement were corrected using ship speed and heading. More information of instrumentation can be found appendix A.

Figure 1.1 Cavity ring-down spectroscopy analyzer at the CRDS container.

3D sonic anemometer

Infra-red gas analyzer

Intake of CRDS

Figure 1.2 Open-path eddy covariance at the foremast of Araon.

Figure 1.3 LIDAR.

2D sonic anemometer

Short-wave radiation sensor

2D sonic anemometer

Long-wave radiation sensor

Temperature & humidity sensor

Figure 1.4 Instruments at the main mast of Araon.

1.3. Expected result

1.3.1. Meteorological condition

During the cruise, air temperature (Ta) ranged from -4 to 2 ℃. Sometime, Ta showed abnormal behavior, compared to sonic temperature from the 3D sonic anemometer. But the 3D sonic anemometer was frozen and not working when the air temperature was below zero after it had rained. Relative humidity was in the range of 85 – 97 % during cruise in Chukchi Sea. Air temperature underwent sudden increase associated with a dramatic drop of relative humidity depending on wind direction suggesting that ship's combustion gas possibly affected the sensor probe when wind came from the stern. Air temperature and relative humidity was filtered out when relative wind direction is in the range of 180 to 240 degrees. Wind speed was less than 20 ms^{-1}. Southerly wind was dominant with a frequency of ~33 %. Air pressure ranged from 98.3 kPa to 101.6 kPa. Variation of daily- averaged temperature, pressure, relative humidity, and wind speed can be found in figure 1.5.
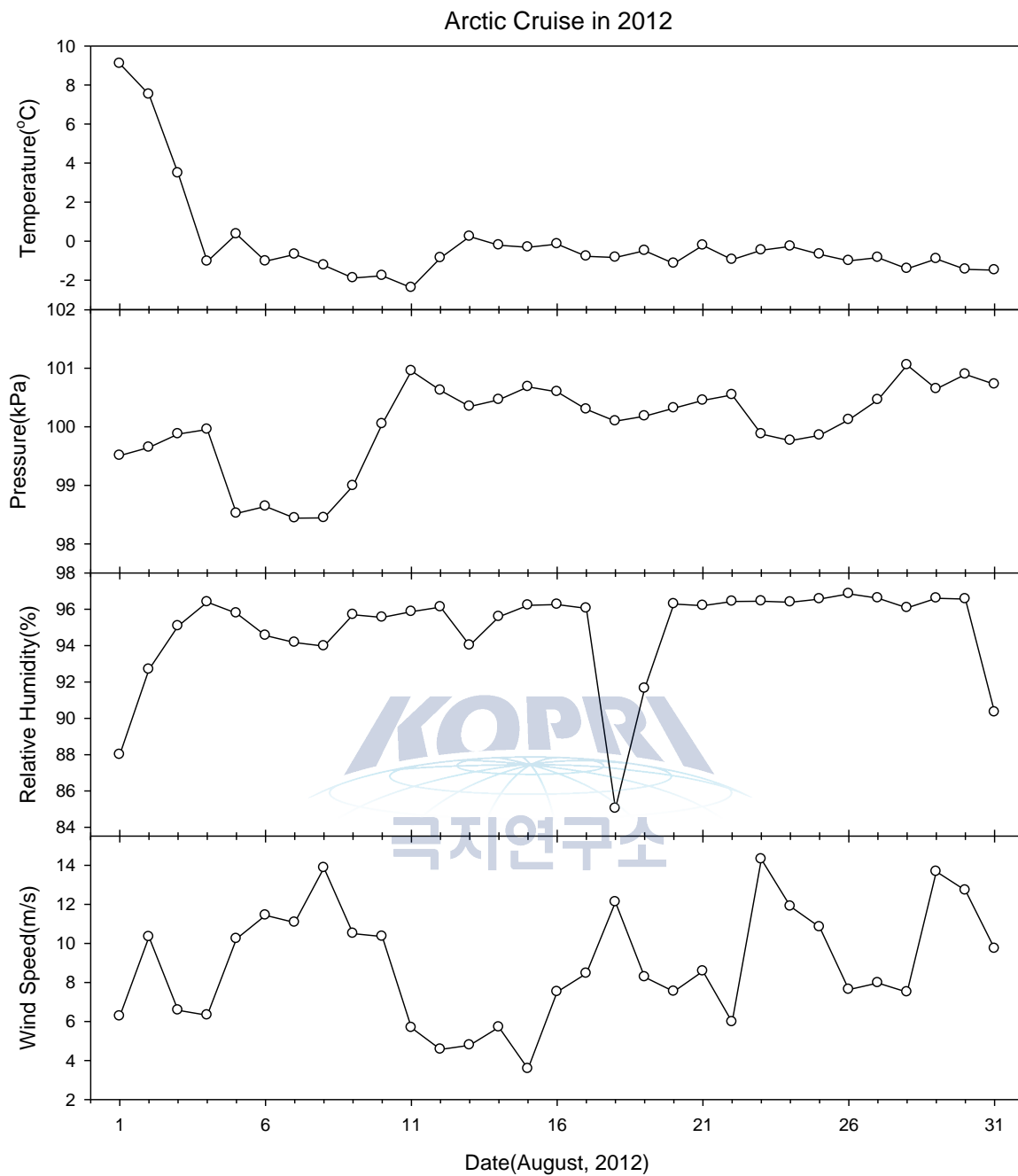
Figure 1.5 Meteorological observation (daily averages during cruise).

1.3.2. Carbon dioxide and methane measurements

During cruise from Incheon to Nome, CRDS was operated in high precision mode in the atmospheric science room (Crosson, 2008). Before departure from Nome, CRDS was moved to CRDS container near the foremast for operation in flux mode. At the begging of

~ 15 ~

the cruise for five days, CRDS was operated in CO_2/H_2O flux mode to compare the performance between CRDS and open path gas analyzer. CO_2 concentration measured by CRDS ranged from 374 ppm to 383 ppm on 1 – 5 August.   After switch to CH_4/H_2O mode on 6 August, CH_4 and H_2O concentration ranged from 1.92 ppm to 2.01 ppm, from 4.2 mmol mol^{-1} to 11.3 mmol mol^{-1}, respectively (figure 1.6).
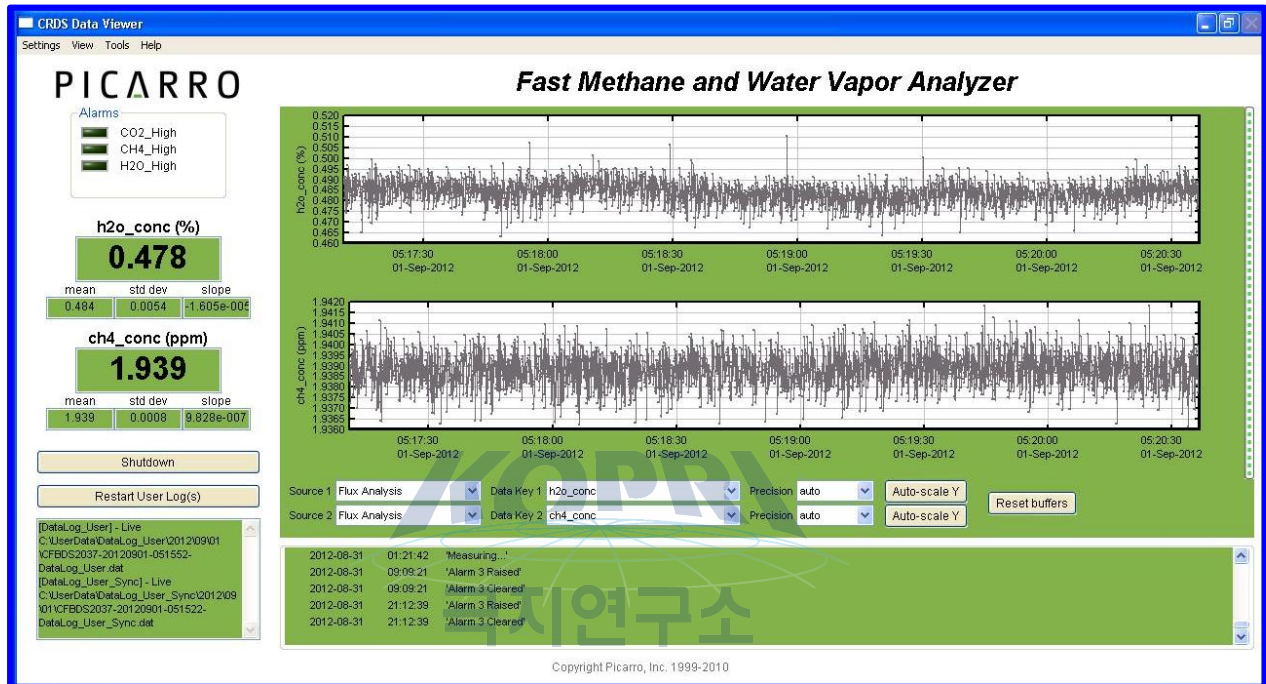
Figure 1.6 Real time variation of CH_4 and H_2O in flux mode.

1.3.3. Eddy covariance system

Eddy covariance system is a direct measurement system of the air-sea turbulent fluxes of momentum and sensible and latent heat in addition to various mean meteorological parameters. The two main aims of the present deployment were 1) to continuously measure a suite of key meteorological variables (wind speed and direction, air temperature, and humidity, radiation and air pressure) and 2) to measure directly the air-sea fluxes of CO_2 and CH_4, sensible heat, latent heat and momentum. The eddy covariance system was installed on Araon in June 2012 and has been running autonomously, with occasional service visits. At the begging of Arctic cruise in 2012, CRDS was deployed as a component of eddy covariance system.

Motion sensor, measuring 3 accelerations and 3 angular rates, is needed for on board eddy covariance flux measurement due to the ship motion. A motion sensor (MotionPakII, BEI, USA) is installed near 3D sonic anemometer to capture the motion of the anemometer. Motion correction will be applied by MatLab code every 30 minutes (Miller *et al.*, 2008), and motion corrected data will be saved for the further analysis. The eddy covariance system was frozen for several days due to frequent precipitation and freezing temperature. This systematic failure is the main limit in operating open-path eddy covariance systems (figure 1.7). More than 50% of total number of measured date is expected to be filtered out during quality control. This drawback draws on attention about closed path eddy covariance system like CRDS-associated system. However, it's highly probable that wind data measured by sonic anemometer is not available either in arctic condition. It is still a big challenge to measure fluxes by eddy covariance system in arctic sea.   Eddy fluxes will be process in post-cruise work. Events log of maintenance during cruise can be found in appendix B.

Figure 1.7 Frozen sensors on 26 August, 2012.

1.3.4. LIDAR

Atmospheric boundary layer process, aerosol and cloud are important factors in polar climate processes. On board elastic LIDAR was operated to measure the profile of aerosol. During arctic cruise, an air conditioner of LIDAR container was out of order. However, because LIDAR room temperature was maintained within operational range, LIDAR was operated.
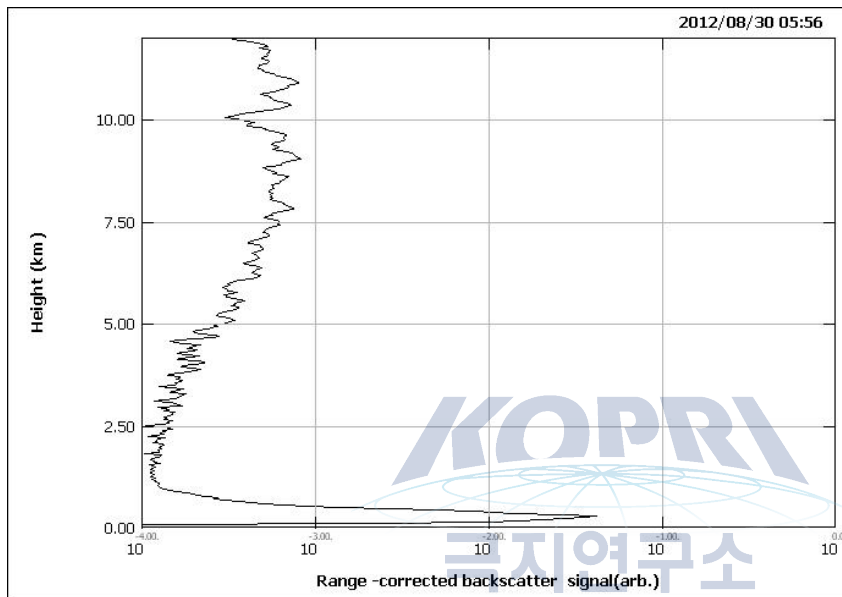
Figure 1.8 Range-correct backscatter signal on 30 August.

1.4. Summary and conclusions

During cruise, CRDS was operated stably in CH_4-H_2O flux mode to quantify methane flux and open-path gas analyzer to quantify CO_2 flux. Further analysis is required to acquire fluxes including motion correction. However, despite the importance of direct observation on sea, there still exist lots of challenges including ship motion, low temperature, sea spray and so on. Those difficulties deteriorated data quality as well as reduced data availability. Various solutions, i.e., heating system to keep the sensor from the ice, can be suggested to resolve the problems revealed in this cruise. But redundant measurement systems are required to assure data availability and quality.

References

Crosson, E.R. (2008) A cavity ring-down analyzer for measuring atmospheric levels of methane, carbon dioxide, and water vapor, Applied Physics B, 92, 403–408.

Hong, J, J. Kim, T. Choi, J. Yun and B. Tanner (2000) On the effect of tube attenuation on measuring water vapor flux using a closed-path hygrometer, Korean Journal of Agricultural and Forest Meteorology, 2(3), pp. 80–86.

Kort, E. A., S. C. Wofsy, B. C. Daube, M. Diao, J. W. Elkins, R. S. Gao, E. J. Hintsa, D. F. Hurst, R. Jimenez, F. L. Moore, J. R. Spackman, M. A. Zondlo (2012) Atmospheric observations of Arctic Ocean methane emissions up to 82° north, Nature Geoscience, 5, 318–321.

Miller, S. D., T. S. Hristov, J. B. Edson, and C. A. Friehe (2008) Platform motion effects on measurements of turbulence and air-sea exchange over the open ocean, Journal of Atmospheric & Oceanic Technology, 25(9), 1683–1694.

Semiletov, Igor P., Irina I. Pipko, Irina Repina, Natalia E. Shakhova (2007) Carbonate chemistry dynamics and carbon dioxide fluxes across the atmosphere–ice–water interfaces in the Arctic Ocean: Pacific sector of the Arctic, Journal of Marine Systems, 66, 204–226.

Appendix A. List of instrumentation (as of September 7, 2012)

Instrument	Model	Manufacturer	Serial Number	Remark
Data Logger	CR3000	Campbell scientific, USA	5953	CRDS container
Data Logger	CR1000	Campbell scientific, USA	7329	Foremast
Data Logger	CR3000	Campbell scientific, USA	2671	Radar mast
Data Logger	CR1000	Campbell scientific, USA	7291	ATM RM
Sonic Anemometer	CSAT3	Campbell scientific, USA	To be updated	Foremast
Infra-red Gas Analyzer	LI7500	Li-cor, USA	1213	Foremast
Cavity-Ringdown Spectroscopy	G2301-f	Picarro, USA	CFBDS2037	CRDS container
Wind Sensor	05106-5	RMYoung, USA	108739	Foremast
Net Radiometer	CNR1	Kipp&Zonen, the Netherlands	080090	Foremast
Short-wave Radiometer	PSP	Eppley, USA	35120F3	Radar mast
Long-wave Radiometer	PIR	Eppley, USA	35408F3	Radar mast
Short-wave Radiometer	Pyarnometer	Li-cor, USA	72851	Radar mast
Rain gauge	WDSA-205	WEDAEN	4089	Radar mast
Temperature & Humidity	HMP45D	Vaisala, the Netherlands	To be updated	Radar mast

sensor				
Motion Sensor	MotionPakII	BEI, USA	0287	ATM RM
Motion Sensor	MotionPakII	BEI, USA	0304	Foremast

Appendix B. Log of events

Date & Time (UTC)	Event
2012.07.31 23:30	Replace the chemical of LI7500(SN:0790), and warm it up
2012.08.01 18:05	Move CRDS from ATM RM to CRDS container and restart CRDS in CO_2/H_2O mode
2012.08.01 20:08	Synchronize the clock of data loggers to DaDis clock
2012.08.02 17:45-21:00	LI7500(SN:0790) calibration
2012.08.03 01:05	Send new program(120802_MotionPak_HMP_PT.CR1) to CR1000(SN:7291)
2012.08.04 06:00-08:00	Replace LI7500(SN:1213) of foremast with LI7500(SN:0709) with PT sensor Install Gelman filter in the upstream of CRDS Install RS485-232 converters for communication between CR1000(SN:7329) and computer in ATM RM
2012.08.04 19:40-20:00	Climb the foremast to check RS485-232 converters and to retrieve the data from CR1000(SN:7329)
2012.08.05 23:10	Reboot computer in ATM RM
2012.08.05 21:00-21:30	Climb foremast to check RS485-232 converter and CNR1
2012.08.06 00:05	Mode switching of CRDS to CH_4/H_2O mode
2012.08.06 00:30-01:00	Climb foremast to check LI7500 wiring, CNR1
2012.08.06 09:10-09:30	Climb foremast to remove PT sensor cable and RS485-232 converter
2012.08.06 12:10-12:35	Climb foremast to reinstall RS485-232 converter
2012.08.06 22:10-23:50	Calibration of LI7500(SN:1213)
2012.08.07 05:30	Reboot CRDS and restart CR3000(SN:5953) program
2012.08.07 06:30-07:30	Climb foremast to replace LI7500(SN:0709) of foremast with LI7500(SN:1213) with PT sensor
2012.08.08 20:30-20:45	Climb foremast to retrieve data from CR1000(SN:7329)
2012.08.08 21:45-22:10	Send new program (update of code for CNR1 temperature, S-B

Date & Time (UTC)	Event
	constant) to CR1000(SN:7329)
2012.08.10 00:30-00:50	Climb foremast to clean the sensors(LI7500, CSAT3, and CNR1)
2012.08.10 01:10-01:30	Climb radar mast to replace AC-DC converter
2012.08.10 17:40-18:00	Climb foremast to clean the sensors(LI7500, CSAT3, and CNR1)
2012.08.11 03:10-03:40	[Chief Observer]Climb foremast to check wind sensor
2012.08.11 06:20-06:40	[Chief Observer]Climb foremast to reconnect wind sensor wiring, Hereafter wind direction is available
2012.08.11 17:50-17:55	Climb foremast to clean the sensors(LI7500, CSAT3, and CNR1)
2012.08.13 18:10-18:30	Climb foremast to clean the sensors(LI7500, CSAT3, and CNR1)
2012.08.14 06:00-06:30	[Chief Observer]Climb radar mast to remove power supply
2012.08.14 18:20-18:35	Climb foremast to clean the sensors(LI7500, CSAT3, and CNR1)
2012.08.16 20:00-20:10	Climb foremast to clean the sensors(LI7500, CSAT3, and CNR1)
2012.08.19 08:40	Reboot computer in ATM RM
2012.08.20 23:10-23:50	Climb foremast to clean the sensors(LI7500, CSAT3, and CNR1)
2012.08.20 23:55	Synchronize clock of data loggers to DaDis
2012.08.21 21:10-21:!5	Climb foremast to clean the sensors(LI7500, CSAT3, and CNR1)
2012.08.22 00:25-00:35	Climb foremast to clean the sensors(LI7500, CSAT3, and CNR1)
2012.08.22 19:05	Restart logging program of CR3000(SN:5953)
2012.08.22 22:15-22:25	Climb foremast to clean the sensors(LI7500, CSAT3, and CNR1)
2012.08.24 17:50-18:10	Climb foremast to clean the sensors(LI7500, CSAT3, and CNR1)
2012.08.24 23:33	Send new program(120825_KOPRI_Araon_flux.CR3, update of diagnostic part of CSAT3) to CR3000(SN:5953)
2012.08.25 04:20-04:35	Climb foremast to clean the sensors(LI7500, CSAT3, and CNR1)
2012.08.25 23:25-23:50	Climb foremast to clean the sensors(LI7500, CSAT3, and CNR1)
2012.08.26 20:40-21:00	Climb foremast to clean the sensors(LI7500, CSAT3, and CNR1)
2012.08.27 22:10-22:20	Climb foremast to clean the sensors(LI7500, CSAT3, and CNR1)
2012.08.28 19:55-20:10	Climb foremast to clean the sensors(LI7500, CSAT3, and CNR1)
2012.08.31 04:50	Stop and restart logging program of CR3000(SN:5953)

Date & Time (UTC)	Event
2012.08.31 19:00-19:15	Climb foremast to clean the sensors(LI7500, CSAT3, and CNR1)
2012.09.01 23:40	Send new logging program(120902_KOPRI_Araon_flux.CR3, update of diagnostic of irga and tp) to CR3000(SN:5953)
2012.09.02 18:15-18:30	Climb foremast to clean the sensors(LI7500, CSAT3, and CNR1)
2012.09.04 01:16	Reboot computer in ATM RM
2012.09.04 02:30-03:50	Calibration of LI7500(SN:0790)

Chapter 2. Hydrographic survey

Tae Wan Kim[1], Koji Shimada[2], Ho Jin Lee[3], Hyun Jung Lee[1], Eri Yoshizawa[2]

[1]Korea Polar Research Institute, Incheon 406-840, Korea (twkim@kopri.re.kr; hyunjung@kopri.re.kr)

[2]Tokyo University of Marine Science and Technology, 4-5-7 Konann, Minato-ku, Tokyo, 108-8477, Japan (koji@kaiyodai.ac.jp; m103046@kaiyodai.ac.jp)

[3]Korea Maritime University, Busan 606-791, Korea (hjlee@hhu.ac.kr)

2.1 Introduction

The Arctic Ocean may be a sensitive indicator of global climate changes. Recently, the extent of summer Arctic sea ice has reduced dramatically. These changes affect both the Arctic and global climate system by altering the heat exchanges between the ocean and atmosphere. Recent observations have shown the warm water inflow from the Bering Sea is recognized as an important driving force for rapid reduction of sea ice associated with increase in the horizontal and vertical flux of heat, salt and momentum (Shimada et al., 2006; Carmack and Melling, 2011). The Pacific-origin Summer Water (PSW) reaches the mouth of the Barrow Canyon along the Alaskan Coast in the Chukchi Sea . After that PSW changes its advective direction toward northwest along the northern slope of the Chukchi Sea and is delivered in the Chukchi Borderland (CBL) region consisting of the Northwind Ridge and Chukchi Plateau. In this area the spreading pathway of PSW strongly affected by the large-amplitude seafloor topography, localized freshwater pool, and variation of in the large-scale oceanic Beaufort Gyre driven by sea ice motion. The horizontal heat transportation and heat release of PSW in this region are key processes to understand the rapid and huge sea ice retreat and changes in water column structure in the Pacific sector of Arctic Ocean. Surprisingly, however, the paucity of knowledge on the hydrographic/physical processes in those areas still exists because of lack of sustaining basin-scale observation and process

oriented small scale measurements against to the rapid Arctic climate changes. To improve our knowledge on the hot spot in the Arctic Ocean, 45-day expedition was conducted by the IBRV *Araon* in the Chukchi Borderland, Mendeleev Ridge, East Siberian Sea, eastern Makarov Basin, and western Canada Basin.

2.2 Materials and methods

An intensive oceanographic survey was conducted in the period of August 4 - September 7, 2012 using the new Korean IBRV Araon to reveal the spatial distribution of water masses in the Chukchi Borderland/Mendeleev Ridge (Fig 2.1). At each hydrographic station, the hydrocast of CTD/Rosette system with additional probes (e.g., transmissometer, PAR, altimeter, fluorometer, oxygen sensor, and etc.) was conducted to measure the profiles of temperature, salinity, depth and other biochemical parameters. To increase the spatial resolution for temperature and salinity, XCTD probes were used at several stations between regular hydrographic stations (see Fig. 2.1). The location of XCTD deployment was determined by the bathymetry and distance between regular stations. During the CTD upcasting, water samples were collected at several depths, and then analyzed in a laboratory. For the precise reading, the salinities of collected water samples were further analyzed by an Autosal salinometer (Guildline, 8400B). The measurement was performed when the temperature of water samples was stabilized to a laboratory temperature, usually within 24-48 h after the collection. A lowered acoustic Doppler current profiler (LADCP, RDI, 300 kHz) was attached with CTD frame to measure the full profile of current velocities. The bin size was chosen as 5 m, and the number of bins was 20. On the cruise track, the vessel-mounted ADCP (RDI, 38 kHz) was continuously operated. In the shallow area (ca. < 1000 m) the bottom tracking mode was applied. In order to avoid any signal interference with other acoustic systems, a synchronization unit was used during the entire running time.

The two moorings are deployed near the critical latitude where the frequency of inertial oscillation coincides with that of M2 tide as a part of GRENE and JAXA-IARC Arctic Research projects. In this area, a resonance between inertial oscillation of sea ice/ sea water

and M2 tide would causes a strong vertical mixing affecting the ice-ocean interaction and water mass formation. The primary purpose of these moorings is to understand the small scale ice-ocean dynamics and their influences on the sea ice. The sea ice motion data acquired by upward looking ADCP is used to validate the AMSR-2 satellite derived sea ice motion. The temperature and salinity data by moored sensor is to detect the water mass formation and modification. The detail configurations and information of deployments are shown in Fig. 2.1. These two moorings are scheduled to be retrieved by the Araon 2013 Arctic cruise. The location and details of deployed moorings are given in appendix Ⅱ.
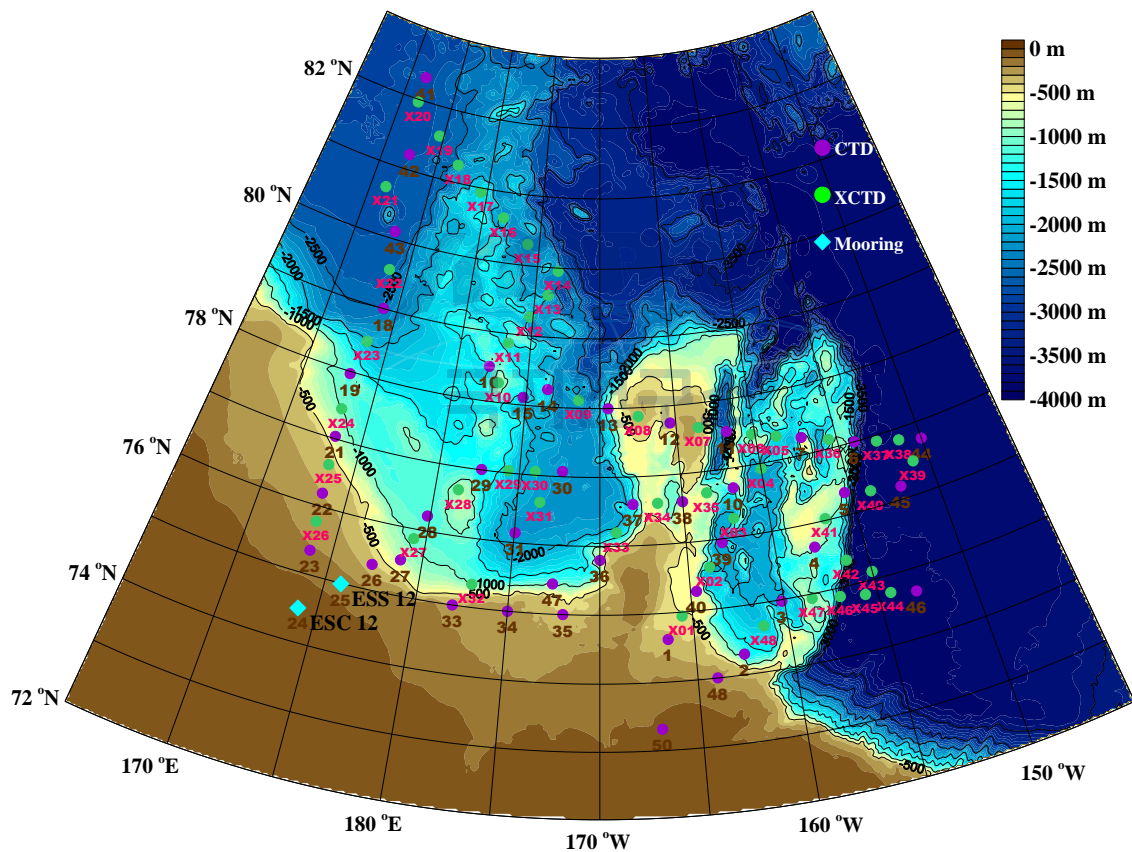

Fig. 2.1. Map showing ARA03B stations. Purple dots are CTD stations and green dots are XCTD stations during 2012 expedition. Ocean mooring stations are marked as diamonds.

2.3 Preliminary results

2.3.1 Chukchi Borderland

During the expedition, a total of 44 CTD (total 102 casts) and 48 XCTD stations were occupied. Water column structure in the Chukchi Borderland and Mendeleev Ridge area is established by layering penetration of distinct water masses: Surface mixed layer water (SMLW), Pacific summer water (PSW), Pacific winter water (PWW), East Siberian Sea winter shelf water (ESWW), oxygen poor lower halocline water (OPLHW), oxygen rich lower halocline water, Fram Strait Branch of Atlantic water (FSBAW), and Barents Sea Branch of Atlantic Water (BSBAW). Here we focus the structure above the main halocline, Fig 2.2 show the vertical section of potential temperature and salinity across the Chukchi Plateau and Northwind Ridge. SMLW has the lowest salinity due to the sea ice melt. PSW is relatively warm, fresh water mass. The salinity at the temperature maximum varies dependent on the wintertime surface mixed layer. In this year the the range was within S=30.0-32.0 psu. In the region east of the Northwind Ridge, upper portion of the PSW was destroyed down to 30m by wintertime convection, as the results huge heat release was occurred during winter. Whereas, in the region west of the Northwind Ridge, winter mixed layer was confined within surface to 20m deep. This geographical difference was a key feature of this year to understand the sea ice retreat in summer. On the Northwind Ridge, the isohaline at the temperature maximum showed a frontal feature with its depth getting deeper toward the east across the Northwind Ridge. The warmest PSW (~0.53 °C), which is identified as the core of PSW, located near the front about 45 m depth. The thickness of PSW layer with salinity range of 30.0~32.0 psu was about 60 m similar to that in 2011.
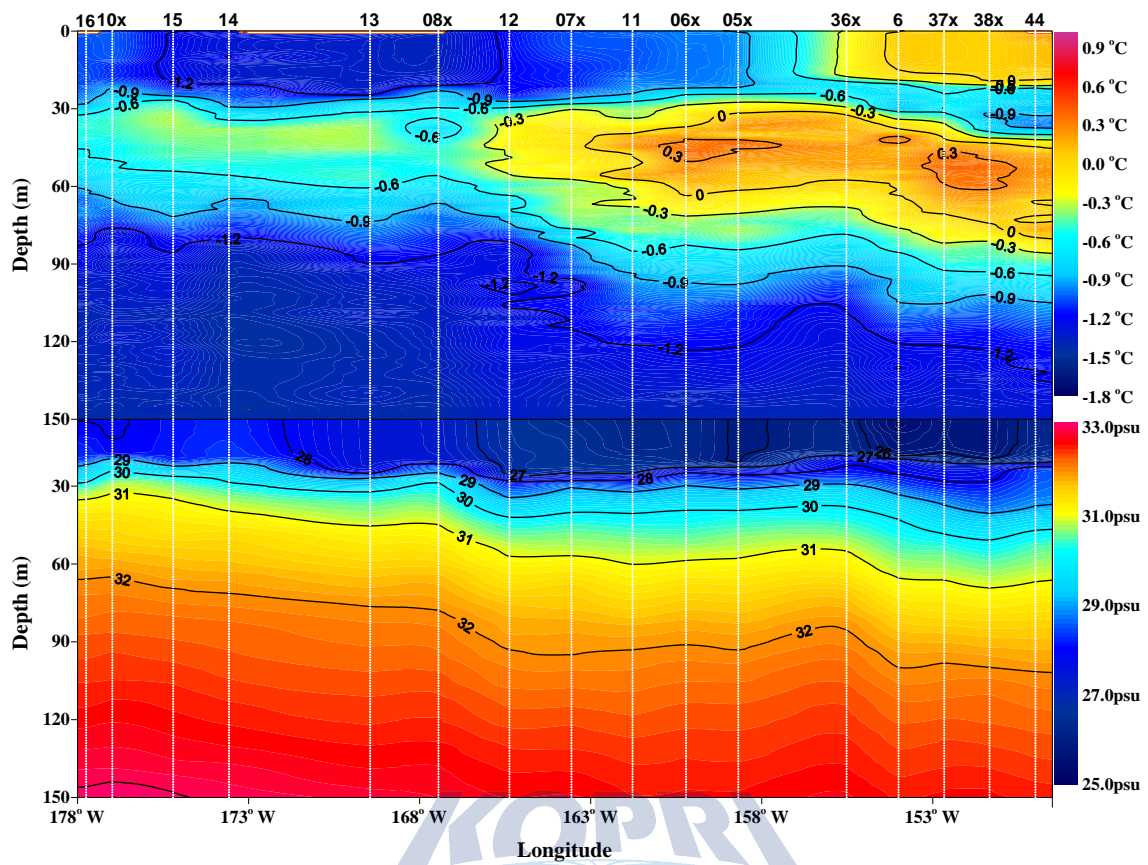
Fig. 2.2. Vertical section of potential temperature (upper panel) and salinity (contours) along the Chukchi Plateau.

Figure 2.3 shows the horizontal distribution of maximum potential temperature from 20 m to 100 m depth and salinity at maximum potential temperature layer. In previously investigation, the center of fresh water anomaly was located in the Canada Basin. And, the major pathway was settled west of the center of the freshwater pool. Similarly, the major pathway of PSW located on the Northwind Ridge in 2012 expedition. Also, PSW has never been observed in the west of 175°W in former data but PSW was identified in this region during 2011 and 2012 cruise. This suggests that some changes in ice and ocean circulation regime occurred in 2011/2012 winter.
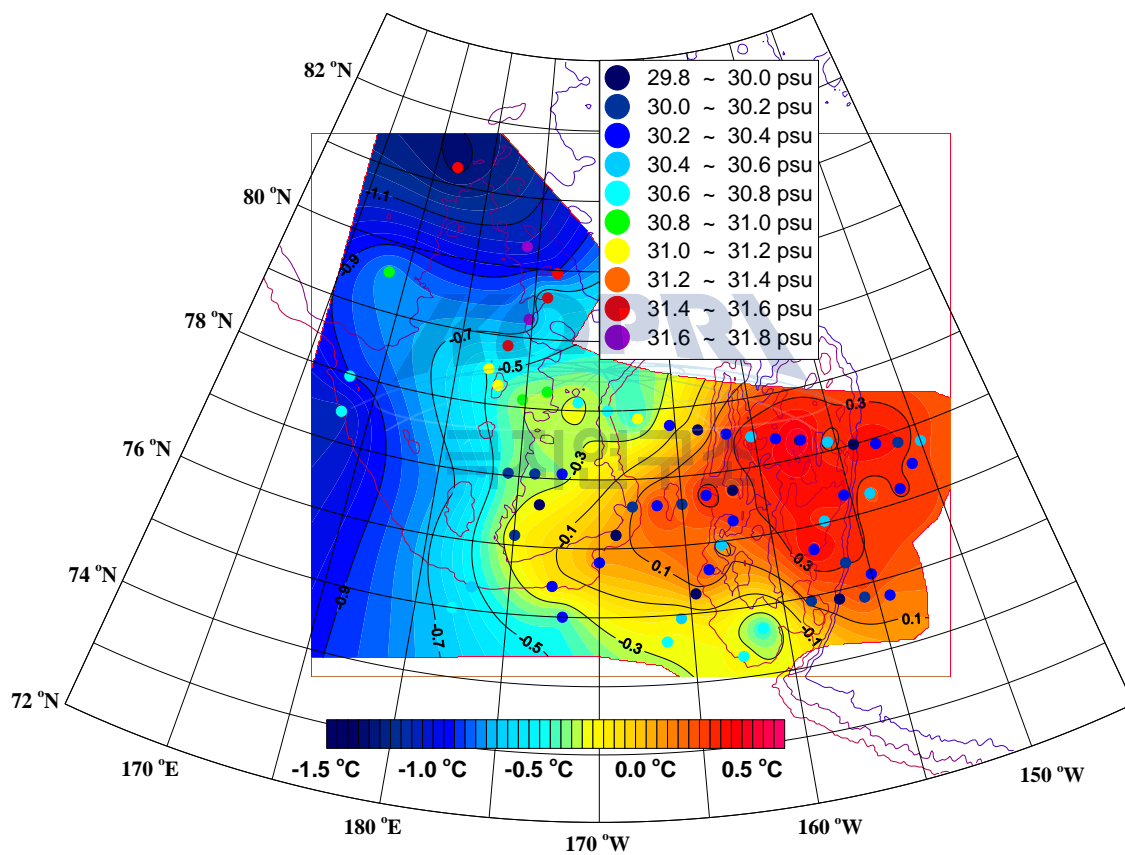
Fig. 2.3. Spatial distribution of maximum potential temperature from 20 m to 100 m depth and salinity at maximum potential temperature layer.

The PWW with nutrient maximum is an important water mass sustaining the Arctic ecosystem. Fig. 2. 4 show the horizontal distribution of potential temperature on S=33.1. In

this year, the PWW spread eastward from the northern Chukchi Slope and entered deep Canada Basin east of the Northwind Ridge. In 2008, the PWW spread northward from Herald Canyon along the Chukchi Plateau. These quantitative difference in the spreading pathway suggests that a certain critical value in surface forcing exist control the switching of the spreading pathway. In the Chukchi Borderland area, the other temerature minimum water (ESWW) with S~32.3 was also identified on the northern slope of the Chukchi Sea east of the Chukchi Plateau. This water delivered from the west of the Mendeleyev Ridge. We introduce this water mass in the following subsection.

Fig. 2.4. Spatial distribution of potential temperature on S=33.1

2.3.2 East Siberian Sea and Makarov Basin

The East Siberian Sea and its offshore Makarov Basin are last frontier area of hydrographic studies in the Arctic Ocean. We have occupied a complete section from shelf

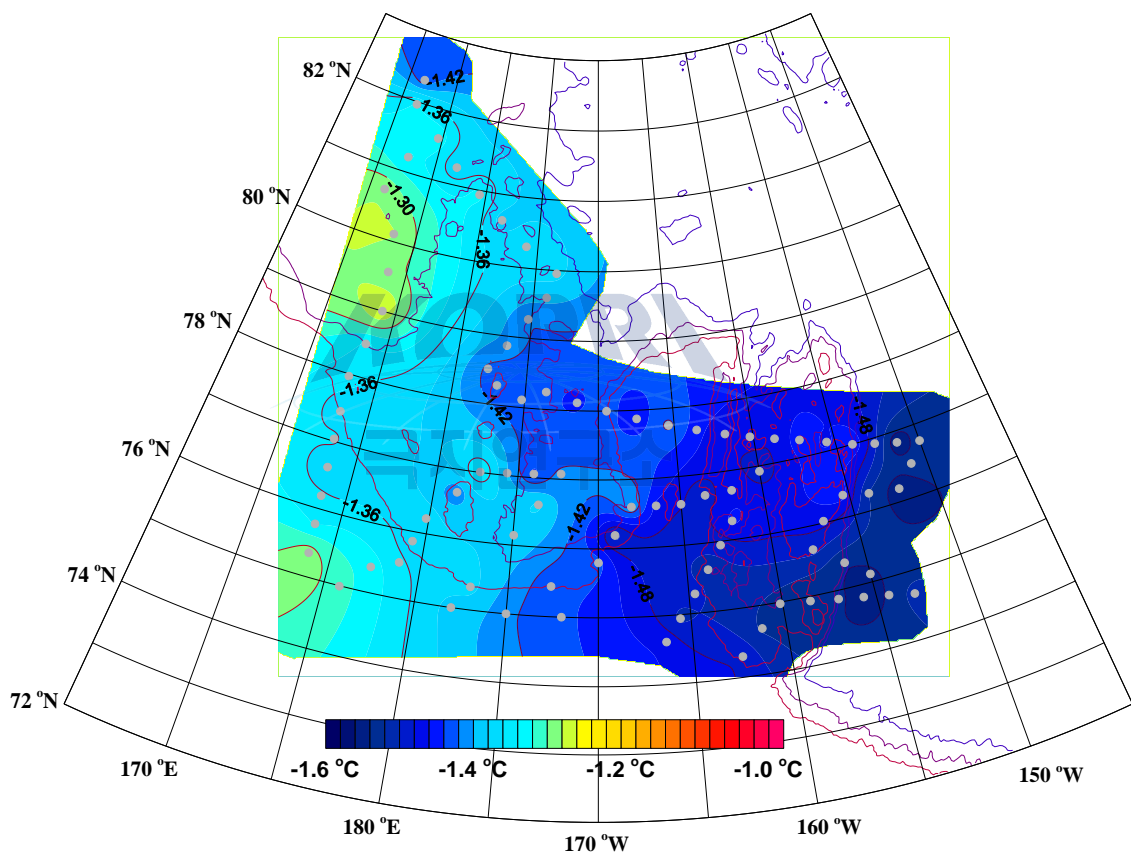region into the deep Makarov Basin up to 82° N. The water mass stratification is classified into two categories according to bottom depths (Fig. 2.5). In the region shallower than 1000m, volumetric cold water with its minimum temperature around S=32.3-32.5 spread from shelf region to the shelf slope about 1000m iso-bathymetry. This cold water is not Pacific Winter Water which is characterized by temperature minimum water around S=33.1. On the section, high biological activities were observed both on ice and in the upper ocean. The spreading pathway and distribution of this winter water will be a key issue to understand physics-biological environment changes associated with huge and rapid sea ice retreat in this region. On the shelf slope, oxygen minimum waters were observed in the lower halocline layer.

This water is delivered along the shelf slope into the western Canada Basin. The property of low oxygen is useful to understand the circulation pattern of the lower halocline water and East Siberian slope water in the Pacific Sector of the Arctic Ocean. In the deep Makarov Basin deeper than 1000m, oxygen rich lower halocline water dominated. T-S curve for the data north of 78° N shows almost straight line in the salinity range between 34.3 and 34.8. This feature suggests the water mass is formed by wintertime convection in surface mixed layer in the Eurasian Basin.
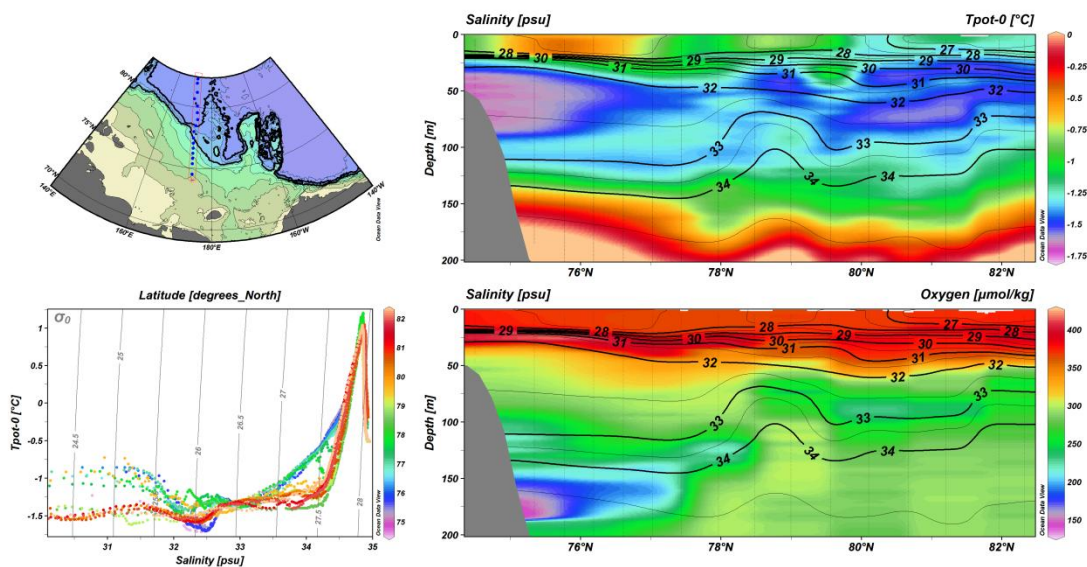
Fig. 2.5. Vertical sections of potential temperature (color) with salinity (contours), oxygen (color) with salinity (contours) along 171-174°E.

2.5. Summary and conclusions

The preliminary conclusions drawn from ARA03B scientific cruise can be summarized as follows:

1. In 2012, the major pathway of PSW located on the Northwind Ridge. And, the PSW has been gradually extended toward the west direction as compared with previously investigation. This suggests that some changes in ice and ocean circulation regime occurred in 2011/2012 winter.

2. The salinity of PWW at minimum potential temperature layer has decreased slightly in 2012. Also, the potential temperature of PWW on the Northwind Ridge was relatively colder than that on Chukchi Plateau.

3. The water mass stratification is classified into two categories according to bottom depths in East Siberian Sea and Makarov Basin. In the region shallower than 1000m, volumetric cold water with its minimum temperature around S=32.3-32.5 spread from shelf region to the shelf slope about 1000m iso-bathymetry. In the deep Makarov Basin deeper than 1000m, oxygen rich lower halocline water dominated.

4. As a further analysis, the current velocity field to be derived by LADCP and vessel-mounted ADCP data will directly provide an implication of pathways and spatial distribution of Pacific-origin warm water.

References

Carmack, E., and Melling, H., 2011. Warmth from the deep. Nature Geoscience, 4, 7-8.

Shimada, K., Kamoshida, T., Itoh, M., Nishino, S, Carmack E., McLaughlin, F., Zimmermann, S.,

and Proshutinsky, A., 2006. Pacific ocean flow: Influence on catastrophic reduction of sea ice cover in the Arctic Ocean. Geophysical Research Letters, 33, doi:1029/2005GL025624.

Jackson, J. M., Carmack, E. C., McLanghlin, F. A., Allen, S. E. and Ingram, R. G., 2010, Identification, Characterization, and change of the near-surface temperature maximum in the Canada Basin, 2993-2008. Journal of Geophysical Research, 115, C05021. Doi:10.1029/2009JC005265

WH-ADCP- 600KHz

Viny 12B-3 x4

20kg x 4 =80kg ↑

52.36m →

Mooring ESC12
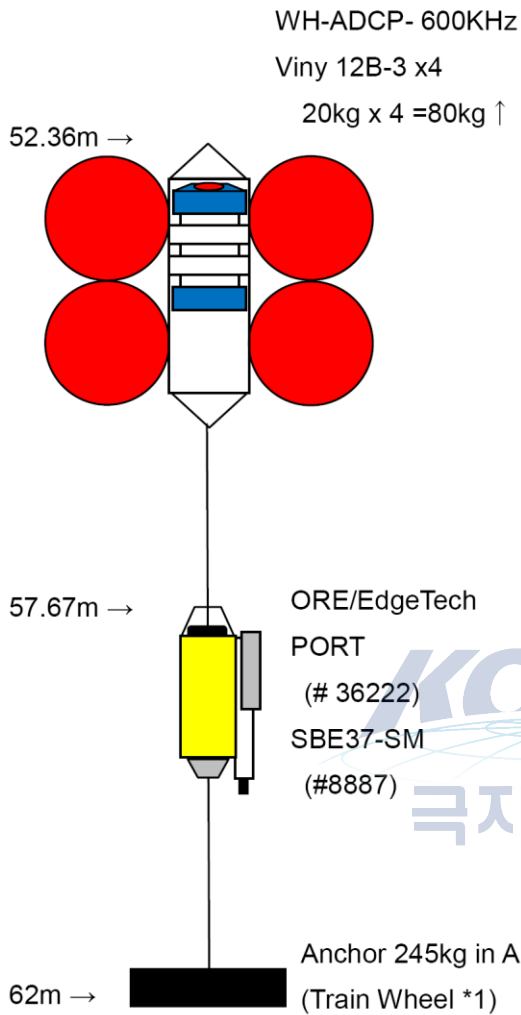
Position:

(Anchor dropped position near the crane on after deck)

74°30.002' N,   173° 59.902' E

Deployment time (Anchor):

August 20, 2012 15:36 (UTC)

Bottom depth: 62m

CTD:

SBE37-SM   S/No. 8887

57.67m →

ORE/EdgeTech

PORT

(# 36222)

SBE37-SM

(#8887)

Current Meter:

WH-ADCP-600kHz Sentinel

S/No. 17731

Acoustic Releaser:

ORE/EdgeTech PORT   S/No. 36222

Int. Frequency: 11.0kHz

Rep. Frequency: 12.0kHz

Pulse Width: 10m/sec.

Release Command: 426464

Enable Command: 406755

Disable Command: 406776

Anchor 245kg in Air

62m →

(Train Wheel *1)

Mooring ESS12

46.17m → ● UBE455×4
49.70m → ● 34.8kg×4＝139kg↑
49.89m → SBE37-SM (#8882)

59.91m → SBE56 (#01178)

68.97m → SBE37-SM (#8889)
69.16m →

79.18m → SBE56 (#01179)

88.24m → SBE37-SM (#8935(公))
88.43m →

98.57m → SBE56 (#01180)

109.63m → SBE37SM (#8883)
109.82m →

UBE455×6
113.90m → 34.8kg×6＝209kg↑

122.58m → WH-ADCP-300kHz
(# 16952)

128.49m → SBE37SM (#8886:公)

139.28m → SBE56 (#01181)

144.76m →
UBE455×4
34.8kg×4＝139kg↑

149.29m →
149.48m → SBE37-SM (#8888)

153.50m →
153.75m → ORE/EdgeTech   8242XS
Kaiyo-Denshi   TMR-6005B

160m → Anchor 1.1 ton (in Air)
(Train Wheel *4)

→ : Master Link

Position:
 (Anchor dropped position near the A-frame)
  74°59.534'N, 175°51.659'E
Deployment time (Anchor):
  August 21, 2012 2:23 (UTC)
Bottom depth: 160m

CTD:
   SBE37-SM   S/No. 8882, 8883, 8886(公)

CT:
   SBE37-SM   S/No. 8888, 8889, 8935(公)

Temperature:
   SBE56   S/No. 01178, 01179, 01180, 01181

Current Meter:
   WH-ADCP-300kHz Sentinel   S/No. 16952

Acoustic Release:
   ORE/EdgeTech 8242XS   S/No. 36446
      Int. Frequency: 11.0kHz
      Rep. Frequency: 12.0kHz
      Pulse Width: 10m/sec.
      Release Command: 432235
      Enable Command: 415107
      Disable Command: 415124

   Kaiyo-Denshi TMR-6005B   S/No. 0238
      Code: 3A-1

~ 36 ~

Appendix Ⅱ. Daily log sheet

Chapter 3 . Chemical Oceanography

3.1. Inorganic Carbon System

Gil Soo Ahn[1]

[1]Korea Polar Research Institute, Incheon 406-840, Korea (ksahn@kopri.re.k)

Hydrographic survey was conducted in the Arctic-Sea by hydrocasting CTD/Rosette at 50 stations. The area covers open ocean, sea ice zone, and polynya Inorganic carbon system was investigated by measuring dissolved CO_2 (pCO_2), dissolved inorganic carbon (DIC), and total alkalinity (TA) in two dimensions, horizontal monitoring along the ship track and vertical profiling at the hydro-casting stations. pCO_2 was measured using two different instruments: a non-dispersive infrared (NDIR) detecting system mounted on board by NIOZ (Steven van Heuven) and AWI (Mario Hoppema), and a gas chromatographic system by KOPRI. The former was dedicated for measuring pCO_2 underway whereas the latter was both for underway measurement and for analyzing discrete samples collected at the hydro-casting stations. Underway measurement of pCO_2 was carried out by supplying uncontaminated seawater to a Weiss-type equilibrator from which headspace air was delivered to the analytical system. For analyzing pCO_2 in the seawater samples collected at the station, a specially designed glass bottle was used to avoid any contamination from the air during sampling and storage. Atmospheric CO_2 in the marine boundary layer was also analyzed by two different systems, In a regular interval using the same instruments by pumping the ambient air. The pCO_2 analyzing systems were calibrated using a series of standard gases.

To investigate the distribution of Dissolved inorganic carbon (DIC) and TA(total alkalinity), CH_4 and N_2O pH in the water column, aliquots of seawater samples were drawn into glass containers from the Niskin bottles mounted on CTD-rosette. Especially, the sampling of CH_4 and N_2O in the laboratory a precisely known volume of "zero air" was injected into the glass containers to make headspace. New kinds of micrometeorological methods are used to measure CO_2 flux over sea in this project. The methods is to measure atmospheric CO_2 concentration combined with turbulent mixing coefficient yields CO_2 flux between the two levels. CO_2 concentrations were measured continuously with Li7000 using

NDIR(Non Dispersive Infra Red Absorption Method). Comparison of above two methods under this project would help to reduce CO_2 flux measurement and quantify CO_2 exchange over sea surfaces ranging from this ship track. The NDIR detecting system for pCO_2, CO_2 equips a streamline of software that provides the values in situ, while the gas chromatographic technique requires computation to determine pCO_2, CO_2 based on the calibration runs which were carried out between sample runs. In the cruise report we use preliminary data from the NDIR detecting system. As we expectation, the positive xCO_2 indicates supersaturation of CO_2 with respect to the atmospheric CO_2 above the seawater, ending up with emission of CO_2 and negative values for undersaturated surface. In general, most of the surface seawaters along the cruse track were undersaturated and act as a sink of atmospheric CO_2. However, more precision analyzing will be conducted at the KOPRI. We also conducted the operation of aerosol and VOC(volatile organic compound) measurement systems(AMS) base on Time of flight Mass spectrometer, CO measurement system base on CRDS(Cavity ring-down spectroscopy) technology and NO_X, $_jNO_2$, PAN, Hg measurement systems also operation to understanding for the atmospheric chemistry mechanism in this area. These detecting systems conducted along a streamline of software as a in situ measurements. However more precision analyzing will be conducted at the KOPRI.
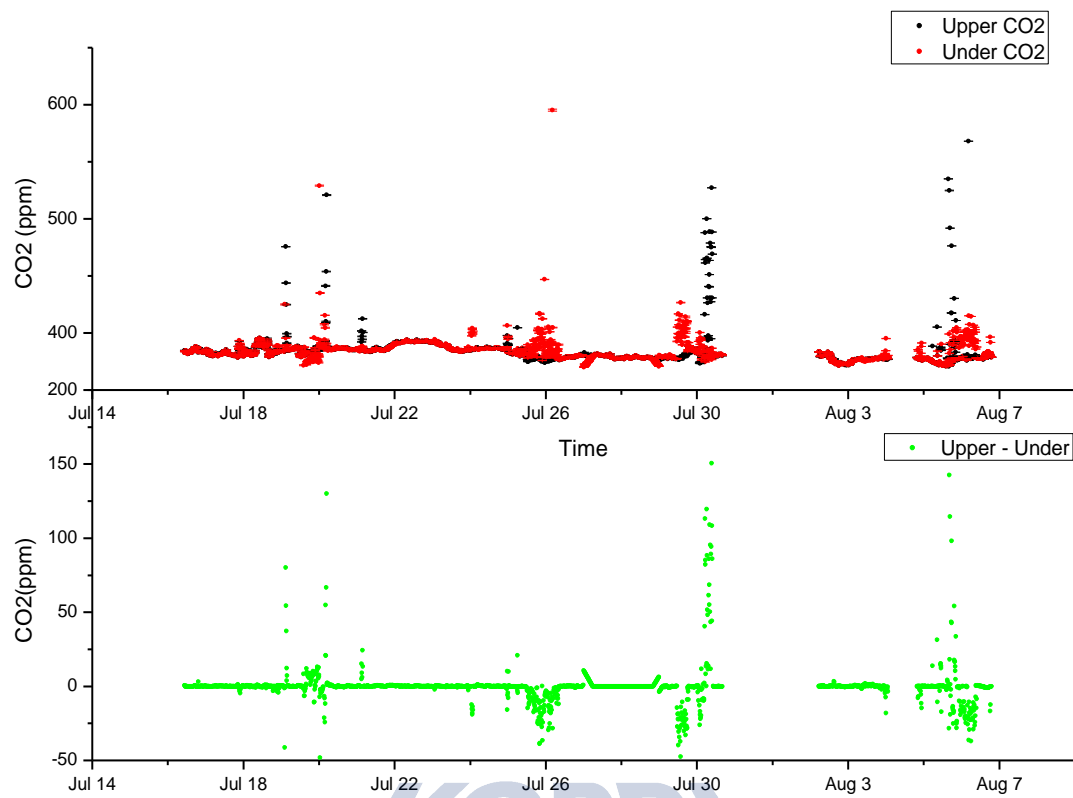
Time series of the uncorrected CO_2 concentrations of 8 m (Cell A) and 22 m (Cell B) above sea level.

3.2. Organic Carbon Measurement

Kyung Ho Chung[1] and Jun Oh Min[1]

[1]Korea Polar Research Institute, Incheon 406-840, Korea (khchung@kopri.re.kr; jomin@kopri.re.kr)

1. Introduction

It is generally known that the Arctic Ocean may significantly affect and be affected by global climate changes. In addition the Arctic Ocean has been shown to have large seasonal changes in sea-ice coverage and thickness, irradiance regime, fresh water input. Due to the impact of these, the Arctic Ocean has dynamic ecosystem and extremely regional contrasts in biological production and biogenic matter concentration in water column. The Chukchi Sea Shelf, one of the major shelf seas in the Arctic Ocean, particulate production rate is 208 $mmolCm^{-2}d^{-1}$ because inflow of nutrient-rich North pacific water through Bering Strait (Cota et al., 1996; Wheeler., 1996) whereas dissolved organic carbon exhibited only minor seasonal variations. Concentration of DOC did not show a significant seasonal change in surface waters of the Canada Basin (Davis and Bener, 2005) but particulate organic carbon concentration were strongly correlated with chlorophyll-a, indicating a plankton source of freshly produced organic matter. The central Arctic Ocean is the notably low productive area but dissolved organic carbon concentration in surface waters are among the highest in the world ocean (Anderson et al., 1998; Bussman and Kattner, 2000). On the other hand, the wide shelves of the Arctic Ocean receive large riverine input, suggesting that terrigenous organic carbon is one of major source of organic matter together with autochthonous production. However the distribution pattern and role of DOC and POC in response to the regional extreme environmental condition in the Arctic Ocean is rarely defined.

The objective of this study to better understanding of the controls on distribution and variability of organic carbon in both the dissolved and particulate form in different region of the Arctic Ocean; particularly Chukchi Sea, Makarov Basin, Canada Basin and East Siberian Sea, which is characterized with a discrete physical and biological properties respectively.

2. Materials and methods

Study area and Sampling

During Korea Icebreaker R/V ARAON cruise from 1 August to 10 September 2012, seawater sampling was carried out using aCTD/rosette sampler holding 24-10LNiskin bottles (OceanTest Equipment Inc., FL, USA). 33sampling stations for analysis organic carbon were occupied between 73N and 82N, and 170E and 150W region (Fig. 1, Table 1)

Water column samples for analysis dissolved organic carbon (DOC) and particulate organic carbon (POC) were drained from the Niskin bottles into amber polyethylene bottle.

DOC samples were collected with precombusted (6 hrs. at 450C) GF/F filters using a nitrogen gas purging system under low (<1.0 atm) pressure (Fig. 2). After 20 ml of DOC samples were collected into a precombusted amber glass vial, 0.1ml MgSO4 was added to samples to remove inorganic carbon.

POC samples were collected with same procedure as DOC sample by filtration of known seawater volume. Both DOC and POC samples were stored frozen at -20C until analysis in the home laboratory.

The hydrographic characteristics of the sampling stations were measured using a CTD (Seabird 911+).
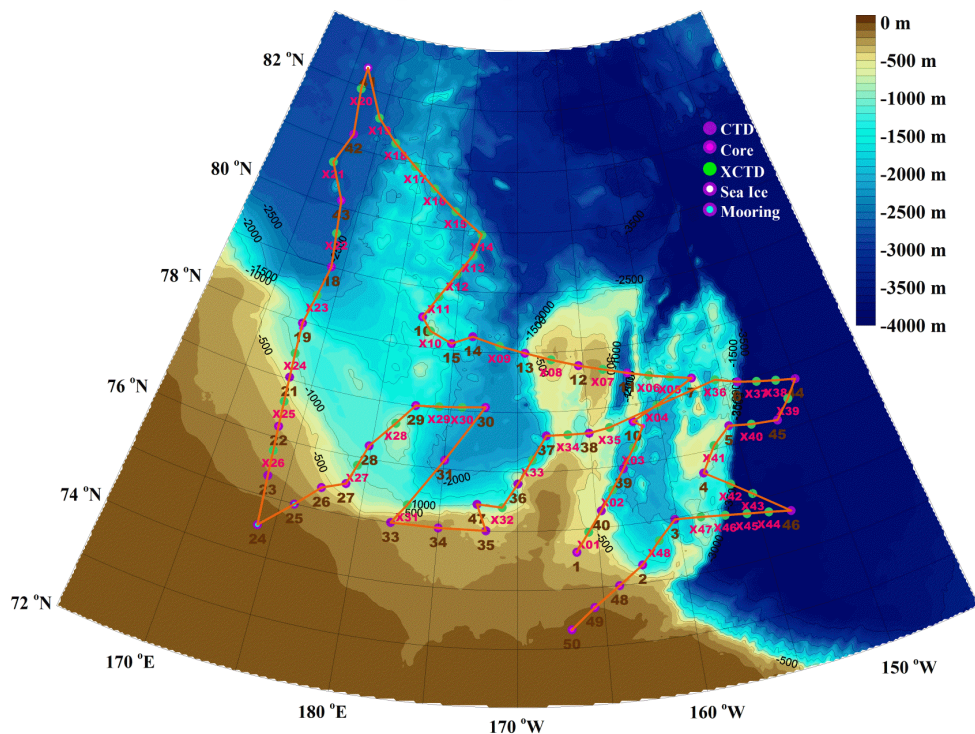
Fig. 1. A map of study site surveyed during 2012.

Analysis

DOC samples will be analyzed with high-temperature oxidation (HTCO) method (Sugimura & Suzuki, 1988) using a Shimadzu TOC-V system. To maintain quality control of sample analysis, 3~4 point calibration curve of seawater DOC reference standards will be made.

POC samples will be determined with a CHN analyzer according to JGOFS protocol (JGOFS, 1996).

Table 1.Sampling location and sampling depth at each station for organic carbon analysis

Station	Lat.	Long.	Sampling depth(m)
ARA03B_#01	73°18.49'N	166°56.36'W	0, 10, 25, 50, 75, 100, 150, 200, 250, 350
ARA03B_#02	74°18.00'N	162°30.00'W	0, 20, 40, 58,70, 100, 150, 300, 500, 1000
ARA03B_#03	74°58.56'N	160°07.84'W	0, 20, 40, 65, 75, 100, 150, 300, 500, 1000
ARA03B_#04	75°39.00'N	157°45.07'W	0, 20, 30, 50, 70, 100, 150, 300, 500
ARA03B_#05	76°15.00'N	153°51.63'W	0, 20, 45, 61, 70, 100, 150, 300, 500, 1000
ARA03B_#06	76°59.95'N	153°59.99'W	0, 20, 45, 57, 70, 100, 150, 300, 500, 1000
ARA03B_#07	77°15.11'N	157°09.20'W	0, 10, 25, 55, 75, 100, 150, 200, 500
ARA03B_#10	76°42.74'N	161°51.73'W	0, 10, 25, 55, 75, 100, 150, 200, 300, 500
ARA03B_#1	77°44.77'	165°19.60'	0, 10, 25, 60, 75, 100, 150, 200, 300, 400

2	N	W	
ARA03B_#13	77°59.81'N	165°26.86'W	0, 10, 25, 60, 75, 100, 150, 200, 300, 500, 1000
ARA03B_#14	78°15.09'N	173°37.48'W	0, 25, 45, 55, 70, 100, 150, 300, 500, 1000
ARA03B_#15	78°11.11'N	175.20.48'W	0, 10, 25, 55, 70, 100, 300, 600, 800, 1000, 1100, 1162
ARA03B_#16	78°30.01'N	177°43.08'W	0, 10, 40, 50, 70, 100, 150, 300, 500, 1000
ARA03B_#18	78°57.00'N	174°00.00'E	0, 10, 30, 40, 70, 100, 150, 300, 500, 1000, 2000
ARA03B_#19	78°29.01'N	173°31.14'E	0, 10, 20, 30, 40, 70, 100, 150, 300, 500, 1090
ARA03B_#21	77°02.12'N	173°18.00'E	0, 10, 30, 43, 50, 75, 100, 150, 300, 500
ARA03B_#22	76°11.41'N	173°31.98'E	0, 10, 30, 43, 50, 75, 100, 150, 300, 500
ARA03B_#23	75°20.70'N	173°45.96'E	0, 10, 32, 39, 70, 100, 150
ARA03B_#25	75°05.88'N	177°12.48'E	0, 10, 34, 45, 70, 100, 150
ARA03B_#27	75°31.13'N	178°46.90'E	0, 10, 38, 45, 70, 100, 150, 300, 500
ARA03B_#28	76°13.11'N	179°50.18'E	0, 10, 31, 45, 70, 100, 150, 300, 500, 1000
ARA03B_#29	77°0.81'N	177°21.08'W	0, 10, 37, 45, 70, 100, 150, 300, 500, 1100
ARA03B_#30	77°4.03'N	172°19.62'W	0, 10, 35, 50, 70, 100, 150, 350, 500, 1000, 2000

| ARA03B_#31	76°08.65'N	174°54.93'W	0, 20, 40, 52, 70, 100, 150, 300, 500, 1000
ARA03B_#33	75°20.00'N	177°5.645'W	0, 20, 34, 55, 70, 100, 150, 200, 315
ARA03B_#35	75°0.00'N	172°0.00'W	0, 20, 34, 55, 70, 100, 150, 200, 315
ARA03B_#36	75°48.00'N	170°0.00'W	0, 20, 35, 46, 70, 100, 150, 200, 500, 700
ARA03B_#37	76°35.98'N	168°00.11'W	0, 20, 45, 55, 70, 100, 150, 300, 500, 1000
ARA03B_#40	75°16.91'N	164°40.07'W	0, 10, 25, 55, 75, 100, 150, 200, 300, 500
ARA03B_#41	82°19.42'N	171°37.05'E	0, 10, 20, 40, 75, 100, 150, 300, 1000, 2000
ARA03B_#42	81°12.62'N	172°24.13'E	0, 10, 20, 40, 70, 100, 150, 350, 500, 1000, 2500, 2750
ARA03B_#48	74°00.10'N	163°59.96'W	0, 20, 40, 50, 70, 100, 150, 200
ARA03B_#50	73°18.80'N	166°56.52'W	0, 15, 24, 40, 50
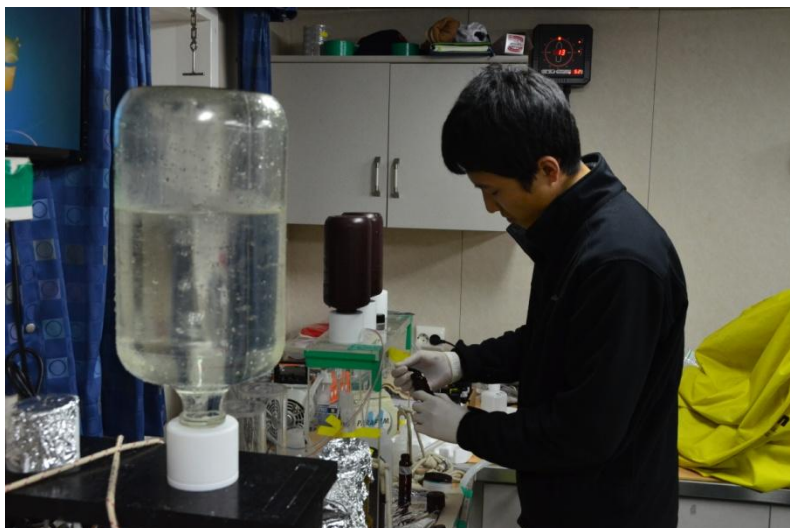
Fig. 2.Nitrogen gas purging system for collecting DOC and POC

References

Cota, G, F., Pomeroy, L. R., Harison. W. G., Jones, E. P., Peters, F., Sheldon Jr., W. M. Weingartner, T. R., 1996. Nutrients, primary production and microbial heterotrophy in the southeastern Chukchi Sea; arctic summer nutrient depletion and heterotriphy. Mar. Ecol. Pro. Ser., 135:247-258

Wheeler, P. A., Gosselin, M., Sherr, E., Thibault, D., Kirchman, D. L., Benner, R., Whitledge, T. E., 1996.Active cycling of organic carbon in the central Arctic Ocean. Nature 380:697-699

Anderson, L, G., Olsson, K., Chierici, M., 1998.A carbon budget for the Arctic Ocean. Global Biogeochemical Cycles, 12(3): 455-465

Bussman, I., Kattner, G., 2000. Distribution of dissolved organic carbon in the central Arctic Ocean: the influence of physical and biological properties. J. of Marine System, 27:209-219

Davis J and R. Benner, 2005. Seasonal trends in the abundance, composition and bioavailability of particulate and dissolved organic matter in the Chukchi/Beaufort Seas and western Canada Basin. Deep-Sea Res., 52:3396-3410.

Chapter 4. Plankton Ecology

4-1. Bacteria and Viruses

Chung Yeon Hwang[1], and Yoon Yong Yang[1]

[1]Korea Polar Research Institute, Incheon 406-840, Korea (cyhwang@kopri.re.kr; tazmenia@kopri.re.kr)

1. Introduction

Microbes (e.g. bacteria and viruses) are ubiquitous in marine ecosystems extending from the sea surface microlayer to the deep abyss. These organisms are at the bottom of the marine food web and play vital roles in global biogeochemical cycles. Heterotrophic bacteria are known to remineralize nutrients that support microbial production and transform dissolved organic carbon (DOC) into bacterial biomass supporting bacterial grazers (Azam 1998). Viruses are the most abundant entities in marine environments and significantly influence the production of DOC and the recycling of nutrients *via* viral lysis of host organisms (Fuhrman 1999).

Bacterial community structure is susceptible to physical environmental conditions (e.g. temperature and salinity). Simultaneously, bacterial community structure can be regulated by bottom-up and top-down mechanisms; the former includes the variables of chlorophyll *a*, nutrients and organic matters, whereas the latter includes viral lysis and grazing by protists. Advances in massively parallel sequencing technologies (e.g. pyrosequencing; Margulies et al. 2005) for the 16S rRNA gene, a molecular marker for phylogenetic analyses, have allowed us to gain deeper insight into bacterial communities and their relationships with physiochemical and/or biological variables.

In the Chukchi Sea, there are 4 distinct water masses during summer; surface mixed layer water, Pacific summer water, Pacific winter water and Atlantic water (Ha et al. 2011). These water masses can be distinguished by its unique properties of temperature and salinity (Ha et al. 2011), suggesting that spatial distribution of microbes and bacterial community structure might be reflected by these different ecological regimes. The objectives of the present study are to investigate the distribution of bacteria and viruses, and to examine

bacterial community structure in the Chukchi Sea.

2. Materials and methods

Seawater sampling for microbiological study was made at 35 stations during the icebreaker R/V Araon expedition (ARA03B; Aug 1 to Sep 10 in 2012; 73.3-82.3^{o}N, 173°E-153°W) in the Chukchi Sea (Fig 1). Samples were collected from 4-9 depths (surface to 2750 m) with 10 l Niskin bottles mounted on a CTD rosette.

For measurements of viral (VA) and bacterial abundance (BA), seawater samples (1.4-6.3 ml) were fixed with 0.02 μm filtered formalin (final conc. of 2%), and were filtered through 0.02 μm pore size Anodisc filters (Whatman). Filters were then laid on a drop of 100 μl of diluted SYBR Gold (final dilution, 2.5×10^3-fold; Noble and Fuhrman 1998) for 15 min in the dark. To avoid loss of microbes due to long-term storage (Hwang and Cho 2008), bacteria and viruses were counted within a day of sampling on aboard by using an epifluorescence microscope (Olympus BX35) isolated from the vibrations of the research vessel. Bacteria were distinguished from viruses on the basis of their relative size and brightness (Fig. 4.2). Contour plots of VA and BA were created in Ocean Data View (ODV version 4.5.0; Schlitzer, 2012) using DIVA Gridding with the default parameters.

Seawaters (4-6 L) for bacterial community analysis were pre-filtered through 3.0 μm pore-sized Nuclepore filters (Millipore) and collected onto 0.2 μm pore-sized cellulose nitrate membrane filters (Advantec). Filters were immediately transferred to cryovial tubes containing 1 ml RNAlater (Ambion) to avoid decomposition of nucleic acids, and stored at -80°C. In a land-based laboratory, extraction of nucleic acids and pyrosequencing of the 16S RNA gene will be made as previously described by Bowman et al. (2012).

3. Expected result (or preliminary results)
3.1. Spatial distribution of bacteria and viruses

Bacterial abundance (BA) ranged from 0.1×10^5 cells ml^{-1} to 16.4×10^5 cells ml^{-1} in the study area. In most stations, BA showed the maximum value at the surface or at the subsurface chlorophyll maximum (SCM) depth, and tended to decrease with depth in water

column. In a case of the transect at the westernmost stations between Stn 23 to 41 (Fig. 4.3), BA was higher in low latitude than in high latitude area. In this transect, a pronounced high BA (16.4×10^5 cells ml^{-1}) was observed at SCM depth in Stn 21, where was located above the continental slope (Fig. 4.3). In the study area, the value of integrated BA (ΣBA) in upper 100 m depth at Stn 21 (855.6×10^{11} cells m^{-2}) was also higher than other stations, whereas the lowest was observed at Stn 37 (159.9×10^{11} cells m^{-2}; Fig. 4.4).

Viral abundance (VA) ranged from 0.1×10^6 viruses ml^{-1} to 22.7×10^6 viruses ml^{-1}. VA was ca. 19-fold higher than BA, but depth profiles of VA showed similar patterns to those of BA. In a case of the transect at the westernmost stations between Stn 23 to 41 (Fig. 4.5), VA was generally higher in low latitude than in high latitude area as shown in the case of BA. However, a pronounced high VA (16.9×10^6 viruses ml^{-1}) was observed at SCM depth in Stn 23, where was located above the end of continental shelf (Fig. 4.5). In the study area, the value of integrated VA (ΣVA) in upper 100 m depth at Stn 23 (1164.9×10^{12} viruses m^{-2}) was also higher than other stations, whereas the lowest was observed at Stn 31 (372.3×10^{12} viruses m^{-2}; Fig. 4.6).

3.2. Bacterial community structure

Preliminary results of bacterial community structure were not available on aboard since further analyses need to be made in a land-based laboratory. However, it is expected that bacterial community structure in the study area may show spatial variability in horizontal and vertical distributions based on the preliminary observations of hydrographic properties and spatial heterogeneity in microbial abundances.

4. Summary and conclusions

Bacteria and viruses are at the bottom of the marine food web and play important roles in biogeochemical cycles of organic matters and nutrients. To understand the characteristics of microbial ecology in Arctic subzero waters, distributions of bacteria and viruses were investigated along with bacterial community structure in the Chukchi Sea during summer 2012. Our interim results showed that there was spatial heterogeneity in bacterial and viral abundances, probably influenced by physiochemical and biological

conditions in the study area. In-depth analyses of relationships between microbial variables and environmental variables will be made in the near future.

References

Azam, F. (1998) Microbial control of oceanic carbon flux: the plot thickens, Science 280, 694-696

Bowman, J. S., Rasmussen, S., Blom, N., Deming, J. W., Rysgaard, S., and Sicheritz-Ponten, T. (2012) Microbial community structure of Arctic multiyear sea ice and surface seawater by 454 sequencing of the 16S RNA gene, The ISME Journal, 6, 11-20

Fuhrman, J. A. (1999) Marine viruses and their biogeochemical and ecological effects, Nature, 399, 541-548

Ha, H. K., Shimada, K., Kim, T. W., Lee, H. J., Yoshizawa, E., and Kawashima, S. (2011) Chapter 1. Hydrographic survey, KOPRI Cruise Report

Hwang, C. Y., and Cho, B. C. (2008) Effects of storage on the estimates of virus-mediated bacterial mortality based on observation of preserved seawater samples with TEM. Aquatic Microbial Ecology, 52, 263-271

Margulies, M., Egholm, M., Altman, W. E., Attiya, S., Bader, J. S., Bemben, L. A., Berka, J. et al. (2005) Genome sequencing in microfabricated high-density picolitre reactors. Nature, 437, 376-380

Schlitzer, R. (2012) Ocean Data View, http://odv.awi.de
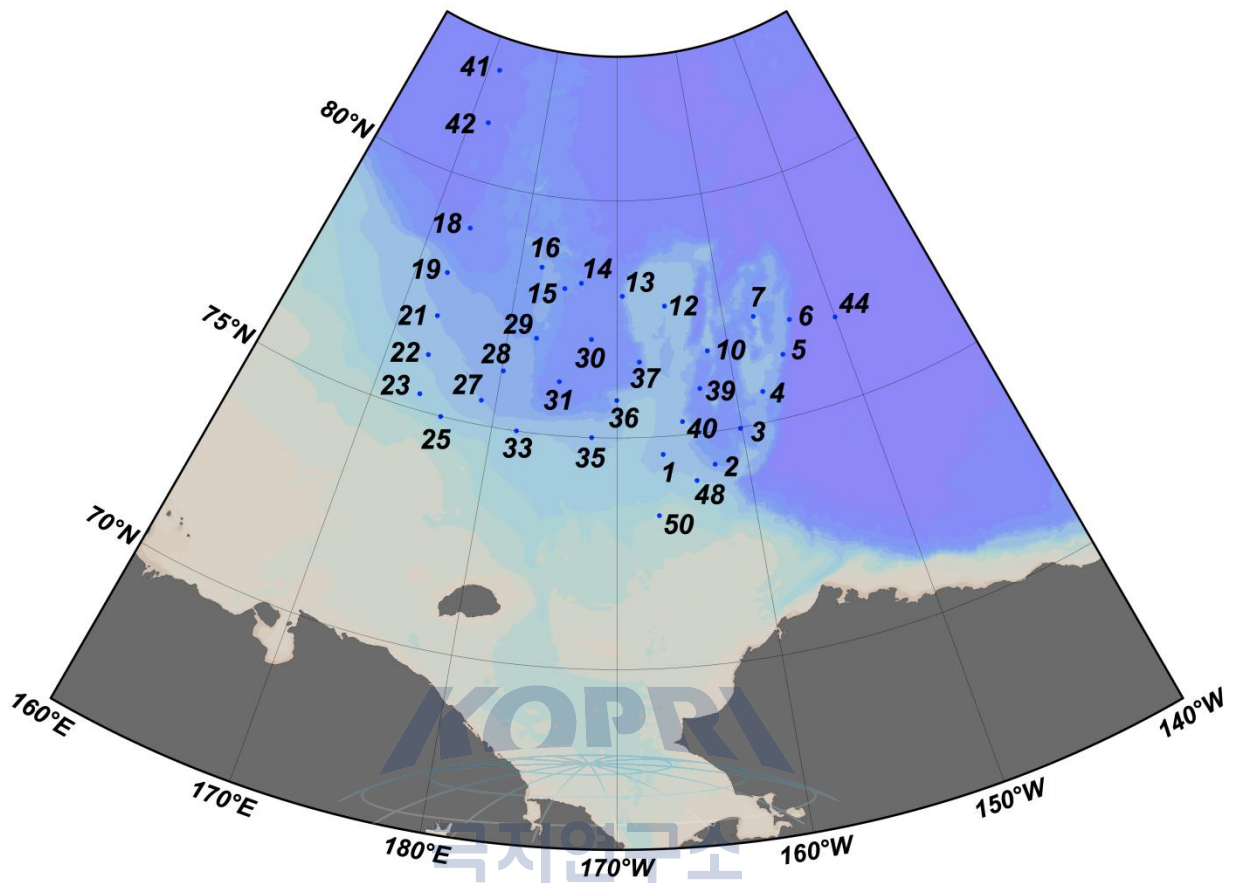
Figure 4.1. Study area and sampling stations for microbiological study in the Chukchi Sea during summer 2012.
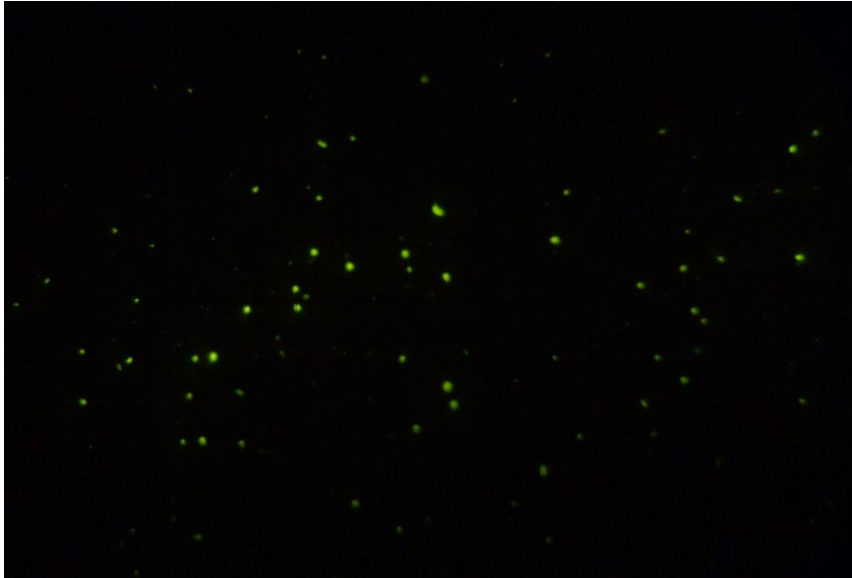
Figure 4.2. Epifluorescence photomicrograph of bacteria (larger green dots) and viruses (small green dots), collected from 200 m depth at Stn 48 in the Chukchi Sea during summer 2012.
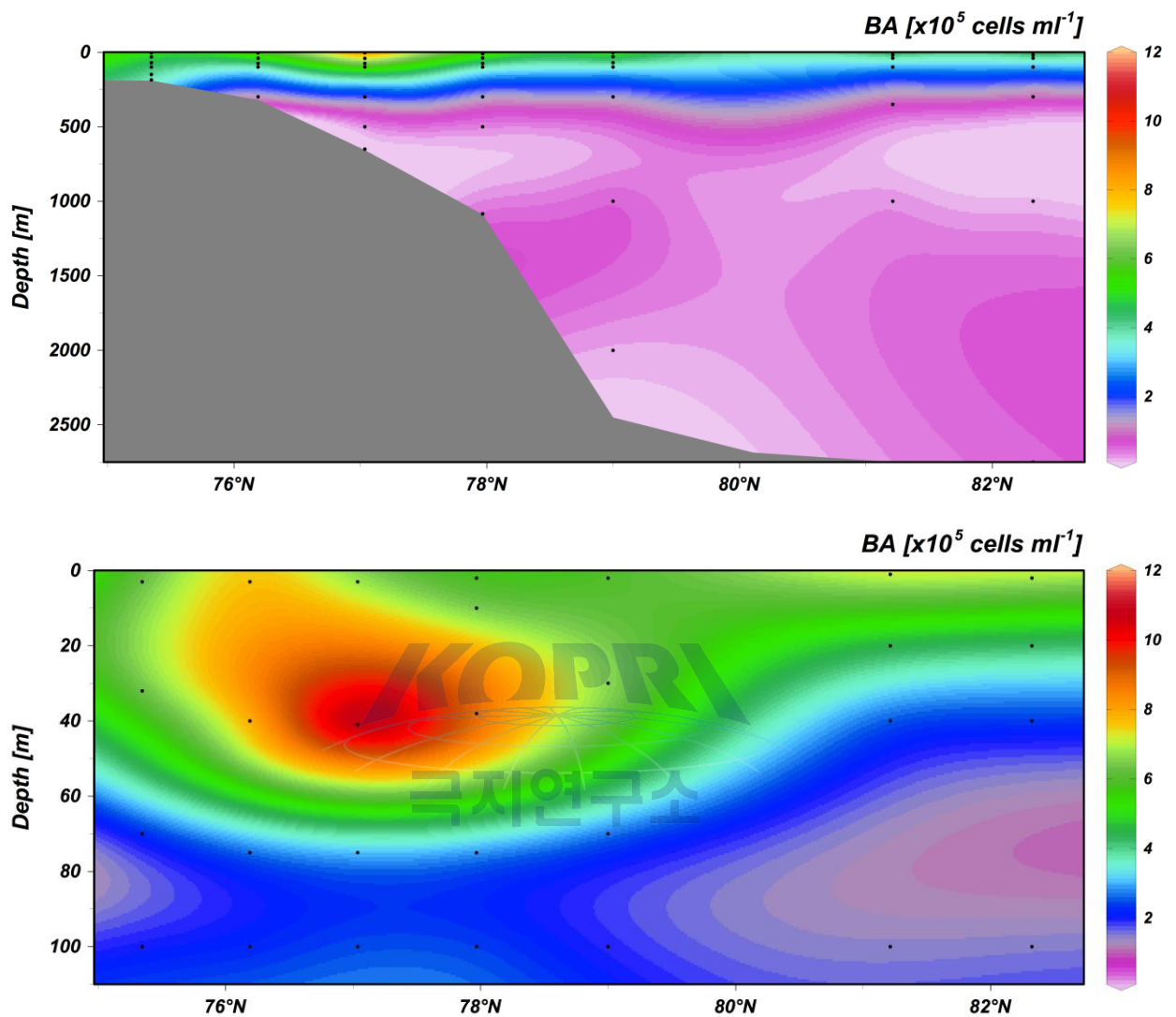
Figure 4.3. Spatial distribution of bacterial abundance (BA) along the transect at the westernmost stations between Stn 23 to 41 (see Fig. 4.1 for the location) in the whole depth (upper panel) and the upper 100 m (lower panel). Each dot represents an individual sampling depth.
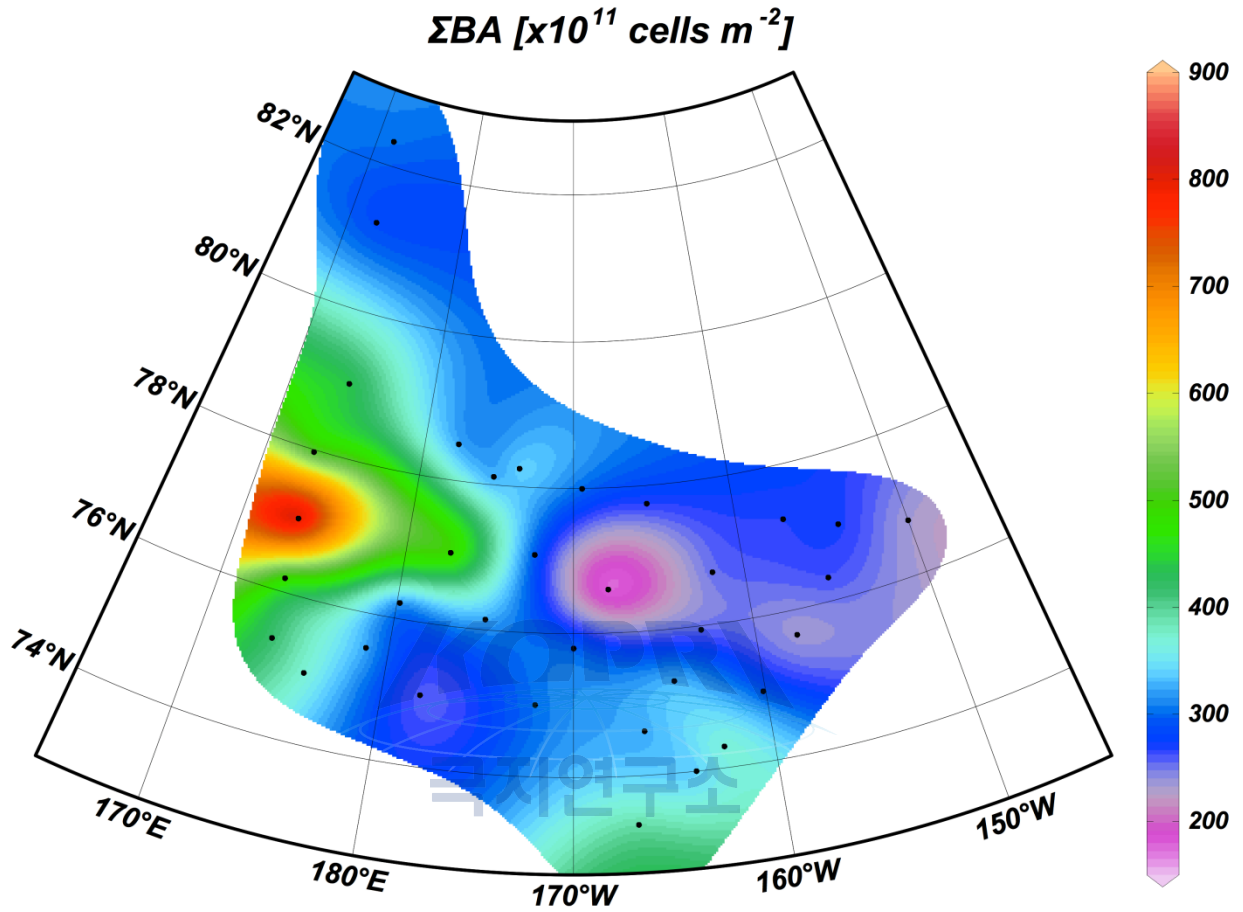
Figure 4.4. Horizontal distribution of the depth-integrated bacterial abundance (ΣBA) in the upper 100 m. Each dot represents an individual sampling station.
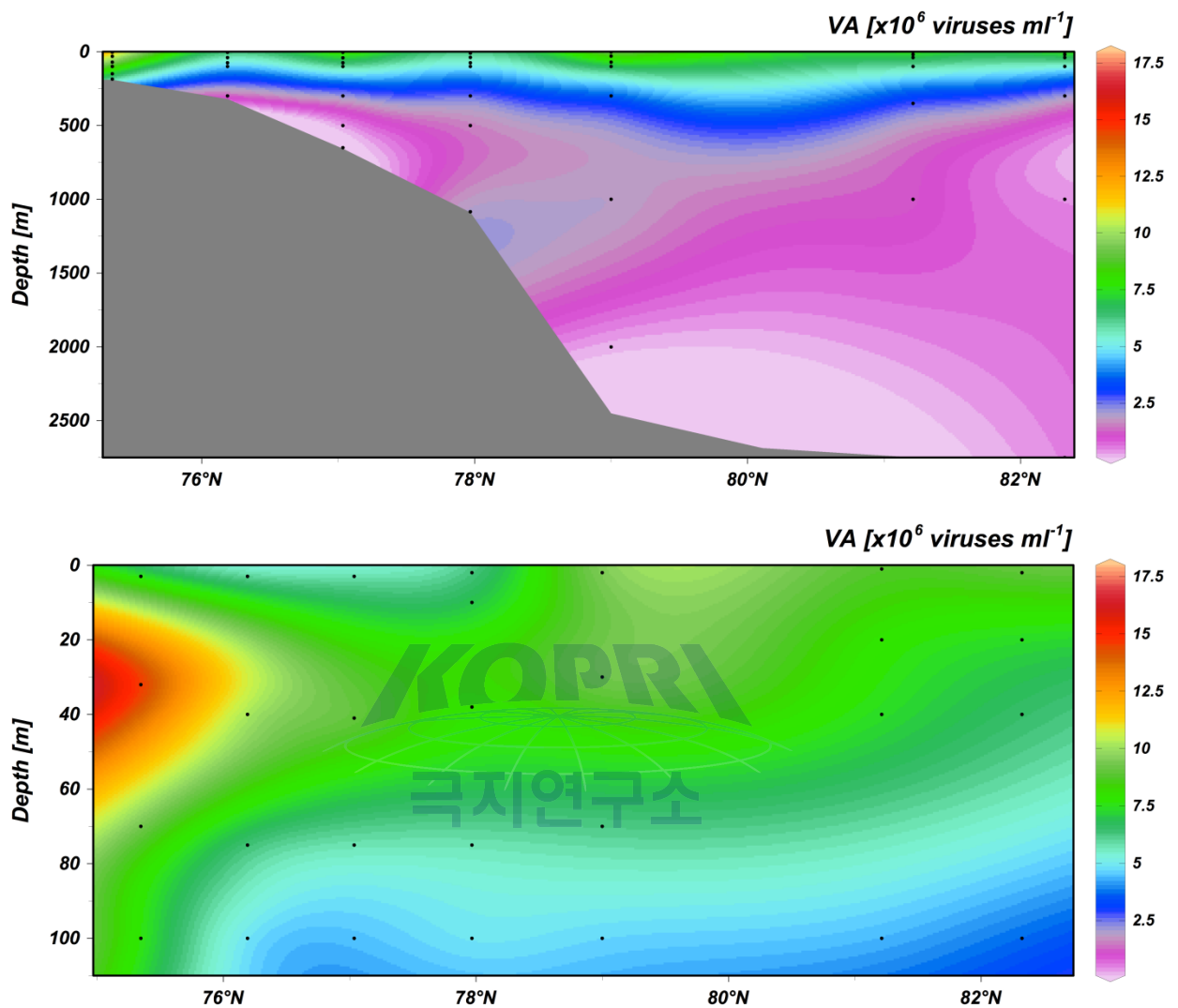
Figure 4.5. Spatial distribution of viral abundance (VA) along the transect at the westernmost stations between Stn 23 to 41 (see Fig. 4.1 for the location) in the whole depth (upper panel) and the upper 100 m (lower panel). Each dot represents an individual sampling depth.

Figure 4.6. Horizontal distribution of the depth-integrated viral abundance (ΣVA) in the upper 100 m. Each dot represents an individual sampling station.

4.2. Phytoplankton

Recent species compositions of phytoplankton and chlorophyll a concentration in the Western Arctic Ocean

Hyoung Min Joo

Korea Polar Research Institute, Incheon 406-840, Korea (hmjoo77@kopri.re.kr)

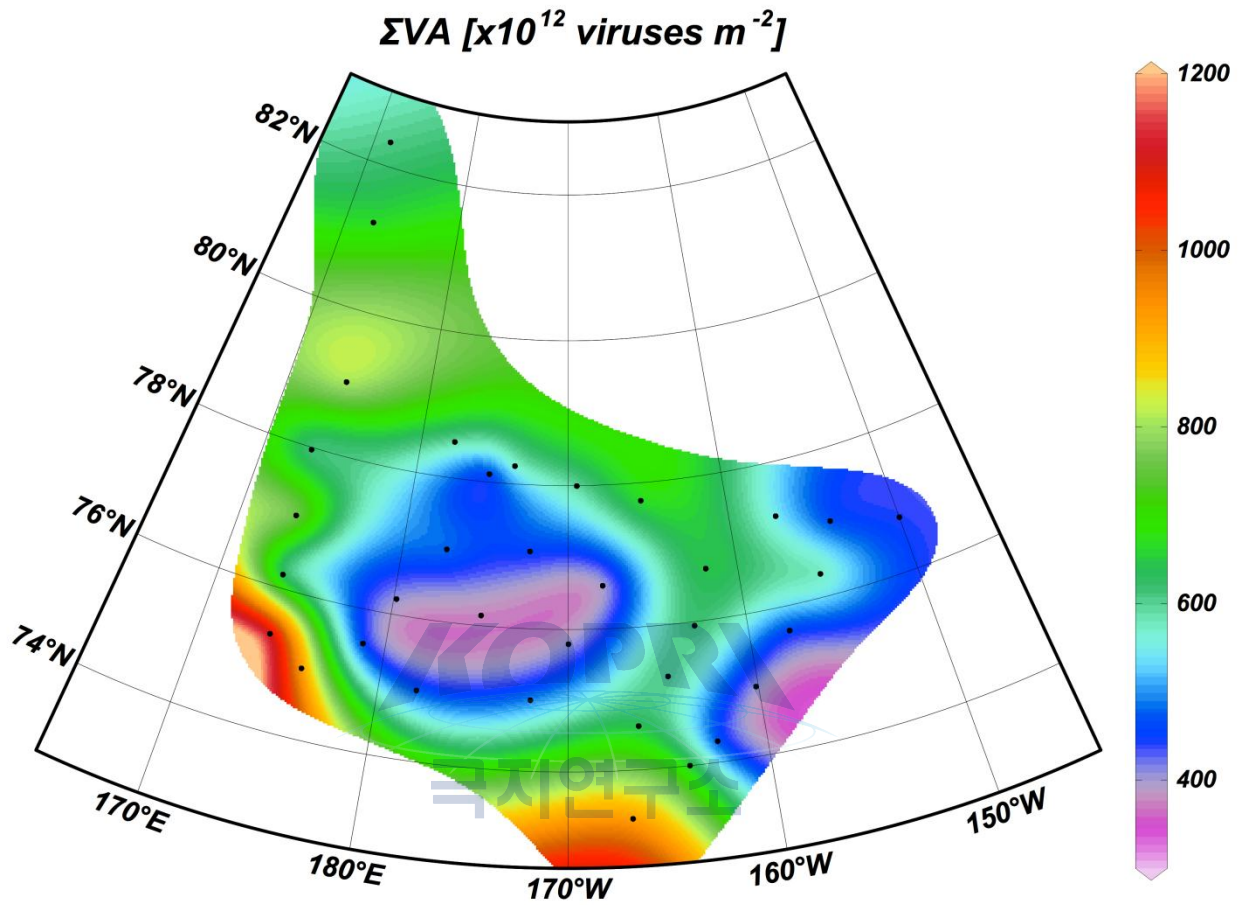### 4.2.1 Introduction

Phytoplankton communities and their contribution to primary production in this area of the Arctic are controlled by seasonal environmental changes in solar irradiation, ice cover, water temperature, and vertical stratification, as well as by the inflow of warm Pacific waters through the Bering Strait. Waters from the south influence the timing of the seasonal ice melting in spring as well as ice formation in the fall, which is different from other Arctic shelves. These warm and nutrient-rich waters flow northwards with the Anadyr Current through the Bering Sea into the Chukchi Sea. This northward flow is caused by a sea-level difference between the Bering Sea and the Arctic Ocean. The variability of the pelagic environment affects phytoplankton and controls their taxonomic composition, abundance, biomass, in situ primary production, and succession. Previous taxonomic analysis of samples in the western Arctic Ocean indicated that populations on the Chukchi Shelf are often dominated by centric diatoms in summer. The aim of the present study was to characterize the systematic composition of phytoplankton assemblages, their distribution, abundance, and size composition and associate them with varying abiotic factors during a limited period of time in summer 2011 in the Chukchi Sea.

4.2.2. Materials and methods

The data were collected in the Chukchi Sea from August 4 to September 6 in 2012 (Table 4.2.1, Fig. 4.2.1). A total of 32 stations were visited. Water samples were collected at 8-9 depths (Surface, 10m, 20m, 30m, 50m, 80m, 100m, 150m, and subsurface chlorophyll a maximum depth) with a rosette sampler equipped with 20 L Niskin-type bottles, an in situ fluorometer, and a high-precision Sea-Bird plus CTD probe. The subsurface chlorophyll

maximum layer depths were estimated by CTD profiles.

To analysis phytoplankton community composition, water samples were obtained with a CTD/rosette unit in 20 L PVC Niskin bottles during the 'up' casts. Aliquots of 125 mL were preserved with glutaraldehyde (final concentration 1%). Sample volumes of 50 to 100 mL were filtered through Gelman GN-6 Metricel filters (0.45 μm pore size, 25 mm diameter). The filters were mounted on microscopic slides in a water-soluble embedding medium (HPMA, 2-hydroxypropyl methacrylate) on board. The HPMA slides were used for identification and estimation of cell concentration and biovolume. The HPMA-mounting technique has some advantages over the classical Utermöhl sedimentation method. Samples were also collected via phytoplankton net tows (20 μm mesh) and preserved with glutaraldehyde (final concentration 2%); these samples were used only for identification of small species in the phytoplankton assemblage. Since the results from this can be biased towards larger specimens, these data were not used for statistical analysis, but only for morphological and systematic analysis. Based on the HPMA slide method, the total 228 slides were made for identifying species compositions of phytoplankton later at the laboratory in KOPRI. To identify small sizes plankton (nano-pico size), phytoplankton net samples were cultured by F/2 media (1 station).

The chl a concentration was estimated by Fluorometer. Particulates were collected on 25 mm glass fiber filters (GF/F) and the filters were then left in the dark for 12 h in 90% acetone at 4°C for pigment extraction.

Table.4.2.1. Sampling locations of phytoplankton species compositions during the ARA02B 2012 cruise.

Station No.	Sampling Date Mm/dd/yy	Sampling time [UTC]	Latitude	Longitude	Bottom Depth [m]
1	08/04/12	22:10	74.617 N	166.397 W	367
2	09/03/12	21:00	74.300 N	162.502 W	1217
3	09/03/12	10:00	74.976 N	160.131 W	1733
4	09/02/12	5:30	75.650 N	157.751 W	917
5	09/01/12	19:40	76.323 N	155.356 W	1031
6	08/31/12	20:00	76.996 N	153.983 W	1837
7	08/08/12	4:10	77.252 N	157.149 W	711
10	08/07/12	8:55	76.714 N	161.856 W	1037
12	08/09/12	8:20	77.746 N	165.327 W	483
13	08/10/12	2:40	77.997 N	169.448 W	1224
14	08/10/12	15:20	78.250 N	173.625 W	1592
16	08/11/12	17:00	78.500 N	177.718 W	1187
18	08/17/12	8:00	79.000 N	174.000 E	2452
19	08/08/12	0:00	77.968 N	173.042 E	1098
21	08/18/12	18:30	77.026 N	173.263 E	639
22	08/19/12	6:50	76.190 N	173.533 E	311
23	08/19/12	18:20	75.337 N	173.766 E	180
25	08/21/12	6:40	74.993 N	175.859 E	151
27	08/21/12	23:10	75.521 N	178.784 E	680
28	08/22/12	13:00	76.218 N	179.836 E	1200
29	08/24/12	21:00	77.006 N	177.369 W	1398
30	08/25/12	23:30	77.075 N	172.327 W	2013
31	08/27/12	1:20	76.144 N	174.916 W	2179
33	08/27/12	15:30	75.000 N	177.998 W	318

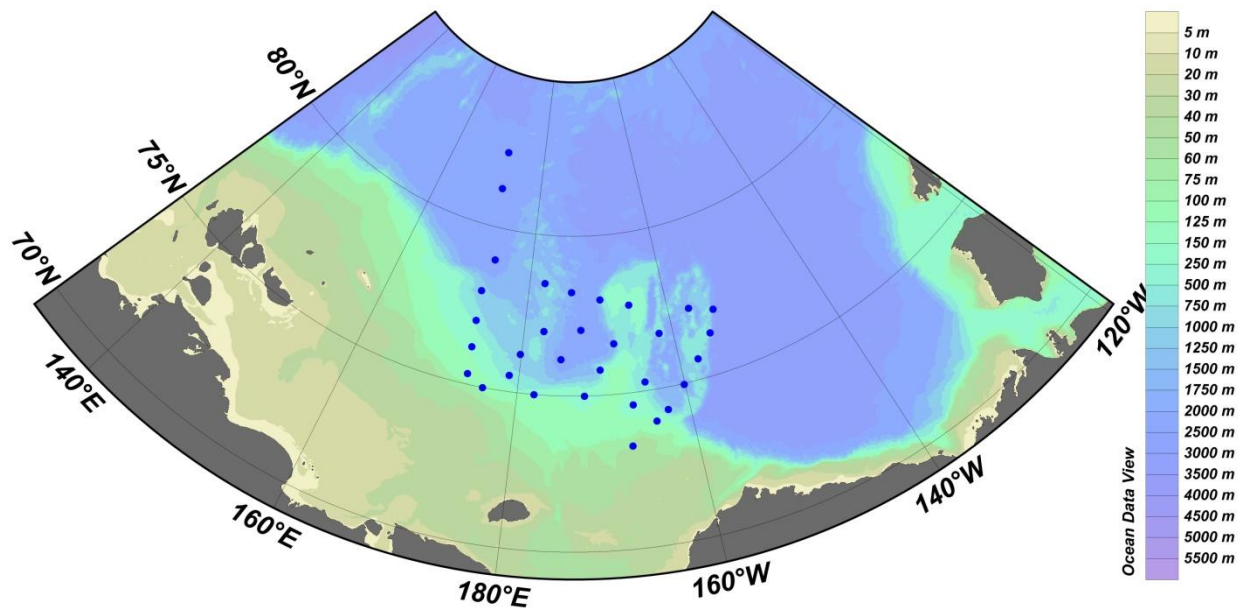| 35	08/28/12	13:30	75.000 N	171.999 W	376
36	08/29/12	5:15	75.799 N	169.998 W	751
37	08/30/12	12:30	76.600 N	168.002 W	1776
40	08/05/12	12:00	75.282 N	164.668 W	618
41	08/15/12	8:50	82.324 N	171.618 E	2760
42	08/16/12	7:30	81.202 N	172.280 E	2757
48	09/05/12	4:30	74.002 N	163.999 W	249
50	09/06/12	6:00	73.314 N	166.942 W	65

Figure 4.2.1.Station map of phytoplankton species compositions during the ARA02B 2012 cruise.

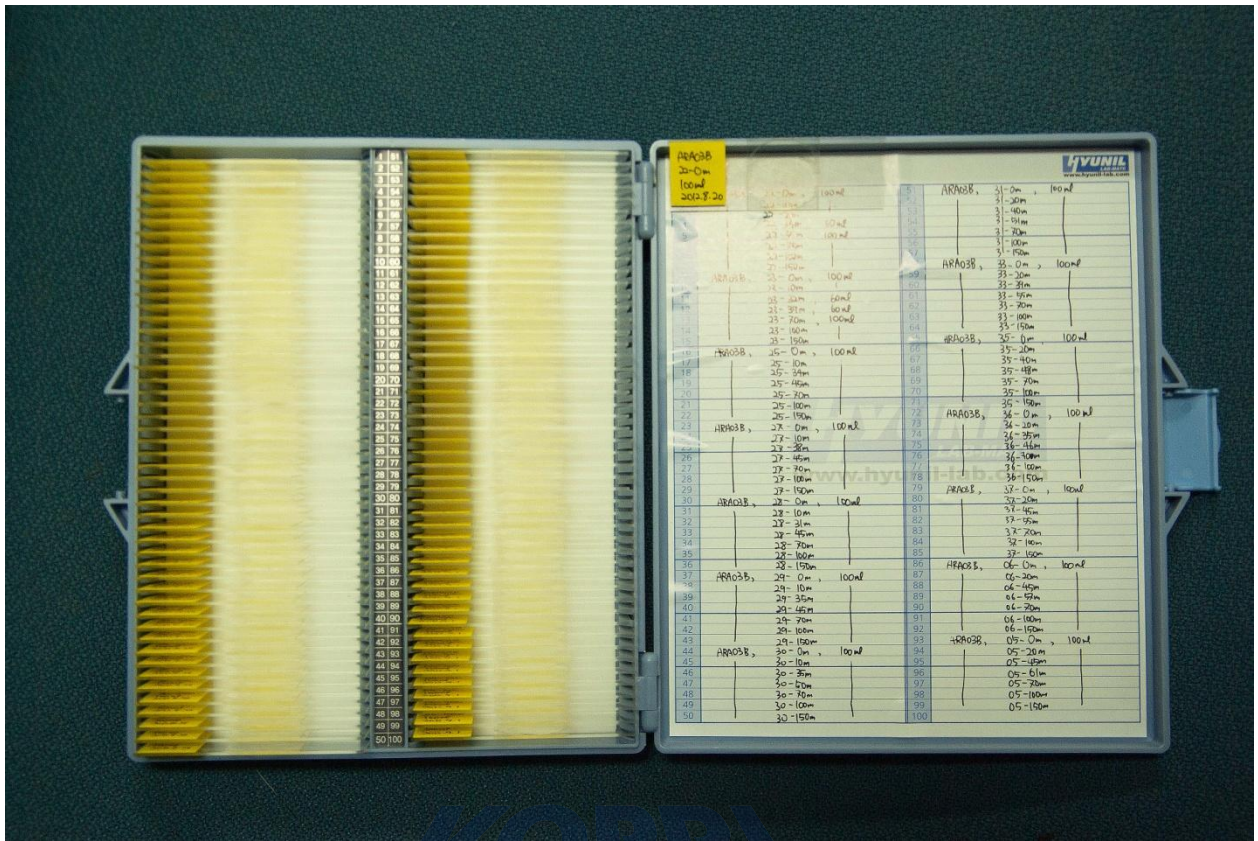**Figure 4.2.2.Sampling by 20um messhed Phytoplankton Net (photo by Dae-sik Hwang).**

Figure 4.2.3.HPMA Slides for Quantity analysis of phytoplankton communities.

4-3. Primary Production

Carbon and nitrogen productions of phytoplankton in the Northern Chukchi Sea

Bo kyung Kim[1], Jaejoong Kang[1](bokyung85@naver.com, jaejung@pusan.ac.kr)

[1]Department of Oceanography, Pusan National University, Korea

1. Introduction

Over the past several decades, higher temperatures have decreased the extent of sea-ice cover as well as its thickness in the Arctic Ocean. In addition, the overall amount of perennial sea ice in the Arctic Ocean, especially in the western Arctic Ocean became reduced (Perovich et al., 2009). The removal of seasonal and permanent sea ice cover altered several important processes, such as the depth of mixing, stratification, light penetration, nutrient supply, temperature-related processes, and possibly photochemical reactions (Tremblay et al., 2008; Codispoti et al., 2009; Lee et al., 2010). These recent changes in climate and ice conditions could change the patterns and the total amount of carbon production of phytoplankton and consequently the production at higher trophic levels. However, whether these climate change conditions enhance or reduce the overall production in the Arctic Ocean is controversial. Therefore, the main objectives are to determine main controlling factors for phytoplankton production and to find the effects of current environmental changes, especially decrease in sea ice extent and thickness, on the overall production in the Arctic Ocean.

2. Methods and Materials

To estimate carbon and nitrogen uptake of phytoplankton at different locations, productivity experiments were executed by incubating phytoplankton in the incubators on the deck for 3-4 hours (Fig. 1) after stable isotopes (^{13}C, $^{15}NO_3$, and $^{15}NH_4$) as tracers were inoculated into each bottle. Total **17** productivity experiments were completed during this cruise. At every CTD station, the productivity waters were collected by CTD rosette water samplers at 6 different light depths (100, 50, 30, 12, 5, and 1%). In addition, Along with the small (1 L) productivity bottle experiments, **8** large volume (8.8 L) productivity experiments

for three depths (100, 30, and 1% light depths) were executed to study the physiological status and nutritional conditions of phytoplankton at the productivity stations (Fig. 2). These filtered (GF/F, ø = 47 m) samples will be chemically analyzed for the macromolecular level end products (such as lipids, proteins, polycarbonates and LMWM) of photosynthesis.

Fig. 1. In situ incubation on deck for 3-4 hours.

After the incubation, all productivity sample waters were filtered on GF/F (ø = 25 mm or 47 mm) filters for laboratory isotope analysis at University of Alaska Fairbanks after this cruise.
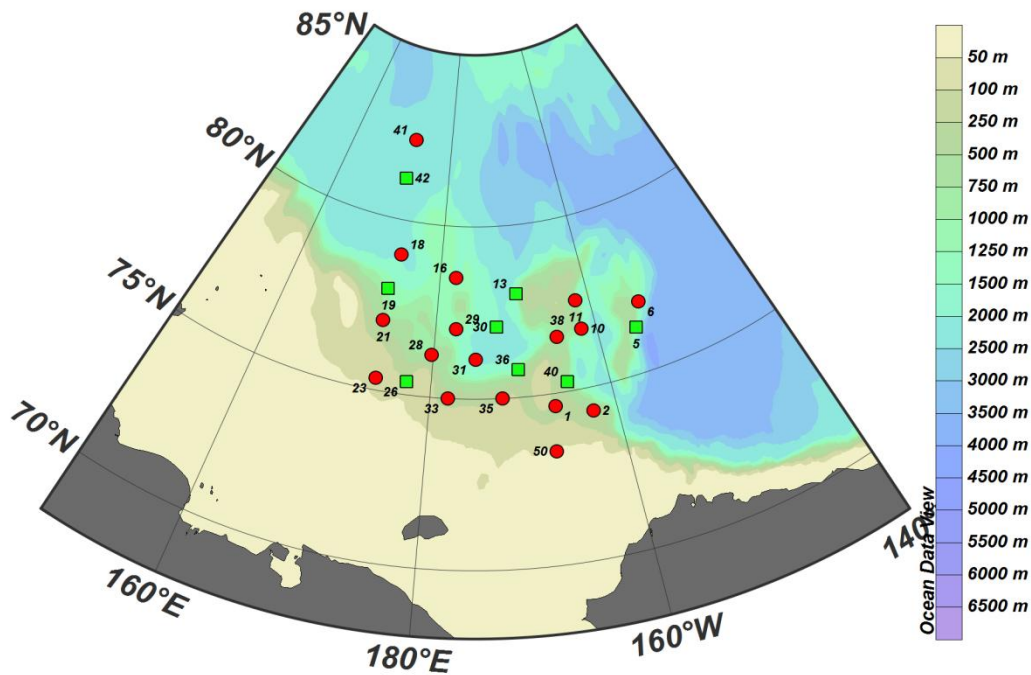
Fig. 2. Stations for primary(red circle) and macromolecular(green square) productivity during the 2012 Arctic cruise.

For the base data at the productivity station, waters were collected for alkalinity, macro nutrient concentrations (Nitrate, Nitrite, Silicate, Ammonium, and Phosphate), and total and size-fractionated (only for 100, 30, and 1% of light depth) chlorophyll-a concentrations.

3. Preliminary Results

3.1. Light and UV intensity during the cruise

Air surface light intensity measured during the cruise ranged from about 300μE m^{-2} s^{-1} for day time(Fig. 3).
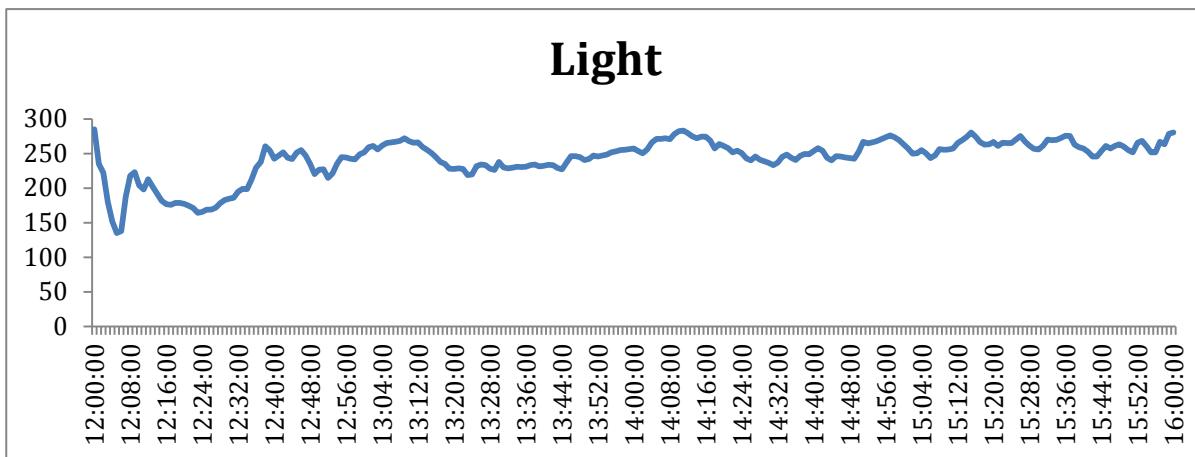
Fig.3. Air surface light intensity during the cruise in 2012
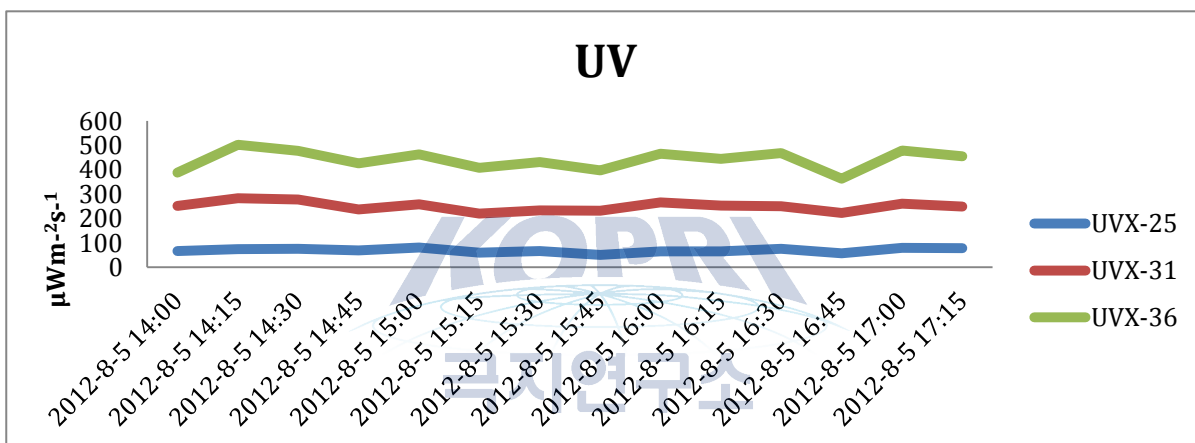
Fig.4. Air surface UV intensity during the cruise in 2012

Night time is not dark at all most of time during the arctic summer. But, the incubation time for phytoplankton productivity experiments should be executed during the day time when the light intensity high enough for their growth.

4. Summary and Conclusions

Phytoplankton production in this region since the nutrient concentrations are very important controlling factors for phytoplankton growth in the Arctic Ocean during the summer time with enough light. More data such as carbon and nitrogen uptake data from our experiments will clearly identify whether phytoplankton production in 2012 is relatively higher or lower compared to 2011 cruise.

References

Codispoti LA, Flagg CN, Swift JH (2009) Hydrographic conditions during the 2004 SBI process experiments. Deep-Sea Research II 56:1144-1163.

Lee SH, Stockwell D, Whitledge TE (2010). Uptake rates of dissolved inorganic carbon and nitrogen by under-ice phytoplankton in the Canada Basin in summer 2005. Polar Biology.33:1027-1036

Perovich DK, Richter-Menge JA (2009) Loss of sea ice in the Arctic. Annual Review of Marine Science 1:417-441

Tremblay, J.-É., Simpson, K., Martin, J., Miller, L., Gratton, Y., Barber, D., Price, N.M., 2008. Vertical stability and the annual dynamics of nutrients and chlorophyll fluorescence in the coastal, southeast Beaufort Sea. Journal of Geophysical Research 114, C07S90, doi:10.1029/2007JCoo4547, 2008.

4-4. Protozoan Ecology

The role of heterotrophic protist in the pelagic ecosystems of the Western Arctic Ocean

Eun Jin Yang and Jin Dong Lee

Korea Polar Research Institute, Incheon 406-840, Korea (ejyang@kopri.re.kr and DJLee@kopri.re.kr)

4.4.1Introduction

Heterotrophic protists ingest a broad size spectrum of prey, from bacteria to microphytoplankton, and are themselves important prey items for mesozooplankton. Many researchers suggest that heterotrophic protists contribute to the trophic linkage between phytoplankton and mesozooplankton and are important in the pelagic food webs of many oceanic waters. The importance of heterotrophic protists in pelagic ecosystems has become increasingly evident in the past two decades, and trophic interaction between heterotrophic protists and phytoplankton has been reported in various marine. However, there is no information on the relative importance of heterotrophic protists in the pelagic ecosystem of the Western Arctic Sea.   The Arctic Ocean is currently experiencing rapid environmental change due to natural and anthropogenic factor that include   warming, sea ice loss and other physical change as well as biology and ecosystem structure change.   In this study area, we investigated the meso-scale variations and structure of heterotrophic protist communities and grazing rates on phytoplankton in the various environmental conditions such as open ocean, sea ice zone and melting ponds. During this cruise, we investigated protozoa abundance, biomass and grazing rate in total 32 stations (Table 4.4.1).

4.4.2. Materials and methods
Abundance and community structure of heterotrohic protists

To determine the abundance of heterotrophic protists, a CTD-Niskin rosette sampler was used to take water samples from the following 7depths. For ciliates and sarcodina, 500 ml water from the vertical profiles was preserved with 1% acid Lugol's iodine solution these samples were then stored in darkness. For heterotrophic nanoflagellates and heterotrophic

dinoflagellates smaller than 20 µm, 500 ml of water was preserved with glutaraldehyde (0.5% final concentration) and stored at 4° C.

▪ **Grazing experiments**

Grazing rates of heterotrophic protists were determined by the dilution method (Landry and Hassett 1982). Water for grazing experiments was collected from 3 depth (surface, SCM, 1% light depth) of each station, and gently filtered through a 200-µm mesh. At each station, 30L seawater were collected in a Niskin bottle and transferred to a polycarbonate carboy. Part of this water was filtered through the 0.22-µm filtration system. Dilution series were set up in ten 1.3-l PC bottles. Ten bottles were used to establish a nutrient-enriched dilution series consisting of replicate bottles with 11, 28, 50, 75, and 100% natural seawater. The bottles were incubated on deck for 24 – 48 h at ambient sea surface temperatures and screened to the ambient light level with neutral density screening. Subsamples were collected from replicate bottles at 0 and 24-48h to determine chlorophyll-a concentrations.

Table.4.4.1. Sampling locations of heterotrophic protists community structure and grazing rates   during the ARA03B 2012 cruise.

Station No.	Sampling Date Mm/dd/yy	Sampling time [UTC]	Latitude	Longitude	Community	Grazing
1	08/04/12	22:10	74.617 N	166.397 W	o	o
2	09/03/12	21:00	74.300 N	162.502 W	o	o
3	09/03/12	10:00	74.976 N	160.131 W	o	o
4	09/02/12	5:30	75.650 N	157.751 W	o	o
5	09/01/12	19:40	76.323 N	155.356 W	o	o
6	08/31/12	20:00	76.996 N	153.983 W	o	o
7	08/08/12	4:10	77.252 N	157.149 W	o	
10	08/07/12	8:55	76.714 N	161.856 W	o	o
12	08/09/12	8:20	77.746 N	165.327 W	o	o

13	08/10/12	2:40	77.997 N	169.448 W	o	o
14	08/10/12	15:20	78.250 N	173.625 W	o	
16	08/11/12	17:00	78.500 N	177.718 W	o	o
18	08/17/12	8:00	79.000 N	174.000 E	o	o
19	08/08/12	0:00	77.968 N	173.042 E	o	o
21	08/18/12	18:30	77.026 N	173.263 E	o	
22	08/19/12	6:50	76.190 N	173.533 E	o	
23	08/19/12	18:20	75.337 N	173.766 E	o	o
25	08/21/12	6:40	74.993 N	175.859 E	o	o
27	08/21/12	23:10	75.521 N	178.784 E	o	
28	08/22/12	13:00	76.218 N	179.836 E	o	o
29	08/24/12	21:00	77.006 N	177.369 W	o	
30	08/25/12	23:30	77.075 N	172.327 W	o	o
31	08/27/12	1:20	76.144 N	174.916 W	o	
33	08/27/12	15:30	75.000 N	177.998 W	o	o
35	08/28/12	13:30	75.000 N	171.999 W	o	
36	08/29/12	5:15	75.799 N	169.998 W	o	o
37	08/30/12	12:30	76.600 N	168.002 W	o	o
40	08/05/12	12:00	75.282 N	164.668 W	o	
41	08/15/12	8:50	82.324 N	171.618 E	o	o
42	08/16/12	7:30	81.202 N	172.280 E	o	o
48	09/05/12	4:30	74.002 N	163.999 W	o	
50	09/06/12	6:00	73.314 N	166.942 W	o	o

4-5. Zooplankton Ecology

Mesozooplankton distribution patterns and grazing impacts of major copepods on phytoplankton biomass

Jae Kwang Lee

Chungnam National University, Daejeon, Korea (powermex@nate.com)

4.5.1. Introduction

The Chukchi Sea is one of the major gateways into the Arctic where large quantities of Pacific heat, nutrients, phytoplankton and mesozooplankton enter the region through the shallow Bering Strait in a complicated mixture of water masses. Mesozooplankton abundance and biomass generally have been considered to be low in the Arctic Ocean. Nevertheless, mesozooplankton is numerically important element and plays a major role in the food webs. Mesozooplankton grazing, especially copepods, is a key factor controlling composition and dynamics of phytoplankton communities. In the Arctic Ocean, *Calanus* spp. are regarded as biological indicators of Arctic (*Calanus glacialis* and *C. hyperboreus*) and Atlantic (*C. finmarchicus*) water masses, respectively. They are the most important biomass species and the prime herbivores in these waters. Over the past several decades, atmospheric warming has increased the Arctic Ocean temperature and resulted in decreased extent and thickness of se ice. The removal of seasonal and permanent sea ice can greatly influence a number of important ecological processes such as photochemical reactions, stratification-related nutrient supply, phytoplankton bloom patterns and mesozooplankton distribution. For predicting climate change impacts in the ecosystems by rapid sea ice melting, it is important to understand the dynamics of the mesozooplankton community. The main goal of this study was, 1) to understand the interactions between the environmental factors (i.e. seawater temperature, salinity and chlorophyll *a* concentration) and the mesozooplankton community 2) to estimate the feeding rates of major copepods on the phytoplankton biomass.

4.5.2. Material and methods

Mesozooplankton samples were collected with a Bongo net (60 cm diameter, 330 and 500 μm mesh size) at 25 selected stations. The net was towed vertically within the upper 200 m of the water column. Samples from 330 μm mesh were immediately fixed and preserved with buffered formaldehyde (pH 8, final concentration ca. 5%) for quantitative analyses. From the 505 μm mesh size samples, healthy individuals were immediately sorted out and transferred into 20 ml vials containing filtered seawater. These vials were frozen at -80°C for the gut content analyses.

Table 4.1. Sampling location and depth during the sampling period in the Arctic Sea, 2012.

Latitude	Longitude	Station	Date(local)	Sampling Depth (m)
74.37.05N	166.22.77W	ARA03B01	2012-08-05	200
74.18.00N	162.30.00W	ARA03B02	2012-09-03	200
77.39.00N	157.45.00W	ARA03B04	2012-09-02	200
77.00.00N	154.00.00W	ARA03B06	2012-08-31	200
77.15.00N	157.07.50W	ARA03B07	2012-08-08	200
76.42.75N	161.51.80W	ARA03B10	2012-08-07	200
77.45.00N	165.22.50W	ARA03B12	2012-08-09	200
78.00.00N	169.30.00W	ARA03B13	2012-08-10	200
78.15.00N	173.37.50W	ARA03B14	2012-08-10	200
78.30.00N	177.45.00W	ARA03B16	2012-08-11	200
79.00.00N	174.00.00E	ARA03B18	2012-08-17	200
77.02.12N	173.18.00E	ARA03B21	2012-08-18	200
75.20.71N	173.45.96E	ARA03B23	2012-08-19	150
75.05.89N	177.12.49E	ARA03B25	2012-08-20	150
75.31.13N	178.46.90E	ARA03B27	2012-08-22	200
77.00.81N	177.21.80W	ARA03B29	2012-08-24	200
77.04.53N	172.19.62W	ARA03B30	2012-08-26	200
75.00.00N	178.00.00W	ARA03B33	2012-08-27	200

Latitude	Longitude	Station	Date	Sampling Depth (m)
75.00.00N	172.00.00W	ARA03B35	2012-08-28	200
76.36.00N	168.00.00W	ARA03B37	2012-08-30	200

Table 4.1. Continued.

Latitude	Longitude	Station	Date	Sampling Depth (m)
75.56.70N	162.56.41W	ARA03B39	2012-08-06	200
81.12.68N	172.23.98E	ARA03B42	2012-08-16	200
74.00.00N	164.00.00W	ARA03B48	2012-09-05	200
73.18.84N	166.56.52W	ARA03B50	2012-09-06	200
82.19.00N	171.35.00E	SEAICE	2012-08-14	-

Chapter 5. Biodiversity Study

Il Chan Kim[1], Hari Datta Bhattarai[1], Taikyung Kim[1], Da Sik Hwang[2] and Joung Han, Yim[1]

[1]Korea Polar Research Institute, Korea (ickim@koprr.re.kr, hari@kopri.re.kr, twkim@kopri.re.kr, jhyim@kopri.re.kr)

[2]Hanyang University, Korea (dshwang@hanyang.ac.kr)

5.1. Introduction

The Arctic Ocean, located in the Northern Hemisphere and mostly in the Arctic north polar region, is the smallest and shallowest of the world's five major oceanic divisions (Michael Pidwirny, 2006). The Arctic Ocean is unique. It is the most extreme ocean in regard to the seasonality of light and its year-round existing ice cover. Arctic seas hold a multitude of unique life forms highly adapted in their life history, ecology and physiology to the extreme and seasonal conditions of this environment. Therefore, K-POD project has collected marine organisms from Arctic Ocean for understanding of biodiversity and their metabolites, related adaptation in extreme environment.

5.2. Materials and methods

1)   Marine bacteria was sampled by CTD/Rosette at each station. Niskin bottles were used at different depths for seawater sampling

2)   Metagenome sampling used by SV filters (0.25 um) from Sea water each station

3)   Zooplankton sampling used by Bongo-net at each station

4)   Sediment sampling used by Box & Multi-Core sampler at each station

5)   Marine biology dredge was used for benthic organisms within the smooth muddy floor of the Arctic Ocean at each station

5.3. Expected result

5.3.1. Marine Bacteria

Bacteria are common inhabitants of sea water, and may contribute up to about 50% of the

total biomass within this habitat. K-POD has collected marine bacterial samples from sea water, sea ice and core (Box & Multi). K-POD was isolated marine bacteria from marine samples about 1,000 strains in MA, R2A, SZB, YPG (marine fungi), ISP4 (marine actinomyces) and ASN II (marine microalgae) media (Fig 5-1). K-POD will try to study of biodiversity and metabolic flow for understanding extreme adaptation, and to develop their metabolites as industrial applications.

5.3.2. Metagenome study

Metagenomics is the study of metagenomes, genetic material recovered directly from environmental samples. Metagenomics has the potential to advance knowledge in a wide variety of fields. It can also be applied to solve practical challenges in medicine, bioengineering, agriculture and sustainability (Challenges and Functional Applications, National Research Council, 2007). K-POD has collected the Metagenome samples from sea water sample of Arctic Ocean about 60 samples. From samples, K-POD will try to study biodiversity, useful gene and industrial applications.

5.3.3. Phytoplankton

Phytoplankton is likely the most important primary producers within Arctic Ocean, Currently 731 species have been observed in Arctic sea ice, with the majority of those common on Pan Arctic scales and in both the ice and the pelagic realms.   For the secure of genetic materials from Arctic Ocean, K-POD has collected phytoplankton and makes axenic culture, if possible.

5.3.4. Zooplankton

The information of Arctic Ocean's zooplankton and benthos are poor compared to most other northern regions. From some data, zooplankton community of Chukchi sea is characterized to Acartia *longiremis, Eurytemora affinis, Centropages abdominalis, Pseudocalanus* spp., *Podon leuckarti, Evadne nordmanni*. K-POD was collected some zooplankton by Bongo-net in Arctic Ocean, and we will try to study inner bacteria, useful gene and natural products.

5.3.5. Benthos

Very little research has been done on the benthic realms in Arctic Ocean. K-POD was collected some benthos by biological dredge in Chukchi sea (Fig 5-2), and we will try to study inner bacteria, useful gene and natural products.

5.3.6. Manganese nodules

K-POD was found MN (manganese nodules) by biological dredge work in 2012' Chukchi sea cruise.   The MN characters are black, 2-3 cm size, and crumbly stone type. From 500 m dredge, we had taken sediment soil sample of 30 x 60 x 30 cm^3, and harvested MN about 150 ea in 30 x 15 x 30 cm^3.

5.4. Summary and conclusions

K-POD project was collected various marine samples about 3,000 ea for studying of marine bacteria, metagenome, zooplankton and benthos from Chukchi sea. We will try to study biological natural product and metabolite flow in this area. And K-POD found the MN form this region, and we try to study a research plan in K-POD project.

References

Michael Pidwirny (2006). "introduction to the Oceans".*www.physicalgeography.net*. Archived from the original on 9 December 2006. Retrieved 2006-12-07. Committee on Metagenomics: Challenges and Functional Applications, National Research Council (2007). The New Science of Metagenomics: Revealing the Secrets of Our Microbial Planet" . Washington, D.C.: The National Academies Press. ISBN 0-309-10676-1

Fig 5-1. Marine bacteria from Sea water samples by various media.

Fig 5-2. Benthos form this regions
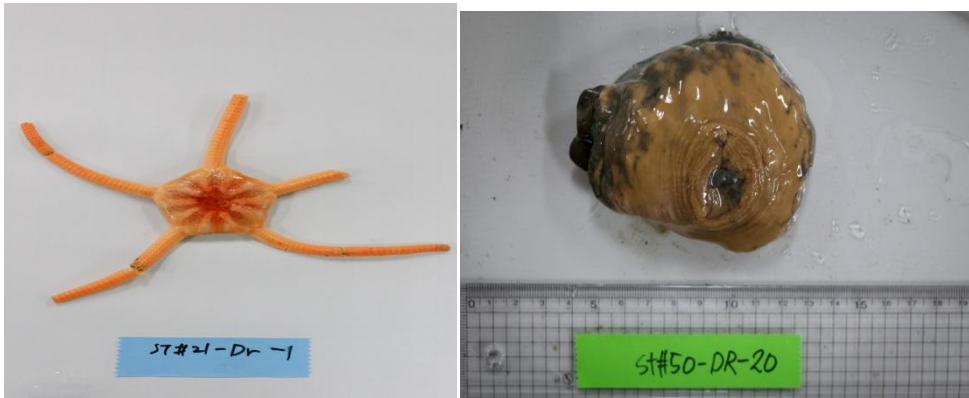
Chapter 6. Ocean Optics

Hyun-cheol Kim[1], Seungkyoem Lee[1], Jinping Zhao[2], Weibo Wang[2], Puneeta Naik[3]

[1]Korea Polar Research Institute, Incheon 406-840, Korea(kimhc@kopri.re.kr, keomnara86@kopri.re.kr)

[2]Ocean University of China, Qingdao, 266100, China (jpzhao@ouc.edu.cn, bobolufei@126.com)

[3]Louisiana State University, Baton Rouge, LA, USA (pnaik2@lsu.edu)

6.1. Introduction

Optical properties are important factors to reflect the physical processes related to the solar energy absorption and distribution in ocean and sea ice. The data of optical properties could be used to analyze the influence from biomasses, including phytoplankton and algae on the light field. Also, the light absorption and scattering will influence the heat transportation and dispersion in the ocean. On the other hand, the optical data, together with the analysis for the inherent optical property of particles in the water, could be used for calibration and validation of visible remote sensing.

In this cruise, we try to get bio-optical relationship to improve ocean color data quality by observing inherent optical properties (IOPs) of water such as absorption by phytoplankton, suspended sediment, and colored dissolved organic matters, and apparent optical properties (AOPs) of water such as downward irradiances (Ed) and upwelling radiance (Lu) over spectrum range of 350~800nm.

Our major goal in this study was to collect bio-optical data in conjunction with measurements of CDOM, phytoplankton and detrital absorption in support of NASA's efforts to develop robust empirical and semi-analytic algorithms for ocean color products in high latitude regions. This effort is part of longer strategic objective of understanding the impacts of changing climate on biological oceanographic processes in the Arctic Ocean using ocean color satellite data.

Also, we are focused our observations and researches on the area of the Chukchi Plateau, Mendeleev Abyssal Plain, Chukchi Abyssal Plain, and part of Markrov Basin, which was less

explored before. The optical properties of the ocean and sea ice in this area are linked with the water structure that might be related to the Arctic Surface Water, Pacific Water, Shelf water, and the rivers' waters. The optical properties might describe the details of the waters from variety of spectral data.

For this purpose, we prepared the instruments for apparent optical property, inherent property, fluorescence, reflectivity, and digital camera to implement the cruise. Our observations include the optical profiles, in situ measurement on sea ice, and the remote sensing by helicopter. On this chapter, we will introduce our instruments and observations, and the potential results.

The optical observations were implemented at about 40 stations as shown in Figure 6.1. The stations information is listed in Table 6.1.
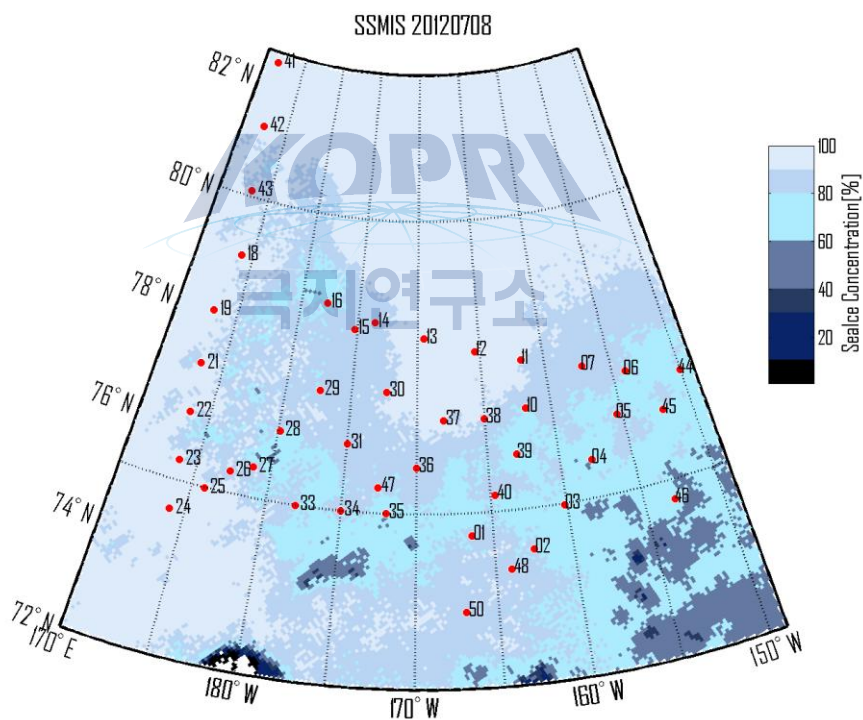

Figure.6.1.Station map for optical observation

Table.6.1. Observation stations information

| St. | Time (UTC) | Latitude (degree N) | Longitude (degree E) | HPRO | APC | | | BOP |
					ACS	PRR	CTD	
Test	08-04 04:03	73°18.03'	-166°56.29'	√	-	√	√	√
01	08-0420:36	74°37.34'	-166°23.91'	√	√	√	√	√
40	08-05 11:46	75°16.90'	-164°40.05'	-	√	√	√	√
39	08-05 22:24	75°56.60'	-162°55.94'	√	√	√	√	√
10	08-07 07:44	76°42.82'	-161°51.37'	√	√	√	√	√
07	08-08 03:09	77°15.06'	-157°08.05'	√	√	√	√	√
11	08-08 18:51	77°32.20'	-161°44.45'	√	√	√	√	√
12	08-09 07:32	77°44.77'	-165°19.61'	√	√	√	√	√
13	08-09 22:41	77°59.83'	-169°27.51'	√	√	√	√	√
14	08-10 13:26	78°14.98'	-173°34.56'	√	√	√	√	√
16	08-11 15:21	78°30.00'	-177°44.96'	√	√	√	√	√
41	08-15 09:02	82°19.79'	171°38.18'	√	√	√	√	√
42	08-16 06:02	81°12.13'	172°17.87'	√	√	√	√	√
18	08-17 06:58	78°59.73'	174°00.70'	√	√	√	√	√
19	08-17 21:28	77°57.77'	173°02.61'	√	√	√	√	√
21	08-18 17:52	77°01.82'	173°16.09'	√	√	√	√	√
22	08-19 05:57	76°11.42'	173°31.96'	√	√	√	√	√
23	08-19 17:06	75°20.70'	173°45.97'	√	√	√	√	√
24	08-20 09:47	74°30.01'	174°00.01'	-	√	√	√	-
25	08-20 21:44	75°00.00'	175°49.98'	√	√	√	√	√
26	08-21 13:40	75°22.27'	177°17.49'	-	√	√	√	√
27	08-21 22:12	75°31.25'	178°47.05'	√	√	√	√	√
28	08-22 13:26	76°13.11'	179°50.18'	-	√	√	√	√
29	08-24 19:27	77°00.34'	-177°22.22'	√	√	√	√	√
30	08-26 00:00	77°04.53'	-172°20.00'	√	√	√	√	√
31	08-26 21:05	76°08.70'	-174°56.87'	√	√	√	√	√
33	08-27 16:05	75°00.00'	-178°00.06'	√	√	√	√	√

St.	Time (UTC)	Latitude (degree N)	Longitude (degree E)	HPRO	APC			BOP
					ACS	PRR	CTD	
34	08-27 22:49	75°00.00'	-174°59.97'	-	√	√	√	√
35	08-28 13:46	74°59.98'	-172°00.00'	√	√	√	√	√
36	08-29 02:41	75°47.81'	-169°59.50'	√	√	√	√	√
37	08-30 11:23	76°36.00'	-168°00.28'	-	√	-	√	√
38	08-30 23:02	76°35.73'	-165°00.25'	√	√	√	√	√
06	08-31 17:27	76°59.77'	-153°58.97'	√	√	√	√	√
05	09-01 17:41	76°19.37'	-155°21.73'	√	√	√	√	√
04	09-02 04:27	75°39.23'	-157°45.76'	√	√	√	√	√
46	09-02 19:21	74°40.01'	-153°00.00'	√	√	√	√	√
03	09-03 09:14	74°58.56'	-160°07.85'	√	√	-	√	√
02	09-03 17:29	74°18.00'	-162°30.09'	√	√	√	√	√
48	09-05 03:31	73°59.99'	163°59.87'	√	√	√	√	√
50	09-06 03:04	73°18.83'	166°56.52'	-	√	√	√	√
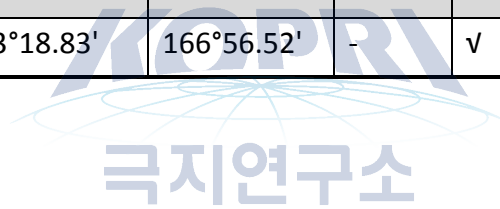
6.2. Materials and methods

6.2.1. Ocean Optical observation 1

We sampled 102 waters at 34 stations (with 3 depths of surface, subsurface chlorophyll maximum, and bottom within euphotic depth). To measure inherent optical properties (IOPs) of water, seawater volumes of 500 ml were filtered on 25mm glass-fiber filters (Whatman GF/F). For absorption by CDOM, seawater volumes of 50 ml were filtered onto disposable syringe filter unit of Advantec (cellullose acetate 0.45 um). Optical densities of total particulate matters were measured directly on the wet filters by methods of Truper and Yentch (1967) with a double-beam recording spectrophotometer of Cary100 in spectral range 350~800nm (spectrum resolution was 1nm) the filter was placed in front of a diffusing windows adjacent to an end-on photomultiplier of large surface area. For a reference blank and baseline variations, an unused wetted filter was taken as were automatically corrected. After the measurement of optical density of total pigments, the spectral absorption by nonalgal material was measured separately with method of Kishino et al.(1985). The filter was placed in absolute methyl-alchol in order to extract pigments.

For the measuring of apparent optical properties (AOPs) of water, we deployed hyper-spectroradiometer of Satlantic Inc. (HPRO II, Figure.6.2.), which is free-fall type (0.5m per second) with 350~800nm of downward irradiance (Ed) and upwelling radiance (Lu). For reference as ambient irradiance variation, downward irradiance (Es) was measured on deck, where is no shaded place of Araon. At the same time, through whole expedition we observed above water reflectance every 15 minutes by using 'Above water spectroradiometer of Satlantic Inc.(HyperSAS, Figure.6.3.)'and Sea-ice monitoring using video camera, mounted on a head of vessel to continuous monitoring of ocean color along the ship's track. This data will be used to calibration/validation currently operated remote sensed ocean color data.
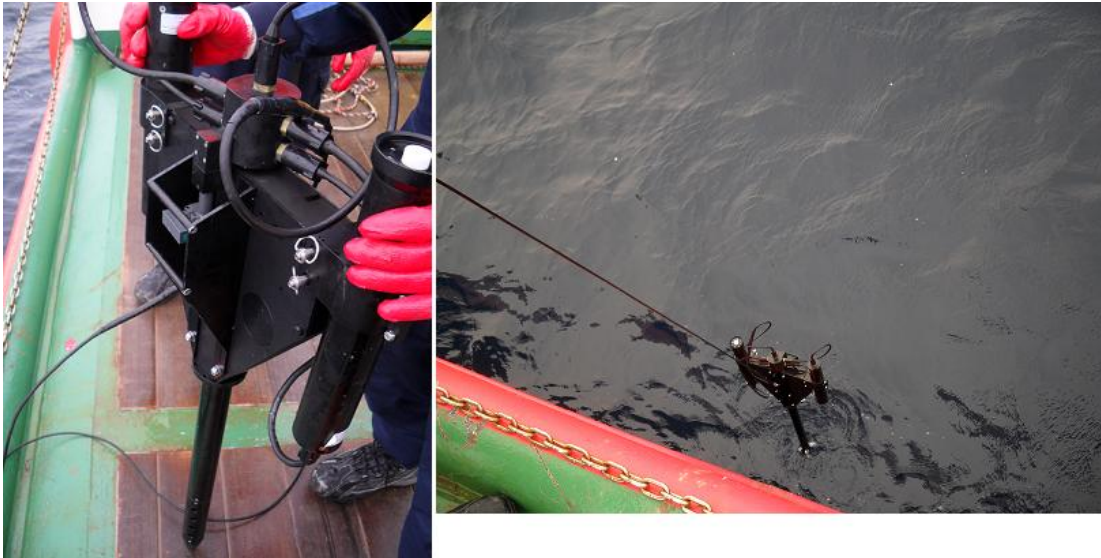
Figure.6.2. Hyper-spectroradiometer

Figure.6.3.   Above   water
spectroradiometer

Figure.6.4. PRR profiling system

6.2.2. Ocean Optical observation 2: APC

6.2.2.1. PRR800/810

The instruments used for optical observation are high resolution Profiling Reflectance

and Radiometer (PRR) made by Bio spherical Instruments Inc.(BSI, USA). The system includes both an underwater profiler PRR800 and a surface unit PRR810, which collect signals simultaneously. Both instruments are all multispectral ones with very high resolution and sensitivity, enough to detect the light in deeper water. The instrument incorporates 15 wavelengths per end standard, with the option to upgrade to as many as 19 wavelengths per end.

PRR-800/810 is a cable-linked system to collect data directly by a computer during the deployment. A unit is adopted to link PRR-800, PRR-810 and computer to control the data acquirement.

Figure.6.5.ACS system

6.2.2.2. AC-S

AC-S aims to measure absorption and beam attenuation coefficients of arctic sea water. Compared with AC-9, the AC-S offers almost an order of magnitude increasing spectral resolution. The AC-S features a proven flow-through system, compact size, and excellent stability. With 80 wavelength outputs from 400-730nm, the 4nm resolution allows for spectral "fingerprinting" and de convolution analysis. The AC-S employs a 25-cm path length for effective measurement of arctic sea water.

DH4 is mounted in the frame to provide for the simultaneous collection, storage, and merging of digital data. The BPA50, which is a non-rechargeable battery pack that provides power to support AC-S and DH4, is also mounted in the frame.

The AC-S, as its sensibleness to the environment condition, receives a special cleaning after each deployment.

6.2.2.3. MCTD (Fluorescence)

A fluorescence sensor was equipped on a Compact-CTD made by ALEC Electronics Co. Ltd (Japan). MCTD is used to measure depth, temperature, salinity, chlorophyll, and

turbidity, simultaneously. MCTD is a shelf containing system. It will start to record when the switch is turn on. The data can be replayed to computer after the cast is over.

The MCTD is integrated on the same frame with PRR and AC-S. The deployment of the system is the same as in 6.2.2.2.

6.2.2.4. Instruments deployment

A frame was designed to deploy PRR-800, AC-S and MCTD at same time. The integrated instruments deployed through the A-frame at the stern of the vessel. The deploying speed was serious limited under 0.5m/sec. In all deep stations, the profile depth reached to more than 120m. PRR 810 was mounted at the top of a crane, where the light was not shaded by any part of the ship in order to get best downwelling radiation. The whole system was rinsed with fresh water after each measurement.

Figure .6.6.The left figure shows the frame designed for deploying PRR800, ACS and MCTD; The right one shows PRR810 at the top of yellow crane

Three crew members help to conduct the optical measurement at each station. One of them operated the winch, while another1-2 members help to deploy the instrument system and watch the ice condition on deck. The two researchers are in charge of operating the logger system, and deploying and receiving the cable.
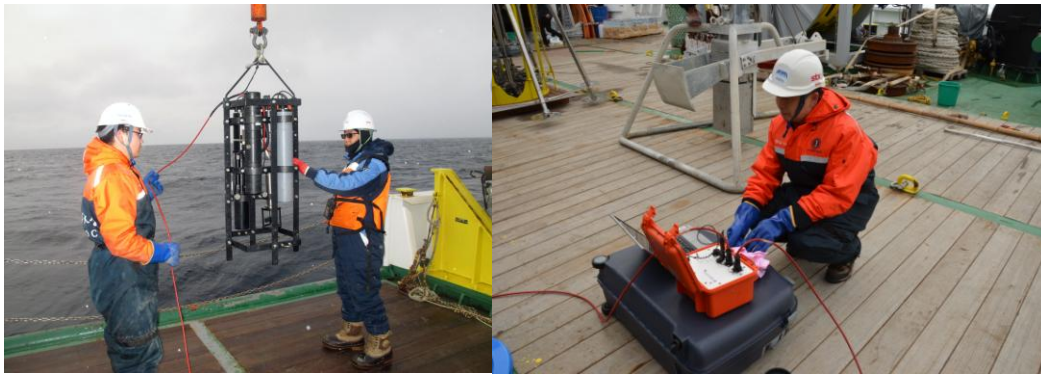
Figure.6.7.APC deployment

6.2.3. Ocean Optical observation 3: BOP

Data required to meet our project goals was acquired from three different streams: 1) Profiling with a bio-optical package 2) Underway measurements with Laser In Situ Scattering and Transmissometry (LISST-100X) and In Situ FIRe Fluorescence Induction and Relaxation System (SAFIRe), and 3) Laboratory based analysis of samples obtained from discrete depths in the water column from the CTD.

6.2.3.1.Bio-optical Profiling

A bio-optical package put together prior to this cruise was used to attain some of the core measurements required to meet our project objectives. This bio-optical profiling package comprised of the following instruments: i) CTD, ii) ECO-Triplet (WETLABS chlorophyll, CDOM fluorometer with scattering sensor), iii) ac-s (WETLABS hyperspectral absorption-attenuation meter), iv) Hyper OCI (Satlantichyperspectraldownwelling irradiance sensor), v) Hyper OCR (Satlantichyperspectral upwelling radiance sensor, and vi) VSF-3 (WETLABS three-angle, three wavelength volume scattering function meter) .

6.2.3.2.Underway measurements

Laser In Situ Scattering and Transmissometry (LISST-100X) and In Situ FIRe Fluorescence Induction and Relaxation System (SAFIRe), were serially interfaced with several ot

her instruments fitted to the ship's underway system to obtain measurements of variable fluorescence as the ship transected through different water types during the cruise. At most stations, the LISST and SAFIRe were operated in discrete mode.

6.2.3.3.Discrete stations:

At each CTD station, water samples were collected for the following measurements: 1) Spectral absorption of CDOM, 2) spectral absorption by phytoplankton and detrital particles at 3 depths: surface, chlorophyll maximum and ~20m below chlorophyll maximum.

Figure.6.8. Bio-optical Profiling

Table.6.2. Observation information

St.	Water Depth	Light condition		HPRO		APC		BOP	
		cloud	light	Obs.	Depth	Obs.	Depth	Obs.	Depth
Test	65m	10	Brightnes	√	50m	√	55m	√	75m
01	379m	10	Darkness	√	85m	√	124m	√	75m
40	618m	10	Darkness	-	-	√	111m	√	75m
39	2074m	10	Darkness	√	80m	√	127m	√	75m
10	1039m	10	Darkness	√	70m	√	83m	√	75m
07	690m	10	Brightnes	√	80m	√	76m	√	75m

St.	Water Depth	Light condition		HPRO		APC		BOP	
		cloud	light	Obs.	Depth	Obs.	Depth	Obs.	Depth
11	2711m	10	Brightnes	√	80m	√	127m	√	75m
12	480m	10	Darkness	√	60m	√	127m	√	75m
13	1250m	10	Brightnes	√	80m	√	126m	√	100m
14	1580m	10	Darkness	√	80m	√	122m	√	100m
16	1229m	10	Darkness	√	70m	√	121m	√	100m
41	1531m	10	Darkness	√	80m	√	118m	√	100m
42	2757m	10	Darkness	√	75m	√	119m	√	100m
18	2446m	10	Darkness	√	70m	√	128m	√	100m
19	1095m	-	Darkness	√	70m	√	117m	√	100m
21	642m	10	Darkness	√	30m	√	117m	√	100m
22	323m	10	Darkness	√	60m	√	128m	√	100m
23	192m	-	Darkness	√	62m	√	115m	√	100m
24	58m	10	Darkness	-	-	√	50m	-	-
25	152m	0	Brightnes	√	60m	√	131m	√	100m
26	354m	-	No sun	-	-	√	129m	√	100m
27	681m	0	Brightnes	√	70m	√	118m	√	100m
28	1196m	-	No sun	-	-	√	125m	√	100m
29	1399m	10	Brightnes	√	80m	√	130m	√	100m
30	2010m	10	Darkness	√	75m	√	130m	√	100m
31	2168m	10	Darkness	√	70m	√	124m	√	100m
33	316m	10	Darkness	√	80m	√	128m	√	100m
34	260m	10	Brightnes	-	-	√	124m	√	100m
35	377m	10	Darkness	√	70m	√	124m	√	100m
36	753m	10	Brightnes	√	70m	√	114m	√	100m
37	1779m	-	No sun	-	-	√	190m	√	100m
38	565m	5	Brightnes	√	72m	√	129m	√	100m
06	1838m	2	Brightnes	√	70m	√	121m	√	100m

St.	Water Depth	Light condition		HPRO		APC		BOP	
		cloud	light	Obs.	Depth	Obs.	Depth	Obs.	Depth
05	1025m	10	Brightnes	√	80m	√	115m	√	150m
04	912m	10	Brightnes	√	80m	√	122m	√	150m
46	3845m	1	Brightnes	√	80m	√	131m	√	200m
03	1729m	-	No sun	√	70m	√	190m	√	200m
02	1220m	5	Brightnes	√	80m	√	130m	√	150m
48	248m	9	Brightnes	√	35m	√	70m	√	150m
50	64m	10	Darkness	-	-	√	57m	√	50m

6.2.4.Melt ponds observation

6.2.4.1 Melt ponds optical observation: FieldSpec Dual VNIR

A field portable spectroradiometer is used to measure the reflectance of melt pond made by Analytical Spectral Devices, Inc. (ASD). The spectroradiometer used double direct path fiber optic input can measure two separate light components simultaneously. It has the nominal spectral range of 350-1050nm for analyzing melt pond with 1nm resolution.

A gray panel is chosen for optimizing machine and calibrating the pond's reflectance. A temporary triple was made to fix a stick which is used to stretch the target fiber above the melt pond. Through careful consideration, an 8⬜FOV (field of view) pistol is picked out in reason. On the one hand it is that pistol can determine whether the target fiber is vertical to ground. On the other hand is that the pistol has a small FOV which only receive the reflected light without noisy, for example the influence of body's shadow.

Table.6.3.Melt ponds observations

St.	Time (UTC)	Latitude (degree N)	Longitude (degree E)	Support	ASD pond	Obs.	CTD	Depth
01	8-14 18:30	82°11.89'	170°58.63'	Ship	7	26	8	√
02	8-15 18:51	82°19.60'	171°30.11'	Ship	7	18	9	√
03	8-16 4:10	81°11.87'	172°07.06'	Heli.	10	×	6	√
04	8-16 20:00	80°05.77'	172°36.38'	Heli.	10	20	6	√
05	8-17 05:08	79°00.83'	173°48.78'	Heli.	5	19	4	√

Figure.6.9. Melt pond observation

6.2.4.2 Sea ice and ponds remote sensing: Digital camera

In consideration of reliability and stability of digital camera, Canon G12 is chosen for sea ice and ponds remote sensing. It is put into a plastic cubic box beside the helicopter. In cubic box, there is much more plastic foam to protect the digital camera. Through a remote controller, the camera can be achieved whenever it is turned on and off.

Several important parameters of the digital camera listed below may be used for future research.

Table.6.4. Digital camera parameters

Manufacturing company	Canon
Model	Canon PowerShot G12
Aperture	f/8
Exposure time	1/60 s
Focal length	6mm
Format	JPEG

Table.6.5. Digital camera observations

Fli.	Time (UTC)	Last time	Latitude (N)	Longitude (E)	images	Average altitude	Camera mount
Test	8-12 07:03	8-12	79°44.77'	172°54.62'	11	200ft	Inside

Fli.	Time (UTC)	Last time	Latitude (N)	Longitude (E)	images	Average altitude	Camera mount
01	8-13 03:54	8-13	-	-	2460	-	Inside
02	8-13 10:23	8-13	-	-	2705	-	Outside
Test1	8-14 03:58	8-14	-	-	823	-	Outside
03	8-14 06:19	8-14	82°13.80'	171°06.84'	2264	2908 ft.	Outside
04	8-15 01:05	8-15	82°18.79'	171°35.48'	322	63 ft.	Outside
05	8-15 06:08	8-15	82°19.60'	171°30.11'	1757	218 ft.	Outside
06	8-16 03:54	8-16	81°12.68'	172°24.10'	1474	213 ft.	Outside
07	8-16 19:45	8-16	80°06.43'	173°10.22'	1548	187 ft.	Outside
08	8-17 04:47	8-17	78°59.98'	173°59.98'	927	203 ft.	Outside

6.3. Preliminary results (or expected results)
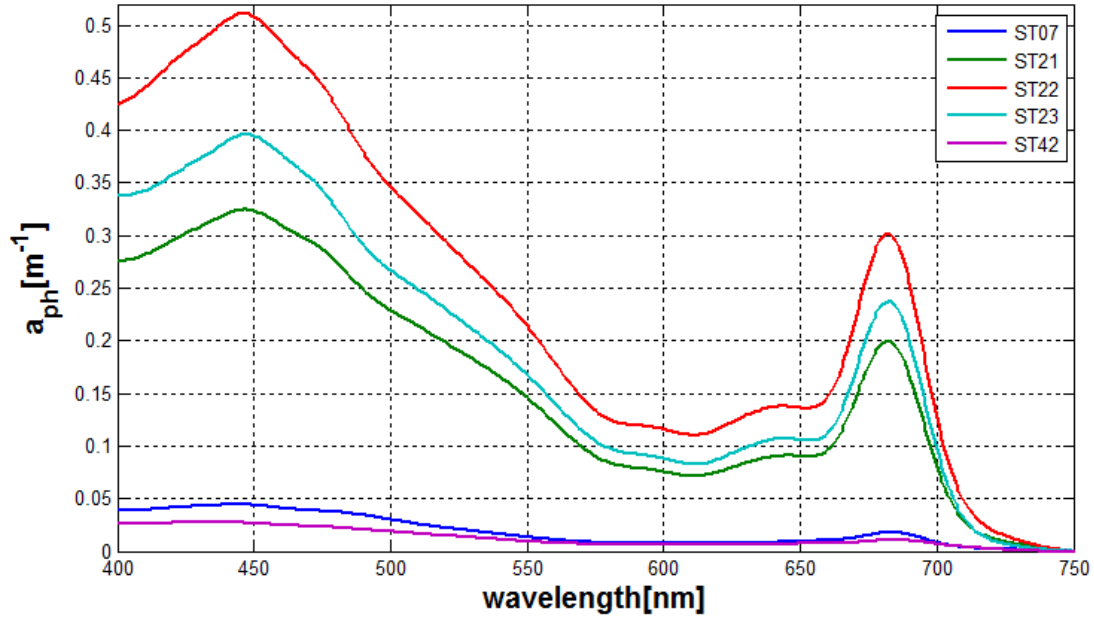
6.3.1. Ocean Optical observation 1

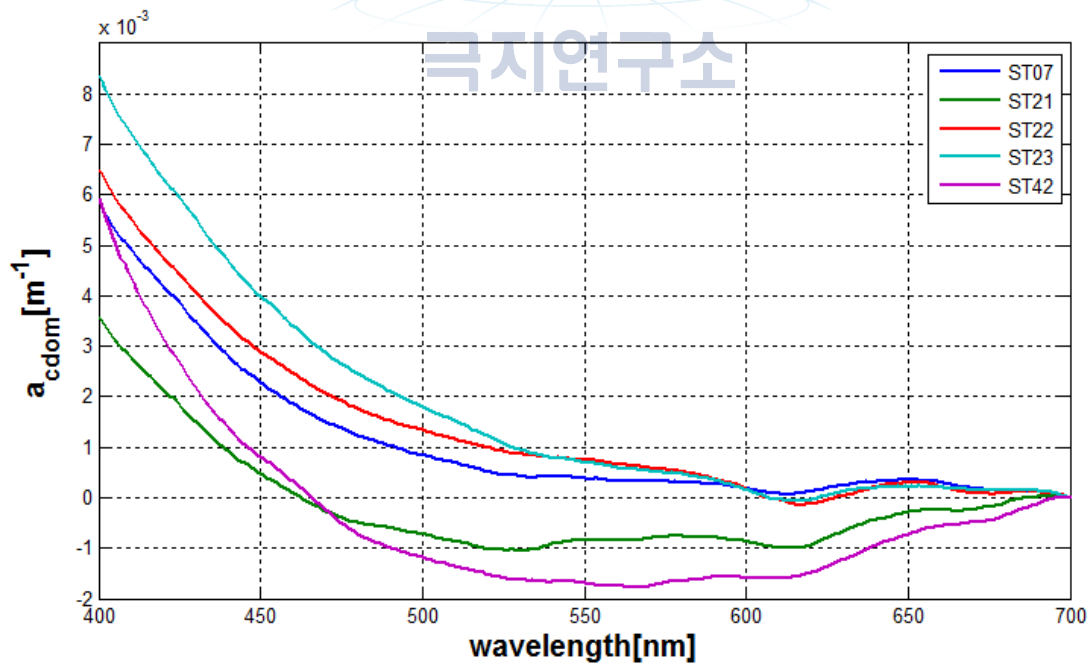Figure.6.10. Phytoplankton absorption in SCM depth (before processing)

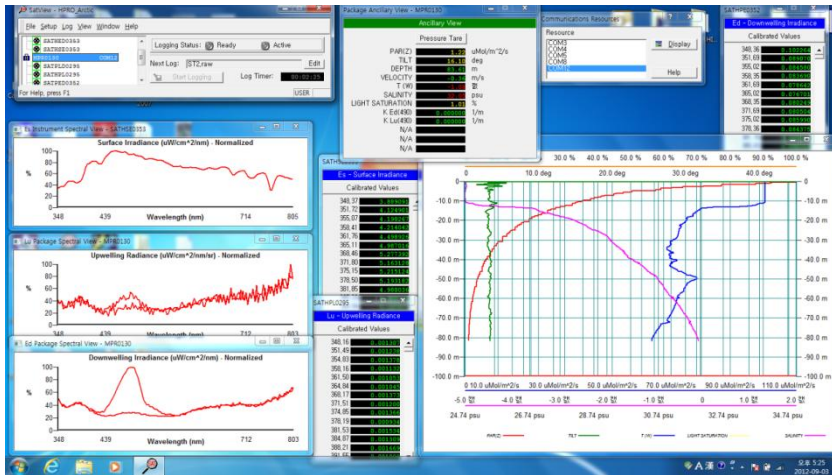Figure.6.11.Colored dissolved organic matter in SCM depth (before processing)

Figure.6.12.Example of HPROⅡ data signal

6.3.2. Spatial distribution of apparent optical property: APC

The stations of this cruise align into four north-south sections and one east-west section. The optical properties along these sections will embody the regional difference of the vertical structure. Compared with the water structure, it is possible to reveal the mechanism of influencing the light field and attenuation characteristics. To match the optical property with the fluorescence data, the connection of spectral optical property with biomasses could be built to express the impact of the primary productivity in the new open area.

A new optical parameter, the representative wavelength, will be calculated based on these data, which is used to provide an overall characteristic of spectral attenuation in the vertical profiles.

6.3.3. Spatial distribution of inherent optical property: APC

Fewer researcher focuses on the inherent optical property in Chukchi Plateau because of sea ice cover, like the absorption and attenuation coefficient of sea water. But during this year summer, great amount of sea ice are being melted all around Chukchi Plateau, and some inherent optical property is acquired by ACS simultaneously. Spatial
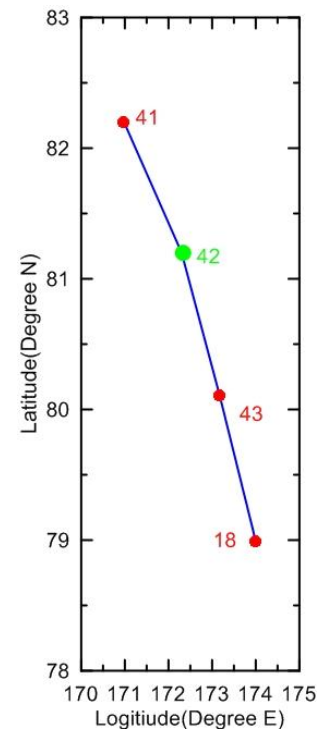
distribution of inherent optical parameters can be rendered during melting season in Chukchi Plateau. Compared with the water structure, inherent optical property is possible to build a relationship with downwellling attenuation coefficient.

Absorption and attenuation coefficient of water are very important parameters to comprehend process of heating sea water by solar radiance. Simultaneously, they may also be used to study on chlorophyll remote sensing.

6.3.4. Spectral reflectivity of ponds and its latitudinal difference: APC

During this cruise, an important section is carried out for spectral reflectivity of ponds from 82.5°N to 79°N, as shown on the right figure. In the sea section, there are four times to measure the reflectance of ponds, two times near 82.5°N, one time near 80°N and one time near 79°N respectively. At 82.5°N, melting ponds both side Araon ship have been measured. In the last two times, we used the helicopter to search and land on sea ice to measure melt pond. Many details about melt ponds in this section was recorded, like size, color, depth and covered by sea ice or not. Comparing with spectral reflectance, the connection of spectral reflectance property could be built to embody the various melt ponds with different latitude in melt reason.
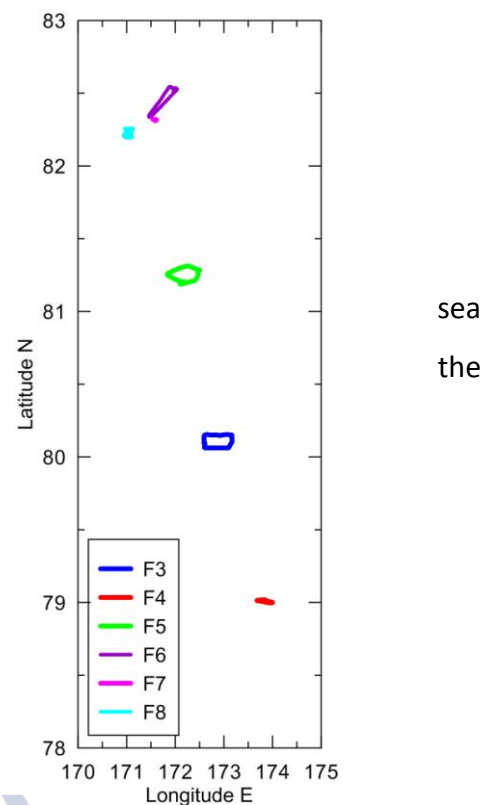
6.3.5. Sea ice concentration and broken degree and their regional difference: APC

A traditional work using digital camera is to process the image and obtain the ice concentration and coverage rate of melt ponds. With exception of these, we will use our data to reflect the latitudinal difference of the ice and ponds as the data have a good coverage from 79°N-82.5°N, as shown on the right figure.

On the other hand, we will use the data to calculate the broken degree of the sea ice, which is a new parameter to reflect the degree of sea ice floes. With this parameter, the ice

melting speed could be better estimated than only using ice concentration.

6.3.6. Ocean Optical observation 3: BOP

Current operational ocean color algorithms do not have data from the region covered in this cruise. We anticipate that the data collected in the cruise could be used to develop robust ocean color algorithms for the Arctic as well as validate ocean color measurements.
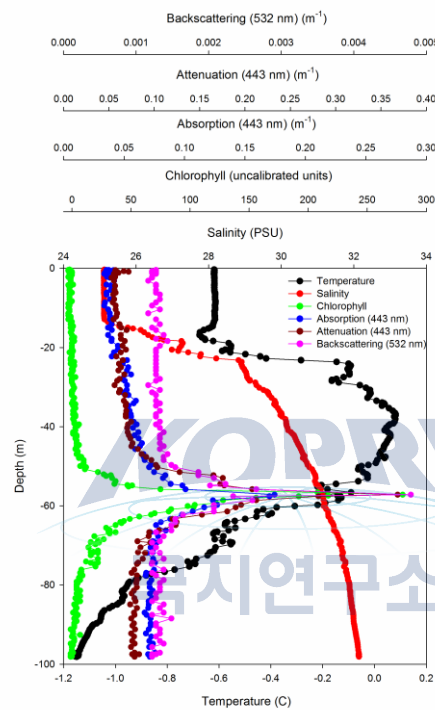

Figure.6.13. Preliminary (uncorrected) data from the Bio-optical Package (BOP) at station 37.

6.4. Summary and conclusions

All items in the observation plan have been realized during the cruise. All the instruments are carefully maintained and worked well in the cold environment and on sea ice. All the three observers worked assiduously to achieve the observational plan and the scientific goal.

This Arctic cruise is to assess the rapid changes of sea ice and calibration/validation of satellite remote sensing ocean color data. We will research using this filed data for examination and correction of satellite data.

PRR is a stable instrument system with which the irradiance has reliably been collected. The AC-S is a new equipped instrument for inherent optical property. With this instrument, along with the PRR, the apparent and inherent optical properties could be compared each other. The ASD is first time for us to use on melt ponds, which not only displays the reflectivity of the ponds, but also benefits to calculate the energy the ponds absorbed. Some of the data are firstly collected in this area, which is expected to provide us new understanding for the optical property.

Here we honestly express our appreciation to the Chief Scientist, Dr. Kang, and the other deputy scientists, Dr. Chung and Dr. Taewan Kim, for their great support to our works. And also we want to express our great appreciation to the Captain and crew for their effective works for the deployment of the instruments every day. We are very enjoyable to work on Araon for its splendid operation capacity that provides us the best observation condition and helps us to get perfect data.

6.5. Reference

Truper, H. G. and C.S. Yentsch, 1967. Use of glass fiber filters for the rapid preparation of in vivo absorption spectra of photosynthetic bacteria. J. Bact.94, 1255-1256.

Kishino, M., N. Okami, M. Takahashi, and S. Ichimura, 1986. Light utilization

efficiency and quantum yield of phytoplankton in a thermally stratified sea.

Limnol. Oceangr., 31, 557-566.

Chapter 7. Sea Ice Dynamics

Phil Hwang[1], and Bernard Hagan[1]

[1]Scottish Association for Marine Science, Dunbeg, PA37 1QA, UK (phil.hwang@sams.ac.uk; bernard.hagan@sams.ac.uk)

7.1. Introduction

Sea ice extent at the end of the summer melt season has been used as a measure of the state of the Arctic Ocean sea ice field since the beginning of the satellite record in 1979. Since then satellite observation showed the decline of sea ice extent by 12% per decade, with the minimum to date occurring in 2007. The second lowest minimum sea ice extent to date was observed in 2011, when the ice extent was slightly (ca. 7%) higher than the 2007 minimum. During that period, the Chukchi Borderland (CBL), in particular, experienced a massive decline in sea ice concentration [*NSIDC,* 2011]. Number of feedbacks and factors discussed for such variability include solar heating, advection of warm current (Pacific), warm air advection, preconditioning of thin ice and simply advection of sea ice away from the region.

Primary drive of our on-going study is to unveil feedbacks/factors controlling such massive sea ice loss in recent years. In 2011 summer, we deployed six SAMS IMBs and two SATICE buoys in the CBL region. The data from six IMBs have shown quite a contrasting sea ice bottom melting (2 cm/day vs. 5 cm/day) even though the buoys were only separated by 90 km apart. Such contrasting melting was attributed to differential ice motion and contrasting solar heating effects (radiative warming of the upper ocean by sun) near the ice edge, e.g. some buoys remained near the deployment site where large fraction of MY ice persisted, whilst the other buoys drifted into the south where sea ice concentration quickly down to zero. This creates more "heat" in the south while less "heat" available near the deployment site. It is still uncertain how horizontal/vertical advection of heat plays a role in sea ice melting. Despite interesting results last year's observations had some technical issues and also suffered from pre-mature failure of the buoys. This limits us to draw more conclusive results on differential ice melt rates and sources of heat.

This year we plan to deploy eight IMBs in the same area as we deployed last year. The technical issues have been corrected and better deployment setting has been designed to ensure longer survival of the buoys. This year we are aiming at measuring water temperatures (4-10 meter depth), more clear distinction between interface (air, snow, ice and water), and coincident hourly GPS measurements. We expect these measurements to last more six months to measure the autumn freeze-up.

The data from two SATICE buoys have shown promising results that stand-alone system can measure GPS vertical displacement with 11-cm RMS errors. Downsides of last year deployment were that the two buoys successfully transmitted only up to 30 days of the data. This summer we are planning to deploy two SATICE buoys. The basic design of the two buoys is the same as last year. However, the two systems have been more rigorously tested and better deployment set-up has been planned (e.g. anchoring the buoys on to the ice and having a camera system).

7.2. Description of buoys and satellite images

7.2.1. Description of buoys

Two SATICE buoys were designed to measure cm-scale variation in three dimensional GPS location. The buoys are also equipped with an automatic weather station, snow sounder, under ice pressure sensor, mini CT (conductivity and temperature), digital camera, and Iridium antenna (Figure 7.1).

Eight SAMS IMB buoys were equipped with a string of thermistors, GPS and Iridium antenna. Standard IMB has a 5-m long chain (240 sensors with 2-cm interval), whilst hybrid IMB has a 10-m long chain (upper 5-m for 240 sensors with 2-cm interval and bottom 5-m for 10 sensors with 50-cm interval) (Figure 7.2). 'Hot-wire' mode is used to delineate the surrounded media (i.e., air, snow, ice and water) based on different thermal conductivity of the media. The tightly spaced thermistors allow us to measure the temperature profile at higher resolution, and allow us to study the detailed thermal characteristics within snow and ice (e.g., internal melting and heat transport). It also has Iridium SBD antenna and GPS.

CRREL seasonal IMB (SIMB) is a floatable buoy to survive melt-out of the ice floe. SIMB is

engineered and owned by US ERDC-CRREL. We have been collaborating with US ERDC-CRREL last two years to deploy their SIMB. It has air temperature and barometric pressure sensors, under ice sounder (distance to the ice bottom), snow sounder (distance to the snow surface), under ice pressure sensor, and temperature string. The buoy is modular and easy to deploy in an hour.

7.3.2. Aerial survey and satellite images

Aerial photographic survey was conducted by using time-lapse camera and video system on board the helicopter. The cameras used for the aerial survey are wide-angle digital video (FOV 135 degree) and a time-lapse camera (FOV 40 degree). We planned "at least" one aerial survey at the ice station to construct mosaic image of ice station (about 6 by 4 km).

Two satellite SAR (Synthetic Aperture Radar) sensors were made available for the pre-planning purpose and the ice monitoring during this cruise; Radarsat-2 ScanSAR Wide and TerraSAR-X ScanSAR imagery. Radarsat-2 ScanSAR Wide imagery has 500-km swath but need at least two weeks of notice to order future scenes. On the other hand TerraSAR-X imagery has 100-km swath but need only 5-day notice to order future scenes.

7.3. Fieldwork summary and preliminary results

7.3.1. Ice Observation

Ice observation was often made throughout the cruise. In particular the ship went through St. 40 to 11 where rapid sea ice decline occurred during the major storm event. We recorded this major event in photos and video with visual description of ice and ocean.

7.3.2. Determining Ice Station

When we arrived at the potential ice station at St. 7 on August 7, the sea ice was mostly broken FY ice with few remaining old ice floes. Solid sea ice retreated to 80N and the wind was too strong (30 knots). It was forecasted the winds would remain strong for the next couple of days. So, we decided to move on to next station to search for the ice.

On August 9 the ice condition from passive microwave sensor showed the ice edge retreated further to 80N. There was a tongue of high ice concentration near the area of 79N and 172.2W. We decided to head up to the area after St. 16. We finished up St. 16 on August

1120 UTC and steamed to the next potential ice station.

When we arrived at 78 44'N and 172 56'W on August 12 UTC, we launched the helicopter to recon the ice condition around. We flew to the northeast in a triangle flight track about 30 km from the ship.   The ice observed from the helicopter was mainly thin FY ice and large area of open water – not ideal ice condition for the buoy deployment.   After the helicopter survey, we decided to go to the northwest (ice station) where area of high ice concentration (< 70%) was observed from the passive microwave data.

As we were approaching to the proposed waypoint, we started to see larger (continuous) ice floes – but mostly FY ice. When the ship reached at 81 40.38'N and 174 15.56'E on August 13 03 UTC, second ice recon was conducted to see ice condition along 40-km north from the ship. We decided to go further to the northwest and the ship parked in an ice floe at 82 8.33'N and 170 44.89'E. One more ice recon was conducted from that site to the north.   Ice condition remained almost the same. So, we decided to have ice station there. The ice floe at the ice station was a FY ice floe about 2-km wide with small areas of blue melt ponded ice (Figure 7.4).

7.3.4. Buoy deployment

Deployment of SATICE#3 and #4

The buoy deployment began on August 13 18 UTC (10 LT) and took about six hours for the deployment.   We deployed SATICE#3 at the Starboard side of the ship on the flat FY ice (Figure 7.5).   The ice thickness varied between 108 cm and 128 cm at the site, and freeboard (between solid ice surface and water level) varied from 4 to 7.5 cm (Table 7.1). SATICE#4 was deployed on August 14 at the Portside of the ship (Figure 7.5). Poor visibility forced us to deploy the buoy near by the ship. Ice thickness was between 100 and 106 cm which were thinner than at the Starboard side (Table 7.1).   Freeboard measurements varied from 4 to 7 cm.

Deployment of SAMS IMBs

SAMS IMB KOPRI#1 was deployed on the flat FY ice which is 5-m away from the SATICE#3 site (Figure 7.5).   Ice thickness and freeboard were close to the SATICE#3 site (Table 7.1). SAMS IMB KOPRI#8 was deployed about 20 m from the SATICE#3 site, at the edge of

depressed (snow-covered) melt ponded area (Figure 7.5).   Freeboard was very shallow (Table 7.1) and observed ice-algae when drilled the hole. SAMS IMB KOPRI#2 was deployed about 5 m from the SATICE#4 site (Figure 7.5). Ice thickness was identical to the SATICE#4 (Table 7.1). SAMS IMB KOPRI#7 was deployed about 20 m from the SATICE#4, at the edge of depressed snow-covered (closed) melt ponded area (Figure 7.5). Freeboard was very small (0.5 cm).

We tried to deploy remaining four IMBs (SAMS IMBs KOPRI#3, #4, #5 and #6) on different ice type.   As the visibility was not still ideal to fly far away, we decided to deploy the IMBs nearby the ship. KOPRI#3/#4 were deployed at the Starboard side about 150 m from the ship where we found layered ice (ridging) (Figure 7.6). When drilling the hole at the KOPRI#3 site, we felt at least one more ice layer about 100 to 150 cm depth. The ice thickness at the KOPRI#3 site was 317 cm and freeboard 37 cm (Table 7.1).   The KOPRI#4 site was selected at the edge of a small closed melt pond (Figure 7.6).   IMBs KOPRI#5/#6 were deployed on layered ice about150-m from the ship (Figure 7.6). The ice thickness at the KOPRI#5 site was thicker than at the KOPRI#6 (Table 7.1).

Deployment of CRREL SIMB

CRREL SIMB was deployed along with SATICE#3 and KOPRI#1/#8 (Figure 7.6).   Ice thickness and freeboard at the CRREL SIMB site were close to KOPRI#8 (Table 7.1).

7.3.3. Preliminary buoy results

Since the beginning of deployment on August 13, the buoy-deployed ice floe drifted to the northeast until August 16, and then it changed its direction to the northwest and drifted that direction until August 20 (Figure 7.7).   After August 20 the ice floe turned back to the southeast and now drifted to the northwest (Figure 7.7).   Primarily estimate of ice melt observed from CRREL SIMB and SAMS IMB was about 20 cm since the deployment (over 20 days) (Figure 7.8). Photographs taken at the SATICE buoys show no sign of surface melt (Figure 7.9), so the total melt observed is likely due to bottom melt.

7.3.4. Helicopter ice survey and satellite imagery

Helicopter ice survey was conducted within 6 by 4 km grid around the ship's location on

August 14 06 UTC for an hour. Helicopter waypoints were set up to have about 400 m grid spacing in "lawn mower" survey pattern to have overlapping of acquired photographs (Figure 7.7).   We kept flight altitude at about 900 m during the survey.

Satellite imagery acquired for this cruise is summarized in Table 7.2. Total 4 Radarsat-2 and 11 TerraSAR-X images were ordered so far. This summer planning satellite imagery was even more difficult due to rapid changing ice condition.

7.4. Summary and conclusions

Despite the fact that we had to go through another record minimum ice year, the deployment of the buoys was relatively successful so far. Good number of on-board ice and wave observations and satellite imagery was acquired to help us to understand rapid sea ice decline in the CBL region this summer.

Experience from this year's cruise cause us to re-think about the concept of ice buoy works. Current buoy system is non-floatable so that we could not find the suitable ice floes to deploy the buoys, as a result this summer we significantly deviated from the ship's transit line to find heavy ice in the north.   This deviation did cost the ship time but more importantly made the ice buoy works to become decoupled from major oceanographic observation within the ship's cruise track. In addition the buoys missed out all interesting processes such as rapid decline of sea ice, solar heating and intrusion of Pacific Summer Water occur in the south.   We suggest that future ice buoy system should be floatable, inexpensive and coupled with the upper ocean observations.

Table 7.1 Summary of buoy deployment

Buoy	Date (UTC)	Time (UTC)	In-situ data	Comments
SATICE#3	Aug 13	18-23h	Snow depth: 7 cm Freeboard: 6 cm Ice thickness: 120	Deployed on flat FY ice

			cm	
SATICE#4	Aug 14	17-20h	Snow depth: 9 cm Freeboard: 7 cm Ice thickness: 106 cm	Deployed on flat FY ice
SAMS IMB KOPRI#1	Aug 13	18-23h	Snow depth: 10 cm Freeboard: 7.5 cm Ice thickness: 128 cm	Deployed on flat FY ice, about 5 m from SATICE#3
SAMS IMB KOPRI#2	Aug 14	17-20h	Snow depth: 11 cm Freeboard: 8 cm Ice thickness: 106 cm	Deployed on flat FY ice, about 5 m from SATICE#4
SAMS IMB KOPRI#3	Aug 15	01-03h	Snow depth: 14 cm Freeboard: 37 cm Ice thickness: 317 cm	Layered ice
SAMS IMB KOPRI#4	Aug 15	01-03h	Ice thickness: 108 cm	At the edge of closed melt pond
SAMS IMB KOPRI#5	Aug 15	04-05h	Snow depth: 5 cm Freeboard: 30 Ice thickness: 300 cm	Layered ice
SAMS IMB KOPRI#6	Aug 15	04-05h	Snow depth: 15 cm Freeboard: 24 cm Ice thickness: 143 cm	Layered ice
SAMS IMB	Aug 14	17-20h	Snow depth: 12 cm	At the edge of depressed snow-

KOPRI#7			Freeboard: 0.5 cm Ice thickness: 101 cm	covered melt ponded area, about 20 m from SATICE#4
SAMS IMB KOPRI#8	Aug 13	18-23h	Snow depth 9.2 cm Freeboard: 1 cm Ice thickness: 107 cm	At the edge of depressed snow-covered melt ponded area, about 20 m from SATICE#3
CRREL SIMB	Aug 14	02-03h	Snow depth: 10 cm Freeboard: 7 cm Ice thickness: 109 cm	On flat FY ice

Table 7.2 Satellite imagery ordered for 2012 Araon fieldworks.

Date	Time (UTC)	Sensor/Mode	Center Lat/Lon Swath Size	Description
3/8/2012	17:48	TerraSAR-X ScanSAR	77N/153W 100 km	Pre-planning acquisition to see ice condition near potential deployment site.
6/8/2012	02:36	TerraSAR-X ScanSAR	77N/153W 100 km	Pre-ordering for potential ice station
6/8/2012	17:42	Radarsat-2 ScanSAR Wide	77N/153W 500 km	Pre-ordering for potential ice station
8/8/2012	17:57	TerraSAR-X ScanSAR	77N/153W 500 km	Pre-ordering for potential ice station
9/8/2012	17:39	TerraSAR-X ScanSAR	77N/153W 100 km	Pre-ordering for potential ice station
9/8/2012	17:39	TerraSAR-X ScanSAR	77N/157W 100 km	Pre-ordering for potential ice station
9/8/2012	17:55	Radarsat-2 ScanSAR Wide	77N/155W 500 km	Pre-ordering for potential ice station
13/8/2012	19:39	TerraSAR-X ScanSAR	79.75N/172.26W 100 km	Pre-ordering for potential ice station
14/8/2012	19:22	TerraSAR-X ScanSAR	79.75N/172.26W 100 km	Pre-ordering for potential ice station
14/8/2012	18:49	Radarsat-2 ScanSAR Wide	78.25N/173.625W 500 km	Pre-ordering for potential ice station
15/8/2012	19:05	TerraSAR-X ScanSAR	79.75N/172.26W 100 km	Pre-ordering for potential ice station

|				
16/8/2012	18:48	TerraSAR-X ScanSAR	79.75N/172.26W 100 km	Pre-ordering for potential ice station
17/8/2012	19:02	Radarsat-2 ScanSAR Wide	78.25N/173.625W 500 km	Pre-ordering for potential ice station
28/8/2012	21:39	TerrSAR-X ScanSAR	83.1N/163.5E 100 km	Capturing buoy deployed floes at Ice Station
29/8/2012	21:22	TerraSAR-X ScanSAR	83.1N/163.5E 100 km	Capturing buoy deployed floes at Ice Station
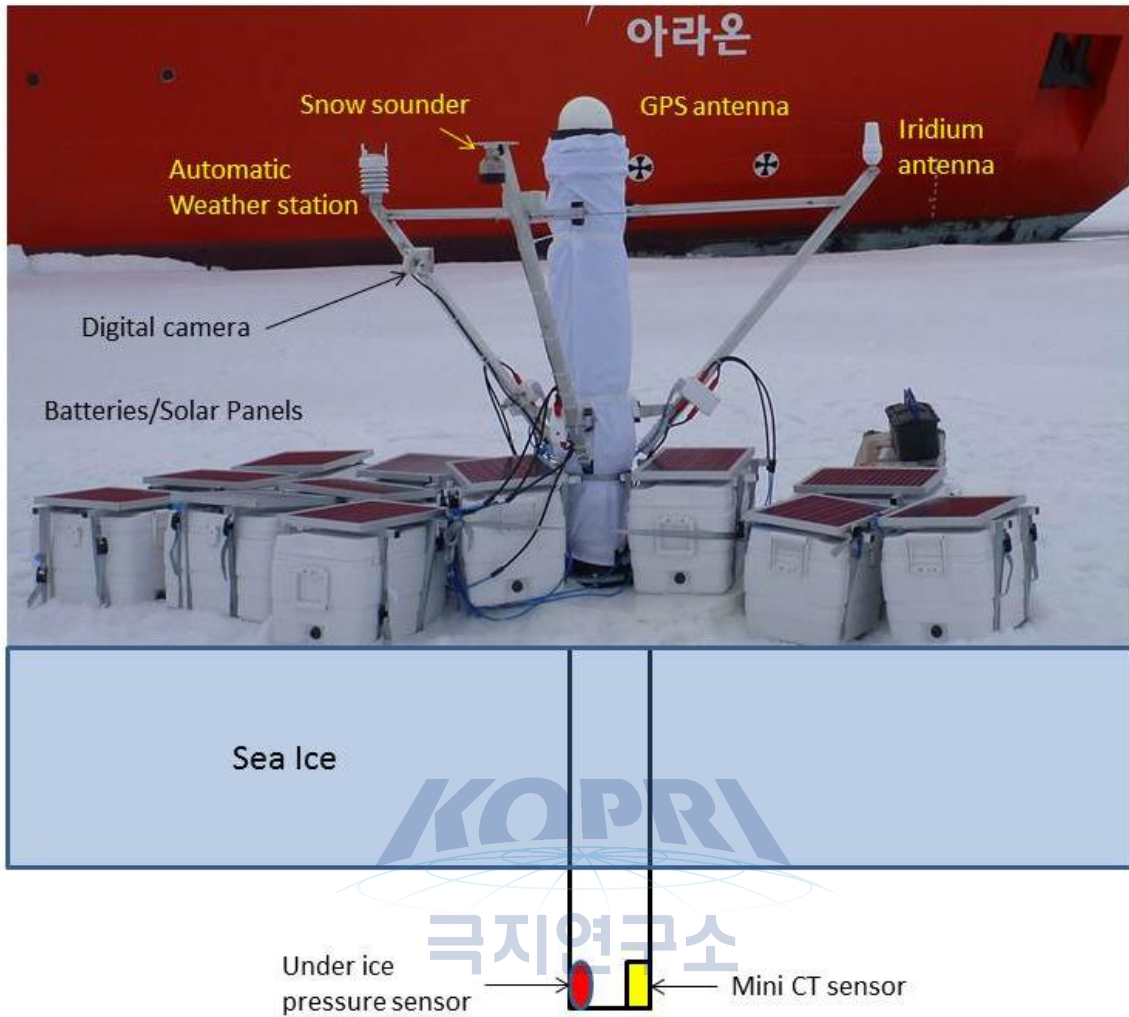
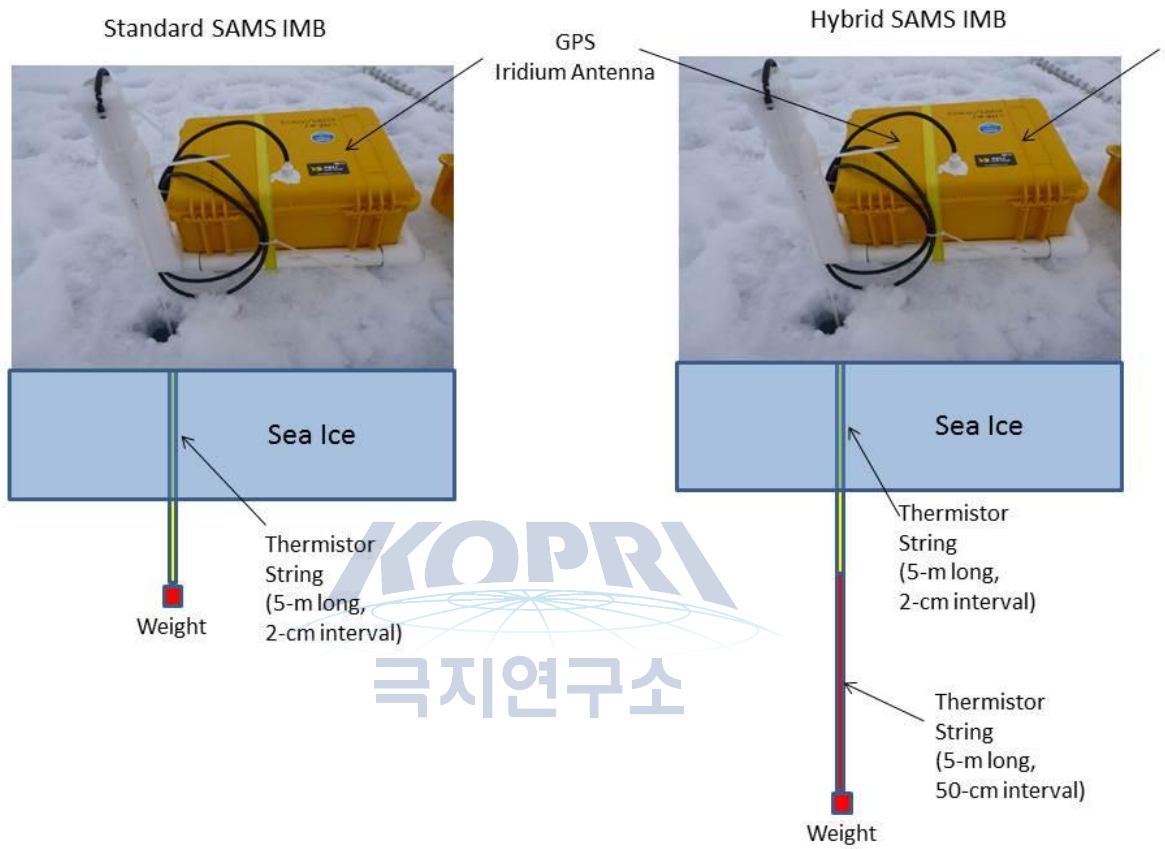**Figure 7.1 Illustrative description of SATICE buoy.**

Figure 7.2 Illustrative description of SAMS IMB buoy.
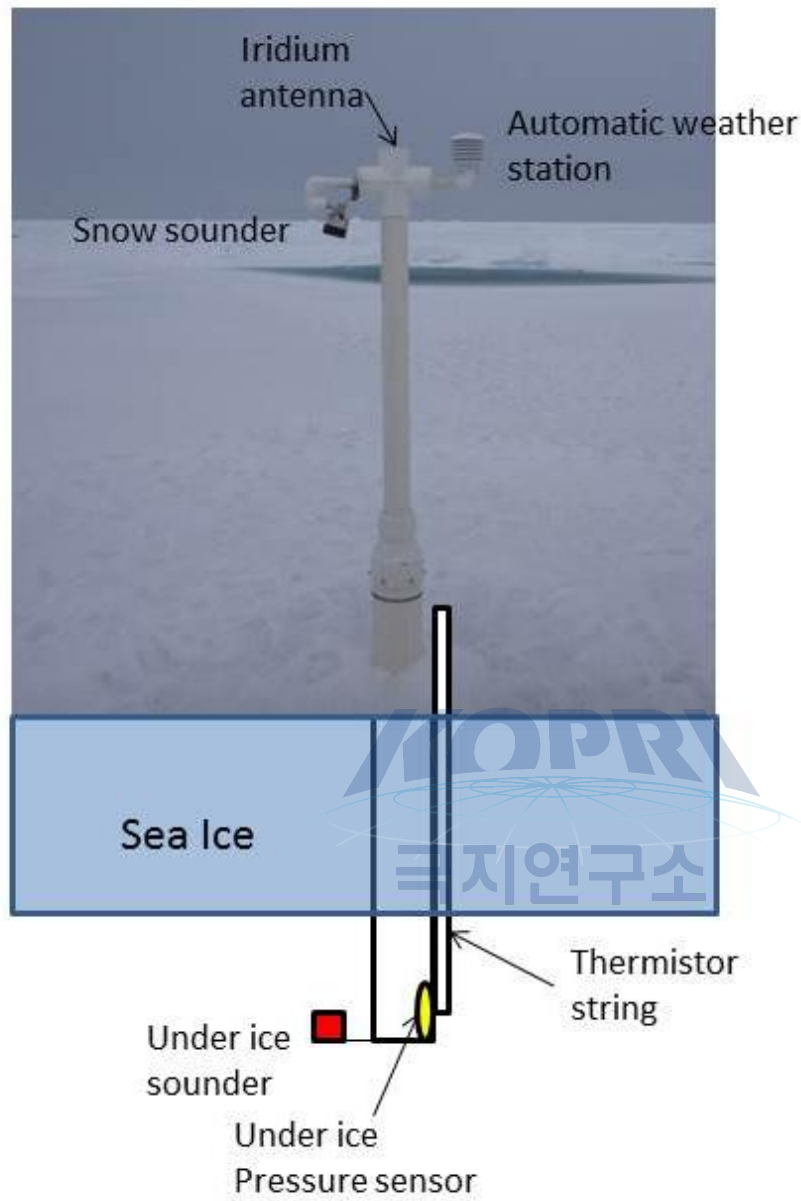
Figure 7.3 Illustrative description of SAMS IMB buoy.

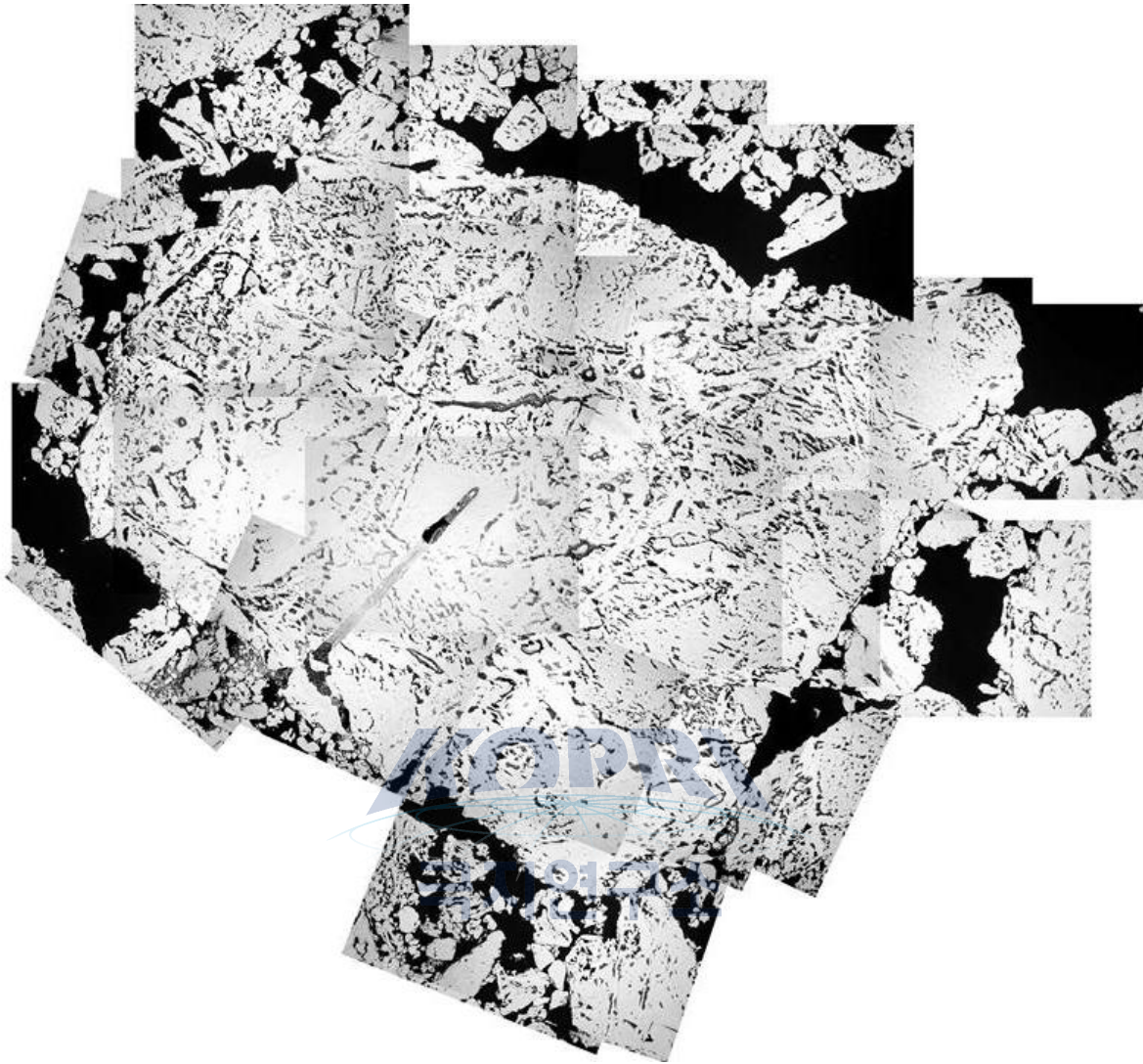**Figure 7.4. Image mosaic of helicopter photographs of ice station.**

Deployment of SATICE#3, KOPRI#1/#8 and CRREL SIMB
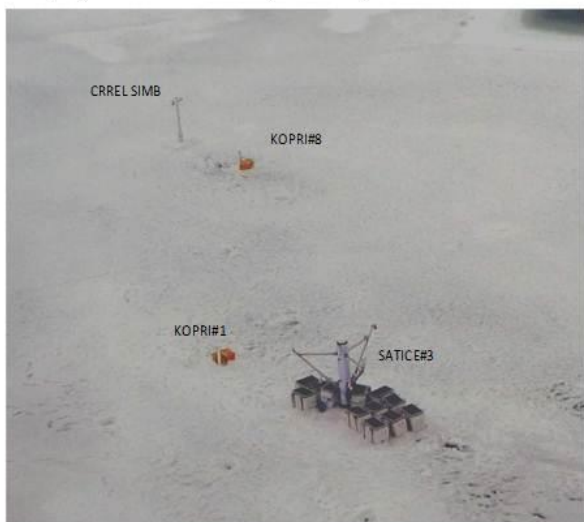
Deployment of SATICE#4 and KOPRI#2/#7

Figure 7.5. Photographs of SATICE#3/#4, SAMS IMBs KOPRI#1/#2/#7/#8, and CRREL SIMB.

Figure 7.6. A aerial view from the helicopter of the location of deployed buoys.

Figure 7.7. GPS track of the deployed buoys from August 15 to September 5.

Figure 7.8. Temporal variation of temperature profile of three selected SAMS IMBs.

SATICE#3

SATICE#4

Figure 7.9. Photographs taken at the SATICE#3 and #4 after the deployment.

Chapter 8. Geophysical Survey

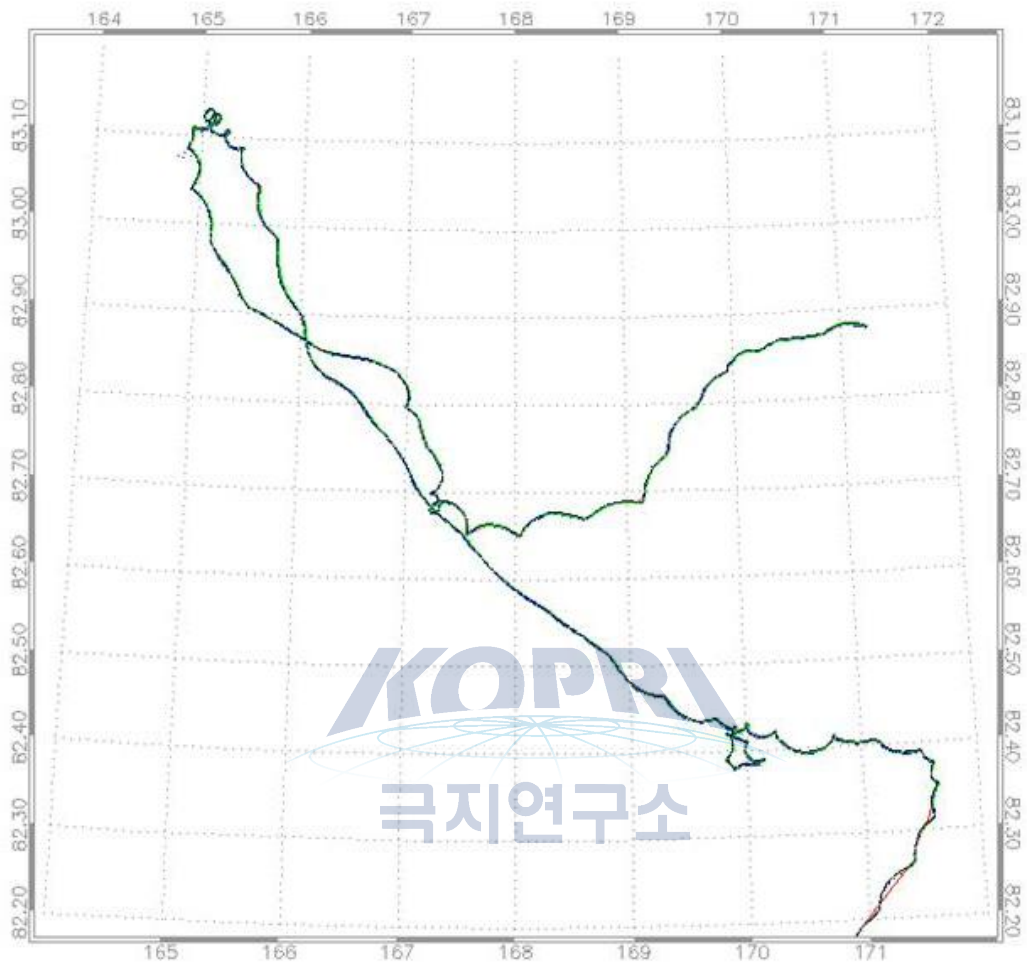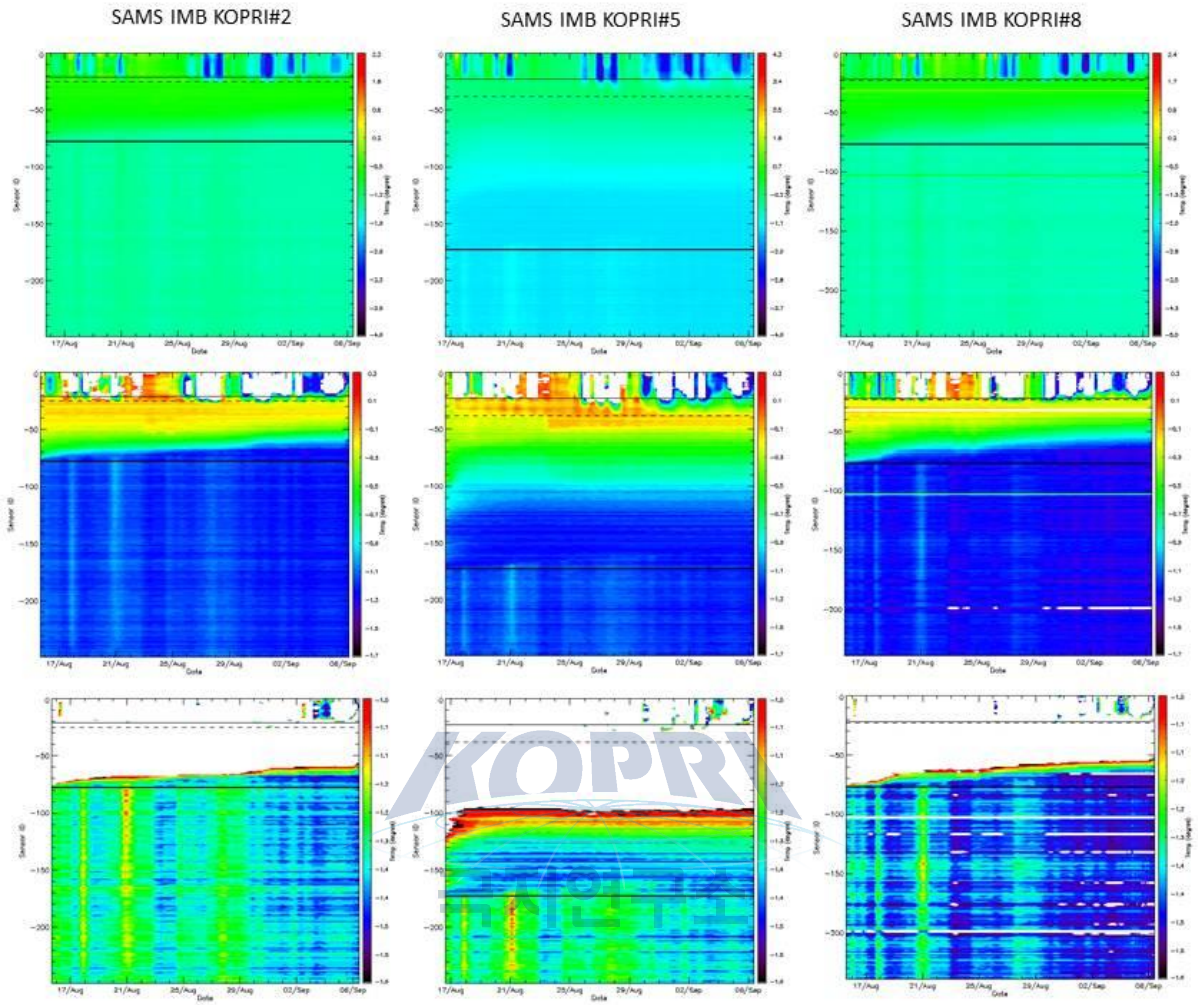Jong Kuk Hong[1], Frank Nissen[2], Dong Seob Shin[1], Hyoung Jun Kim[1], Sookwan Kim[1], Nari Seo[1]

[1]Korea Polar Research Institute, Incheon 406-840, Korea (jkhong@kopri.re.kr; dsshin@kopri.re.kr; hjkim@kopri.re.kr; skim@kopri.re.kr; snari@kopri.re.kr)

[2]Alfred Wegener Institute, Bremerhaven, Germany(frank.niessen@awi.de)

8.1. Introduction

Swath bathymetry and high-resolution reflection data (~3.5KHz) were collected during the ARA03B cruise. On the sea floating ices were not densely distributed and wind and waves were mild and calm. Because of the relatively good sea condition, we could be able to acquire geophysical data with high signal-to-noise ratio. When the ship was ramming to find a thick multi-year ice for an ice station, however, very noisy data were acquired due to the interference to the transducers by crashed ices.

The survey tracks the western part of the Arctic Ocean ranging from Mendeleev Ridge to the Northwind ridge(Fig. 8.1). Most of the Arctic Ocean is poorly surveyed(Kristoffersen and Mikkelsen, 2003) so that new findings were expected through this cruise. The aim of the geophysical survey is to reveal the subsurface feature and sedimentary structures related to the climate change and geological evolution. For this aim, we focused geophysical survey on the following topics. The topics are:

- to map subsurface structure on the unknown area
- to characterize ice sheet lineation
- to survey the distribution of pockmarks
- to examine sedimentary structure below the coring sites
- to investigate shallow sedimentary structure
- to reveal sedimentary structures related to ice ages.
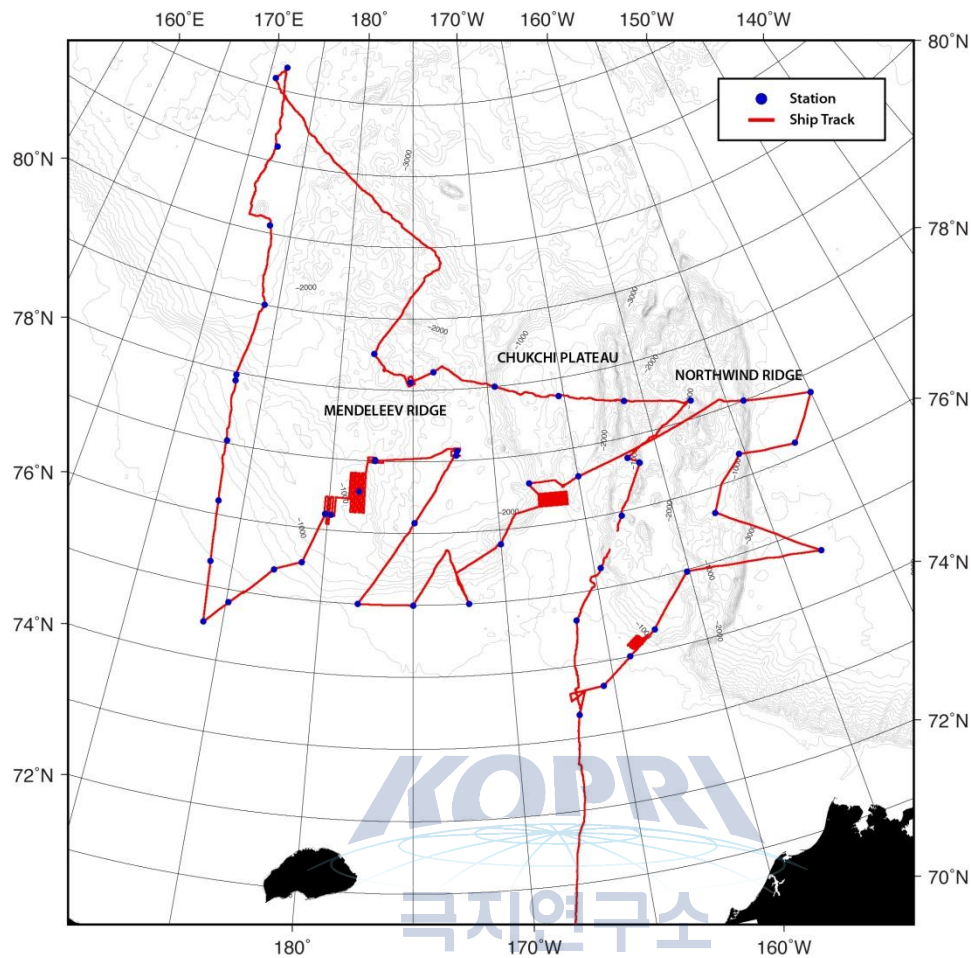
Figure 8.1 Ship track chart. Red line represents tracks for geophysical data acquisition and red closed circles represent station for geological sampling and/or oceanographic measurements.

8.2. Sub-bottom Profiling

8.2.1. SBP120 Sub-bottom profiler

The SBP120 Sub-bottom profiler installed on ARAON in 2008 is an optional extension to the highly acclaimed EM122 Multibeam echo sounder. The receive transducer array shared with the EM122 is wideband. By adding a separate low frequency transmit transducer and electronic cabinets and operator stations, the SBP 120 has a capability of the

sub-bottom profiling. The system beam width is 12 degrees with 24 transducers.

During the survey the SBP120 is synchronized by the Synchronize Unit which controls the triggering timing to reduce interference between acoustic equipment such as EM122 and ADCP. It has a much narrower beam width than a conventional sub bottom profiler with correspondingly lesser smearing. It thus provides deeper penetration into the bottom, and higher angular resolution. The frequency ranges from 2.5 to 7kHz. Its beam is electronically stabilized for roll and pitch. It can also be steered to take into account the bottom slope. The ping rate is synchronized to that of the EM122 if both are running simultaneously.

8.2.2. Data acquisition

Sub-Bottom profiling data were recorded in from the 3rd August to 5th September UTC. The data produced by the SBP120 are logged in the TOPAS raw format and can be saved in SEG-Y format for the postprocessing with a standard seismic package. During the ARA03B cruise applied system parameters are represented at Table. 8.1.

Table 8.1. System parameters of the SBP 120 during the ARA03B cruise.

Used Settings	Value	Unit
Transmit mode	Burst	2~3 depending on the depth
Synchronization	External trigger	From S.U.
Acquisition delay	Manual mode	ms
Acquisition window	400	ms
Pulse form	Linear chirp up	
Sweep low frequency	2500	Hz
Sweep high frequency	6500	Hz
Pulse shape	80	%
Pulse length	30	ms
Source power	0	dB

Beam widths Tx	Normal	
Beam widths Rx	Normal	
Number of Rx beams	1	
Beam spacing	3	1 deg
Calculate delay from depth	X	
Delay hysteresis	30	%
Bottom screen position	50	%
Automatic slope corrections	On	
Gain	36	dB
Time Variable Gain	From the bottom	
TVG control	manual	

There was recording errors which could not record for a few minutes per an hour. This recording errors might be caused by the weak capability of the computer system.   The error was fixed when we replaced the recording system to another computer since the 1st September.

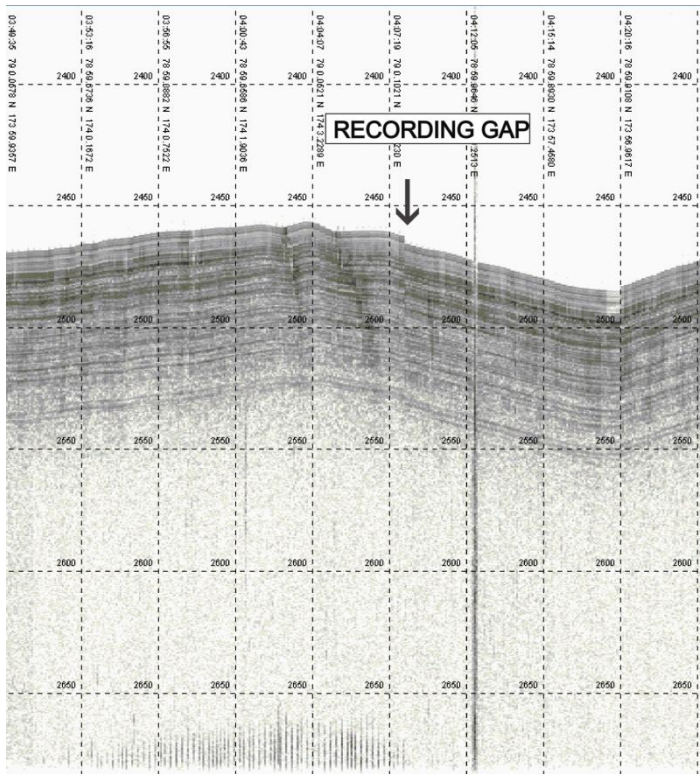**Figure 8.2. An example showing a recording gap for several minutes**

In the Arctic Ocean recording quality is strongly dependent on the sea ice condition. Fig. 8.3 shows a screen image of the recorder captured on the icy sea. No reflection was detected when the vessel passed over the ice.
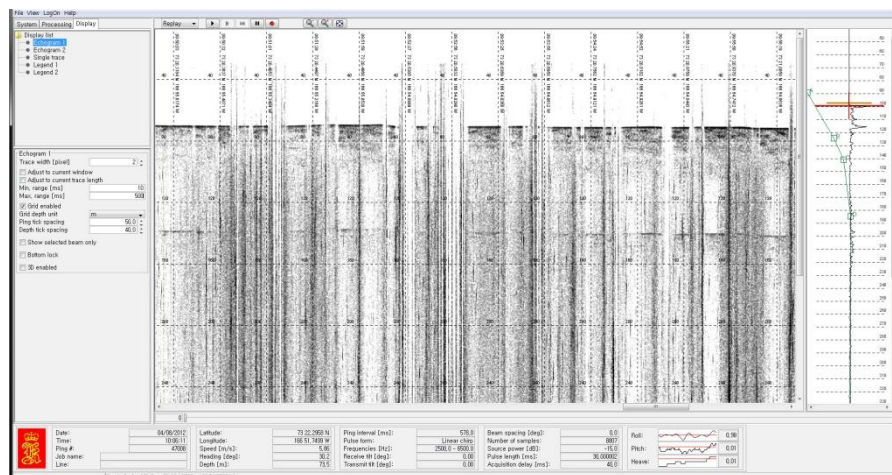

Figure 8.3. A screen image of SBP recorder when the ship sails in the ice-covered sea.

8.3. Seafloor Mapping

8.3.1. Introduction

Swath bathymetry survey was conducted utilizing EM122 multibeam echosounder. Data acquisition was continued for the whole period of the cruise and the survey area is limited to the international waters in the Arctic Ocean. Sound velocity profiles are updated frequently using the profiles obtained from CTD casting. Acquired bathymetry data were processed onboard using CARIS, a specialized bathymetry-processing software, and the results are plotted using Generic Mapping Tools(GMT) software.

The major purpose of the survey is to reveal unknown feature and to convince specific features recognized by other cruise. Results are also utilized for the site survey of geological sampling and dredge by providing the sea floor features. Some of processed data will contribute to international bathymetry data sets of International Bathymetric Chart of the Arctic Ocean(IBCAO) and General Bathymetric Chart of the Ocean (GEBCO).

We conducted detailed mapping on several specific features. These features represent pockmarks, marks by ice and morphological interest. Some of the features are already identified by previous cruises (Jokat, 2009) but need more survey for more evidences.

8.3.2. Data Acquisition

EM122 has a wide beam angle (-70 ~ 70 degrees) and a capability of measuring into the deep ocean. During the survey there were some recording errors mainly originated by supporting navigation system. This kind of errors occurred not frequently and continued only for several minutes therefore these errors are acceptable.   The technical specifications of EM122 are listed at Table. 8.2.

Table 8.2. Technical specifications of EM 122.

Operating frequency	12 kHz
Depth range	20 – 11000 m
Swath width	6 × Depth, to approx 30 km
Pulse forms	CW and FM chirp
No. of beams	432

Swath profiles per ping		1 or 2
Motion compensation	Yaw	± 10 degrees
	Pitch	± 10 degrees
	Roll	± 15 degrees
Sounding pattern		Equi-distant on bottom/equiangular
Depth resolution of soundings		1 cm
High resolution mode		High Density processing
Sidelobe suppression		-25 dB
Modular design, beamwidth		0.5 to 4 degrees

8.4. Preliminary Results

We chose several areas which show pockmarks and lineation and conducted line survey to map details. Also we crossed on a doubtful features existed in the GEBCO data set.

8.4.1. Pockmark

Many pockmarks are reported in the Chukchi ridge, however, there is little report are found in the Mendeleev Ridge(Jokat, 2009). During this cruise, many pockmarks are identified in the Mendeleev Ridge and Chukchi ridge. The size of pockmarks ranges from tens to hundreds meters in diameter. The biggest one we noticed is more 600 meters in diameter. Figure 8.4 represents one of the surface image of the pockmark.
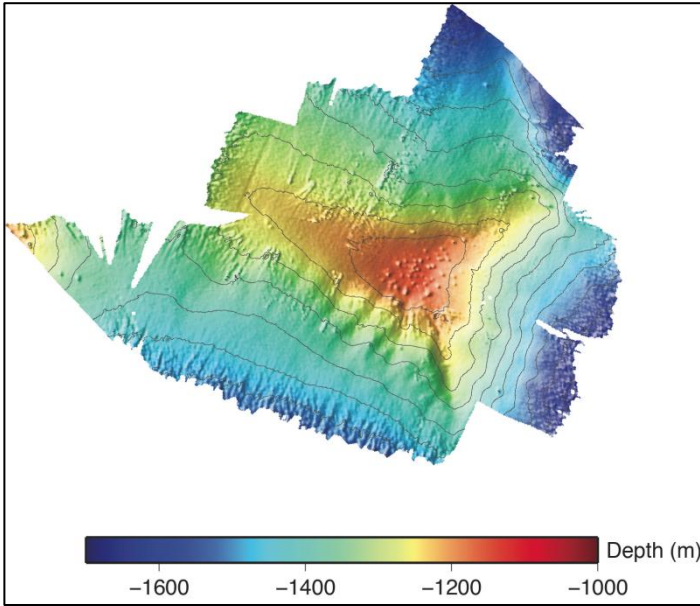
Figure 8.4. An example of seafloor image showing pockmarks.

8.4.2. Iceberg Scours

When a big iceberg is moving by wind or tide, its keel marks on the bottom. Because the wind direction may change to any ways, plow marks show random directional feature. In the Chukchi sea many plow marks made by icebergs on the continental shelf are reported(Jakobson et al., 2008) Fig.8.5 shows a seafloor feature on the Chukchi ridge. On the shallow bottom less than 360 meters many plow marks with random direction are shown. However, within the depth range of 390 ~ 410 meters, a cascade of lineation is aligned with the same direction. Origin of this lineation is different from the plow marks. It is regarded as the mark by ice sheet loaded on the seafloor in a certain ice age.
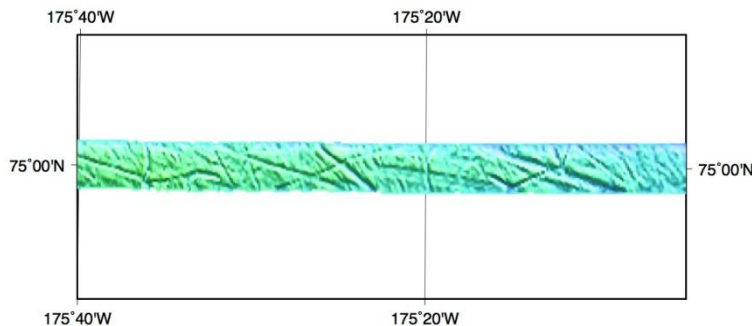
Figure 8.5. Iceberg plow marks. Plow marks are prevail on the shallow are shown in red

color.

8.4.3. Subsurface feature

The Arctic Ocean is mostly covered by ice during winter and it is very remote area from many countries and limited vessels are trying to sail over it. For these reason it is not easy to collect bathymetry data to cover the Arctic Ocean. Current bathymetry data provided by GEBCO dataset is based on previous data collected from many sounding methods. Because there is not enough data coverage in the Arctic Ocean, the dataset may include sounding errors to be corrected. Figure 8.6 shows a bathymetry map crossing an erroneous seamount revealed in the dataset. In the dataset, there is a seamount with the height of 800 meters from the bottom. However, we cannot find any evidence of the seamount. This erroneous seamount was partly surveyed during the Polarstern ARK_XXIII_3 cruise. We have a plan to combine two cruise results and to send them to the dataset provider.
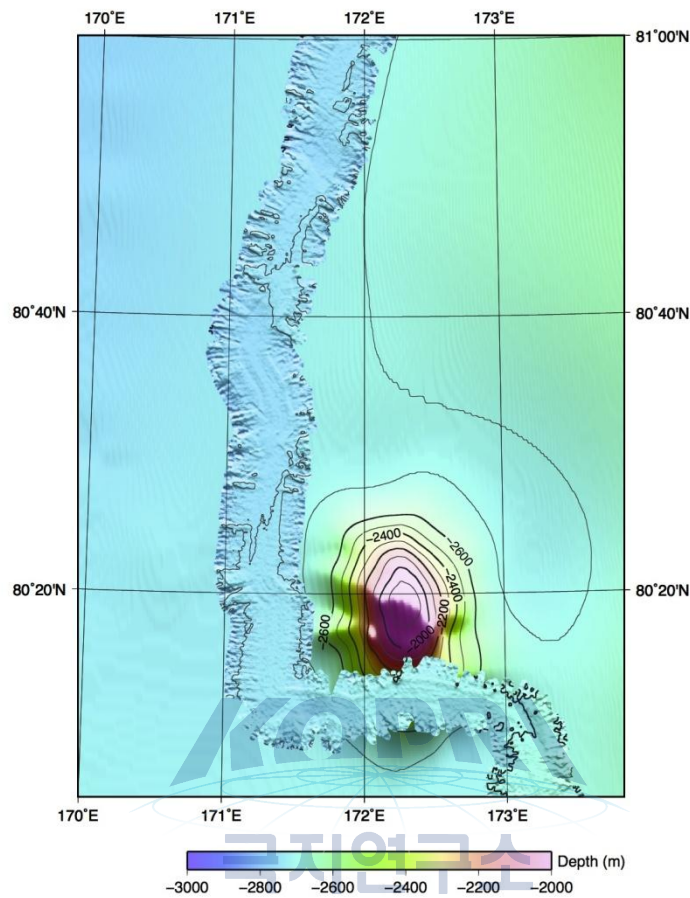
Figure 8.6. A acquired topographic image overlain on the GEBCO data set. We surveyed around a seamount shown in the data set.

References

Jakobsson, M, Polyak L., Edwards M., Kleman J., and Coakley, B. (2008) Glacial geomorphology of the Central Arctic Ocean: the Chukchi Borderland and the Lomonosov Ridge, Earth Surf. Process. Landforms 33, 526–545

Jokat, W. (2009) The Expedition of the Research Vessel "Polarstern" to the Arctic in 2008 (ARK-XXIII/3), Reports on Polar and Marine Research, 226p

Kristoffersen Y. and Mikkelsen N. (2003) Scientific drilling in the Arctic Ocean and the site survey challenge: Tectonic, paleoceanographic and climatic evolution of the Polar Basin JEODI Workshop, Copenhagen, Denmark

Chapter 9. Marine Geology

Seung-Il Nam[1], Frank Niessen[2], Masanobu Yamamoto[3], Duk-Ki Han[4], Hyo-Sun Ji[1], Heung Soo Moon[1], Young-Ju Son[1], Young Sam Sim[1], Young Jin Joe[5], Inka Schade[2] and Saskia Wassmuth[2]

[1]Korea Polar Research Institute, Incheon 406-840, Korea (sinam@kopri.re.kr)

[2]Alfred-Wegener-Institute for Polar- and Marine Research, 47568 Bremerhaven, Germany

[3]Hokkaido University, Japan (myama@ees.hokudai.ac.jp)

[4]Gwangju Institute of Science and Technology, Gwangju 500-712, Korea (dukkihan@gist.ac.kr)

[5]Jeju National University, Jeju, Korea

Introduction

Marine geology program is conducted in combination with geophysics, biomarker geochemistry and microbiology during the 3rd ARAON Arctic Expedition in 2012. Overall goal of marine geology for the 3rd ARAON Arctic cruise is to take new and undisturbed sediment cores from the selected research target areas including the Chukchi Borderland and Northwind Ridge, the Mendeleev Ridge, the East Siberian continental margin and adjacent areas in the western Arctic Ocean (Fig. 7.1). To retrieve the sediment cores at selected geological and oceanographic stations we used different coring gears such as box corer, multiple corers and gravity corer. Undisturbed surface sediments are taken by using box corer and multiple corers, whereas long sediment cores are acquired using gravity corer with 3 to 9 m long barrels. All of the retrieved sediment cores have been logged Onboard ARAON using the Multi Sensor Core Logger (MSCL) manufactured by Geotek (UK) (see details 7.2).

The collection of particulate organic matter (POM) in the water column is also one of the goals of marine geology for the establishment of organic paleo-proxies. POM samples were collected at different depths at selected 6 CTD stations by a Niskin water sampler (see details 7.3). Furthermore, a microbiology program to monitor benthic bacterial assemblages in the Arctic Ocean related to the global warming was also conducted in parallel. The aim of

this study is to understand the effects of environmental factors on the spatial distribution of marine bacteria by monitoring distributions of major phylotypes in bacterial communities in the Arctic Ocean see details 7.4).

1 Sediment coring

1.1 Introduction

Main purpose of marine geological program is to retrieve new sediment cores and then to correlate those with existed sediment cores based on preliminary core logging data such as MS, p-wave and wet density which is conducted onboard ARAON during the cruise. It is necessary to establish a precise and reliable chronostratigraphy of the recovered sediment cores in order to reconstruct glacial history and paleoceanographic changes (sea-ice coverage, brine formation, paleoproductivity in sub/surface water, origin of organic matters, etc.) in the western Arctic Ocean during the Quaternary glacial-interglacial cycles. For this study, multi-proxies such as MSCL-logging data set, XRF-core scanning data, sedimentological characteristics, stable isotopes of planktonic and benthic foraminifers, organic geochemistry (TOC, $CaCO_3$, carbon and nitrogen isotopes of bulk sediment and organic matters), biogenic opal contents, microfossils (e.g., foraminifers, pollen & spores, dinoflagellate cysts) and biomarkers will be applied in details after this expedition.

1.2 Materials and methods

Before starting the 3rd ARAON Arctic cruise (ARA03B), a total of 15 geological stations were already chosen based on data set of detailed multi-beam bathymetric mapping by Hydrosweep and shallow sub-bottom seismic profiles. It was acquired by sub-bottom Parasound acoustic profiling systems which have been conducted during the German Icebreaker "Polarstern Arctic expedition (ARK-23/3)" in 2008. The selected coring sites based on acquired data set of Parasound profiles that were provided by Dr. F. Niessen at the Alfred-Wegener-Institute for Polar- and Marine Research, Germany. In addition, the seismic survey is carried out for acquisition of shallow seismic profiles using sub-bottom profiler (SBP) system as well as for mapping of sea-floor topography using multi-beam

systems during the whole ARAON cruise. As a result, we checked the selected 15 geological stations provided by AWI based on the SBP and multi-beam data acquired during this ARAON cruise.

For recovering undisturbed sediment cores from the western Arctic Ocean, we used different coring gears. Bases on seismic data, we collected surface sediments at 15 geological stations using box corer (BOX) (30x40x60 cm) and multiple corers (MUC) with 8-7 tubes, whereas relatively long sediment cores were taken by using a gravity corer (GC) with 3 to 9 m long barrels (Fig. 7.1). In addition, we selected 9 more geological sites from the CTD stations operating for physical oceanography and marine biology. At these additional 9 stations we used multiple corers or box corer as well as gravity corer in order to collect more undisturbed surface sediments and additional long sediment cores from the western Arctic where there are still wide gaps in terms of reconstructing glacial history and paleoceanographic changes during the Quaternary. Within this context, we occasionally retrieved two gravity cores at the 7 selected same sites (Table 7.X).

8 gravity and box sediment cores including a test site (T01 GC-03) on the shallow inner shelf in the Chuckchi Sea are selected for XRF-core scanning with ITRAX Core Scanner installed in marine geology Lab Onboard ARAON. After splitting the sediment cores (archive and working parts) of the selected box cores and gravity cores, both surface sediments were photographed with a distal camera Canon 5D Mark-II. A split archive part of sediment core is used for XRF core scanning, whereas a half working part of split core is used to take slabs for soft X-radiograph. However, color of surface sediment of split core, its texture and structure, etc. will be described during the post-cruise meeting in November at KOPRI.

In general, two surface sediment cores collected with the multiple cores were sampled in slices of 1 cm interval for sedimentological, micropaleontological and organic geochemical investigation and stable isotope analysis. For sedimentological, micropaleontological (e.g., dinoflagellate, pollen and spores) and organic geochemical analyses, the sliced sediment samples are freeze-dried. Elemental analysis (total carbon, inorganic carbon and nitrogen) will be measured using CHN-Analyzer and/or IR Mass, and then calculated TOC and $CaCO_3$ contents (wt. %) and C/N ratio. Stable carbon and nitrogen isotopes of bulk sediment and organic matters will be determined using Delta Plus V Mass

spectrometer (Thermofishers, Germany) at KOPRI.

On the other hand, for stable isotope analysis and AMS ^{14}C dating, the other sliced sediment samples are sieved with a 63 μm-mesh and dried in oven with about 60℃. The dried sand fraction will be estimated with binocular microscope for hand-picked out the planktonic and benthic foraminifers, sinistral and dextral coiling species of *N. pachyderma* and *C. wuelloides*, respectively. Stable oxygen and carbon isotopes will be measured on *N. pachyderma* sin. and dex., and *C. wuelloides* with Finnigan MAT 253 at the Alfred-Wegener-Institute for Polar and Marine Research, Germany and/or at Hokkaido University, Japan. AMS ^{14}C dating of *N. pachyderma* sin. will be performed at Georgia University, USA.

1.3 Preliminary results

The sediment coring processes were carried out in the western Arctic Ocean in water depths between 57 and 2711 m. The undisturbed surface sediments were recovered with box corer and multiple corers, whereas gravity corer was used acquisition for long sediment sequences. From 24 stations, 27 long sediment cores were obtained during the 3rd ARAON Arctic Expedition (ARA03B) (Table 7.1). At several CTD stations, Box corer or Multiple corer were only used. Surface sediment samples (top to 1 cm) were taken from Box core sediments for separating living from dead benthic foraminifers stained using Rose Bengal with 70 % ethanol solution, and also investigating stable oxygen and carbon isotopes of planktonic and benthic foraminifers. The recovery of the gravity core sediments taken at 24 geological stations varied from 68 cm to 604.5 m (Table 7.6).

Table 9.1 Locations and corer types of geological stations

Date	Station	Corer type		Location		Water depth (m)
				Latitude	Longitude	
03.08.2012	T01	Box	Start	73°18'54.224'N	166°56'38.640'W	73
			Touch	-	-	-
		Multiple	Start	73°18'54.481'N	166°56'36.482'W	73
			Touch	73°18'54.485'N	166°56'36.610'W	
		Gravity	Start	73°18'54.672'N	166°56'37.968'W	67
			Touch	73°18'54.718'N	166°56'37.702'W	
04.08.2012	01	Box		74°37'26.43'N	166°23'82.01'W	377
				74°37'25.54'N	166°23'81.05'W	
		Multiple		74°37'45.61'N	166°23'23.67'W	378
				74°37'45.56'N	166°23'23.72'W	
		Gravity		74°37'45.48'N	166°23'24.05'W	379
				74°37'45.47'N	166°23'24.04'W	
06.08.2012	08	Box		76°36'55.36'N	161°12'74.64'W	2134
				76°36'55.33'N	161°12'74.72'W	
		Multiple		76°36'55.32'N	161°12'74.77'W	2129
				76°36'55.29'N	161°12'74.59'W	
		Gravity		76°36'55.28'N	161°12'74.59'W	2130
				76°36'55.30'N	161°12'74.48'W	
	09	Box		76°36'92.11'N	161°14'82.00'W	2110
				76°36'92.08'N	161°14'82.79'W	
		Multiple		76°36'90.66'N	161°14'78.86'W	2109
				76°36'90.60'N	161°14'78.80'W	
		Gravity		76°36°74.48'N	161°14'11.56'W	2117
				76°36°74.44'N	161°14'11.23'W	

07.08.2012	10	Box		76°42'75.68'N	161°51'89.70'W	1056
				76°42'75.79'N	161°51'89.49'W	
		Multiple		76°42'75.75'N	161°51'89.41'W	1056
				76°42'75.66'N	161°51'89.39'W	
		Gravity	03	76°42'75.72'N	161°51'89.43'W	1059
				76°42'75.79'N	161°51'89.44'W	
			04	76°42'75.48'N	161°51'89.53'W	1056
				76°42'75.53'N	161°51'89.50'W	
07.08.2012	07	Box		77°15'00.50'N	157°07'39.73'W	666
				77°14'99.78'N	==157°07'50.59'W==	
08.08.2012	11	Multiple		77°32'09.53'N	161°46'63.56'W	2711
				77°32'09.50'N	161°46'63.40'W	
09.08.2012	12	Box		77°45'01.23'N	165°22'49.24'W	429
				77°45'01.21'N	165°22'49.14'W	
		Multiple		77°45'01.19'N	165°22'49.14'W	429
				77°45'01.18'N	165°22'49.15'W	
	13	Multiple		78°00'01.12'N	169°30'12.03'W	1312
				78°00'01.12'N	169°30'11.96'W	
10.08.2012	14	Multiple		78°14'99.84'N	173°37'49.24'W	1592
				78°14'99.85'N	173°37'48.94'W	
	15A	Multiple		78°06'67.06'N	175°12'32.43'W	1166
				78°06'66.95'N	175°12'32.22'W	
		Gravity		78°06'66.89'N	175°12'32.10'W	1162
				78°06'66.89'N	175°12'32.13'W	
	15B	Multiple		78°06'54.19'N	==175°14'03.95'W==	1149
				78°06'54.10'N	175°14'08.58'W	
		Gravity		78°06'59.75'N	175°14'01.53'W	1149
				78°06'59.82'N	175°14'01.30'W	
11.08.2012	16	Multiple		78°29'99.63'N	177°44'98.70'W	1228

			78°29'99.65'N	177°44'98.82'W	
15.08.2012	41	Multiple	82°19'22.60'N	171°32'01.64'E	2758
			82°19'39.18'N	171°30'96.41'E	
		Gravity	82°19'21.74'N	171°34'17.26'E	2710
			82°19'22.84'N	171°33'32.45'E	
17.08.2012	18	Multiple	79°00'00.57'N	174°00'00.40'E	2452
			79°00'00.56'N	174°00'00.68'E	
	19	Box	77°58'03.41'N	173°02'24.21'E	1091
			77°58'03.51'N	173°02'21.02'E	
		Multiple	77°58'03.50'N	173°02'28.36'E	1091
			77°58'03.53'N	173°02'28.58'E	
		Gravity	03	77°58'03.57'N	173°02'28.72'E	1093
				77°58'03.52'N	173°02'28.71'E	
			04	77°58'03.51'N	173°02'28.41'E	1097
				77°58'03.53'N	173°02'28.41'E	
18.08.2012	20	Gravity	77°52'84.63'N	173°03'92.00'E	1121
			77°52'84.64'N	173°03'92.25'E	
		Box	77°52'84.67'N	173°03'92.32'E	1119
			77°52'84.65'N	173°03'92.95'E	
19.08.2012	22	Box	76°11'42.10'N	173°32'00.85'E	322
			76°11'42.08'N	173°32'00.51'E	
	23	Box	75°20'82.29'N	173°45'50.40'E	185
			75°20'82.61'N	173°45'50.67'E	
20.08.2012	24	Box-01	74°30'01.14'N	174°00'01.17'E	57
			74°30'01.02'N	174°00'01.19'E	
		Gravity	03A	74°30'00.89'N	174°00'03.14'E	57
				74°30'00.90'N	174°00'03.16'E	
				74°30'00.91'N	174°00'03.10'E	57
			03B	74°30'00.91'N	174°00'03.04'E	

21.08.2012	26	Box	76°22'27.43'N	177°17'48.51'E	354
			75°22'27.43'N	177°17'48.48'E	
		Multiple	75°22'27.43'N	177°17'48.48'E	354
			75°22'27.43'N	177°17'48.47'E	
		Gravity	75°22'27.43'N	177°17'48.39'E	354
			75°22'27.43'N	177°17'48.46'E	
	27	Box	75°31'13.75'N	178°46'93.23'E	676
			75°31'13.74'N	178°46'93.27'E	
		Multiple	75°31'13.90'N	178°46'92.34'E	678
			75°31'13.89'N	178°46'92.35'E	
		Gravity	75°31'13.83'N	178°41'95.98'E	677
			75°31'13.83'N	178°41'95.95'E	
22.08.2012	28A	Box	76°13'11.56'N	179°50'15.79'W	1177
			76°13'11.55'N	179°50'15.78'W	
		Multiple	76°13'11.55'N	179°50'15.87'W	1179
			76°13'11.51'N	179°50'15.73'W	
		Gravity	76°13'11.57'N	179°50'15.83'W	1179
			76°13'11.56'N	179°50'15.74'W	
23.08.2012	28B	Box	76°34'08.16'N	178°15'37.40'W	762
			76°34'08.32'N	178°15'37.45'W	
		Gravity	76°34'07.11'N	178°15'37.75'W	762
			76°34'07.06'N	178°15'37.90'W	
24.08.2012	29	Box	77°00'38.20'N	177°21'69.34'W	1394
			77°00'38.25'N	177°21'69.30'W	
		Multiple	77°00'38.25'N	177°21'69.28'W	1396
			77°00'38.25'N	177°21'69.27'W	
		Gravity	77°00'38.25'N	177°21'69.34'W	1395
			77°00'38.26'N	177°21'69.31'W	
25.08.2012	29A	Gravity	77°00'12.87'N	177°25'42.45'W	1428

			77°00'12.88'N	177°25'42.44'W	
		Box	77°00'12.90'N	177°25'42.39'W	1430
			77°00'12.86'N	177°25'42.38'W	
	30	Multiple	77°04'53.63'N	172°19'61.33'W	2013
			77°04'53.64'N	172°17'61.32'W	
		Gravity	77°04'53.64'N	172°19'61.33'W	2013
			77°04'53.63'N	172°19'61.31'W	
26.08.2012	30A	Gravity	77°08'39.79'N	172°14'26.03'W	1961
			77°08'39.80'N	172°14'26.02'W	
		Box	77°08'39.78'N	172°14'26.98'W	1961
			77°08'39.79'N	172°14'26.03'W	
	31	Box	76°08'66.24'N	174°54'79.11'W	2176
			76°08'66.25'N	174°54'79.01'W	
		Gravity	76°08'66.13'N	174°54'80.39'W	2180
			76°08'66.13'N	174°54'80.38'W	
28.08.2012	35A	Box	75°26'35.47'N	172°37'87.31'W	1077
			75°26'35.37'N	172°37'87.02'W	
		Gravity	75°26'35.42'N	172°37'87.04'W	1079
			75°26'35.40'N	172°37'87.06'W	
30.08.2012	38A	Multiple	76°30'03.97'N	166°00'48.00'W	952
			76°30'03.58'N	166°00'47.80'W	
		Gravity	76°30'03.71'N	166°00'48.00'W	952
			76°30'03.61'N	166°00'48.10'W	
03.09.2012	02A	Box	74°13'79.65'N	162°51'15.18'W	856
			76°13'79.67'N	162°51'15.24'W	
		Gravity	74°13'79.65'N	162°51'15.17'W	856
			74°13'79.64'N	162°51'15.24'W	
04.09.2012	02B	Box	74°08'73.76'N	163°16'29.37'W	376
			74°08'73.73'N	163°16'29.75'W	

|		Gravity	74°08'73.77'N	163°16'29.84'W	375
			74°08'73.77'N	163°16'29.66'W	

7.2.1.3.1 Box Coring

The Box corer equipped with weights of ca. 350 kg that are attached to the top of a rectangular steel tube (30*40*60 cm) have been used 24 times at 23 stations. Recovery of Box cores ranges between 17 and 50.5 cm (Table 7.2) (Fig. 7.12). From the Box corer, surface sediments and 1 or 4 sediment cores (diameter of a plastic core liner 100 cm) were taken. If necessary, box core sediments are for the following investigations;

1 core: Core description, geochemistry and micropaleontology (KOPRI)

1 core: Planktonic and benthic Foraminifers (KOPRI)

1 core: Microbiology used small diameter tube (KOPRI)

1 core: Microbiology (GIST)
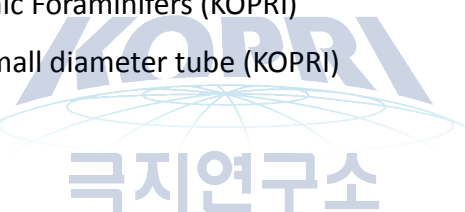
Generally, one of the selected sediment cores was split into work and archive halves. The archive half was photographed with digital camera (Canon 5D Mark-II) and will be described and photographed with spectrophotometer (Minolta) at KOPRI. One core will be used to identify the uppermost part of each gravity core which was always lost during coring process. Surface sediments will be sliced every cm for further geochemical analyses and also wet sieved through 63μm mesh and residues will be oven dried for microfossil analysis.
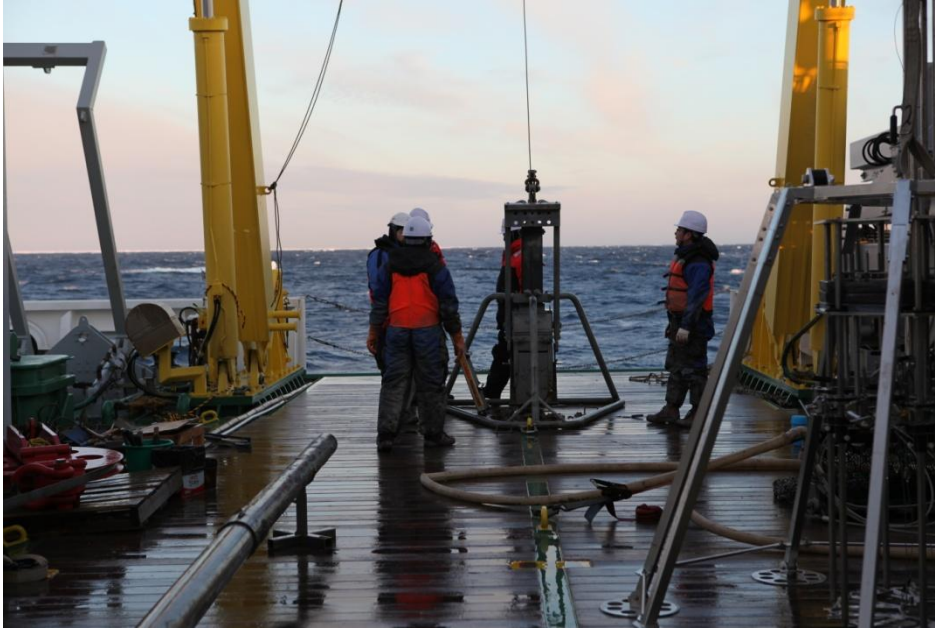
Figure 7.12 Surface sediment recovered with a box corer.

Table 7.3 Box core sampling list.

Core	Water depth (m)	Recovery (cm)	Number of sediment cores
T01Box-01	73	37.5	3
01Box-01	378	34.5	4
08Box-01	2134	43	1
09Box-03	2110	39	1
10Box-01	1056	24	1
07Box-01	666	28	1
12Box-01	429	36	1
19Box-01	1091	37	1
20Box-02	1119	A39.5/B39.5	2
22Box-02	322	A36.5/B	2
23Box-01	185	17	1
24B Box-02	57	A35/B36	2

26Box-01	354	36.5	1
27Box-01	676	37	1
28A Box-01	1177	38	1
28B Box-01	762	A41.5/B40.5	2
29Box-01	1394	A45.5/B45.5	2
29A Box-2	1430	A49.5/B50.5	2
30A Box-01	1961	A35/B32.5	2
31Box-01	2176	A39.5/B39.5	2
35A Box-01	1077	A41/B41	2
02A Box-01	856	A38/B39	2
02B Box-01	375	A41.5/B45.5	2

7.2.1.3.2 Multiple Coring

Multiple cores with 8-7 inner plastic tubes (diameter of ca. 10cm) were used 23 times at 21 stations to obtain undisturbed surface sediments and overlying bottom waters. Recovery of multiple cores ranges between 20 and 64 cm (Table 7.4) (Fig. 7.13). Multiple core sediments are for the following investigations;

1 core: Organic geochemistry and Palynology (KOPRI)

1 core: Foraminifers (KOPRI)

1 core: Biomarker (GDDTs, Lignin) (Hokkaido University, Japan)/Microbiology (GIST)

1 core: Microbiology (KOPRI)

2 cores: Biomarker etc. (AWI)

1 core: used as Box core (KOPRI)

6 sediment cores were sub-sampled in every cm interval for foraminiferal, organic geochemical and palynological analysis as well as biomarker and microbiological analysis onboard ARAON. Any stations where box core was not recovered, one sediment core from multiple cores was prepared for using box core sediment.

Figure 7.13 Surface sediment with overlying bottom water were taken with multiple corers

Table 7.4 Multiple core sampling list

Cores	Water depth (m)	Recovery (cm)	Number of sediment cores
T01 MUC-02	73	20-21	4
01 MUC-02	377	33-36	7
08 MUC-02	2129	49	6
09 MUC-02	2109	40	7
10 MUC-02	1056	21-23	7
11 MUC-02	2711	51-52	7 (1 Box core)
12 MUC-02	429	40	8 (1 Box core)
13 MUC-01	1312	51-54	7 (1 Box core)
14 MUC-02	1592	61-64	8 (1 Box core)
15A MUC-02	1162	49-54	3
15B MUC-02	1149	60	8 (1 Box core)
16 MUC-01	1228	56-57	8 (1 Box core)

41 MUC-03	2579	50-52	7 (1 Box core)
18 MUC-01	2450	52-54	7 (1 Box core)
19 MUC-02	1079	55-56	7 (1 Box core)
26 MUC-02	354	29-30	7 (1 Box core)
27 MUC-02	678	32-33	7 (1 Box core)
28A MUC-02	1179	48	7 (1 Box core)
29 MUC-02	1396	50-60	7 (1 Box core)
30 MUC-01	2013	54	7 (1 Box core)
38A MUC-01	952	54-55	7(1 Box core)

In addition, for analysis of [10]Be and Nd concentrations and its flux in the western Arctic Ocean, 2 liters of water samples were taken, respectively (Tables 7.5, 7.6) and were immediately moved to a refrigerated container. The water samples of [10]Be concentration and flux will be analyzed by Dr. K.J. Kim at KIGAM (Korea Institute of Geoscience and Mineral Resources, Korea) and Prof. Y.S. Huh at SNU, respectively. Also bottom water samples overlying the surface sediment were additionally collected in 2 liters of water samples at selected core sites.

Table 7.5 Water sampling lists for [10]Be analysis for KIGAM taken at selected CCD stations

station	Sampling water depth (m)			
10	(Surface) 0	200	700	1000
16	(Surface) 0	150	500	1220
18	(Surface) 0	100	300	2450
19	(Surface) 0	300	500	-
37	(Surface) 0 (2EA)	150 (2EA)	500 (2EA)	1783 (2EA)

Table 7.6 Water sampling lists for [10]Be and Nd analysis for KIGAM and SNU taken at selected multiple cores

Stations	Sampling water depth (m)
01	377
08	2129
10	1056
11	2711
12	429
13	1312
14	1592
15A	1162
15B	1149
16	1228
18	2450
19	1097
26	354
27	678
28	1179
29	1396
30	2013
38A	952
41	2579

7.2.1.3.3 Gravity Coring

For longer sediment cores, a gravity corer which has a penetration weight of 1.0 ton was used with barrel lengths of 3 to 9 m at 24 geological stations (Fig. 7.14). 26 gravity cores with

total recovery length of 115.94 m were retrieved at 24 selected geological stations. The recovery of the gravity corer varied from 68 to 604.5 m (Table 7.7). Gravity cores arrived on deck, they were cut into 1.5m long sections (diameter of 11.4cm) after recovery. The core sections were labeled and then stored in a refrigerated container.

Figure 7.14 Long sediment cores are recovered with a gravity corer

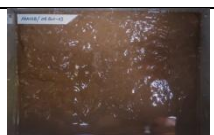**Table** 7.7 Recovery of sediments retrieved with gravity corer and length of barrel (cm)

Cores	Water depth (m)	Recovery/ Barrel length (cm)	Number of core sections
T1 GC-03	67	308/600	3
01 GC-03	379	573/600	4
08 GC-03	2160	475/900	4
09 GC-01	2117	413/900	3

10 GC-03	1059	328/600	3
10 GC-04	1056	332/600	3
15A GC-02	1162	381/600	3
15B GC-01	1149	440/600	3
41 GC-03	2759	465/600	4
19 GC-02	1093	549/900	4
19 GC-04	1097	604.5/900	4
20 GC-01	1121	446/600	3
24 GC-03A	57	68.5/300	1
24 GC-03B	57	68/300	1
26 GC-03	354	458/600	3
27 GC-03	677	466/600	3
28A GC-03	1179	572.5/900	4
28B GC-02	762	448/600	3
29 GC-03	1395	523/900	4
29A GC-01	1430	545/900	4
30 GC-02	2013	209/600	2
30A GC-01	1961	443/600	3
31 GC-02	2180	494/900	4
35A GC-02	1079	570/900	4
38A GC-02	979	541.5/900	4
02A GC-02	856	498/900	4
02B GC-02	375	364/600	3

7.2.1.3.4 Characteristics of surface sediments

Surface sediments were taken from box corer at 23 stations with water depths varying between 73 and 2,176 m. Surface sediments were photographed and then the uppermost 1 cm were sub-sampled in plastic bags for microfossils analysis and its stable isotope measurement and biomarker. The characteristics of surface sediments are summarized in Table 7.8.

Table 7.8 Characteristics of surface sediments recovered by box corer

Cores	Water depth (m)	Color and lithology		Remarks
T01 Box-01	73	Grayish mud		Soft sediment, crabs, shells
01 Box-01	378	Brownish clay mud		Soft sediment
08 Box-01	2134	Grayish brown mud		Soft sediment, some drop stones
09 Box-03	2110	Grayish brown mud		Soft sediment, some drop stones
10 Box-01	1056	Grayish brown coarse sandy mud		Winnowed sediments with high amounts of drop stones & corals
07 Box-01	666	Grayish brown sandy mud		Many drop-stones & corals
12 Box-01	429	Grayish brown sandy mud		Large-sized drop-stones, shells and corals
19 Box-01	1091	Brownish mud		Soft sediments & bioturbated surface
20 Box-02	1119	Brownish mud		Soft sediment
22 Box-02	322	Grayish brown mud		Bioturbated and benthic organisms

Cores	Water depth (m)	Color and lithology		Remarks
23 Box-01	185	Grayish brown mud		Manganese nodules
24B Box-02	57			
26 Box-01	354	Grayish brown mud		Bioturbated surface & worm tubes
27 Box-01	676	Brownish mud		Bioturbated surface with benthic foraminifers
28A Box-01	1177	Brownish mud		Bioturbated surface & some small dropstones
28B Box-01	762			
29 Box-01	1394	Brownish mud		Bioturbated surface & benthic organisms
29A Box-02	1430	Dark brown mud		Tubes & benthic organisms
30A Box-01	1961	Dark brown mud		Living mollusks for AMS dating
31 Box-01	2176	Brownish mud		Benthic foraminifers & shells
35A Box-01	1077	Brownish mud		
02A Box-01	865	Brownish mud		Benthic organisms trace
02B Box-01	375	Brownish mud		Benthic organisms trace

7.2.1.3.5 Digital Camera Photography

The split working and archive halves of both box and gravity cores were photographed by using a digital camera Canon 5D Mark II (Figures 15, 16). All the digital photographs are organized separately for each sediment core under the respective station.
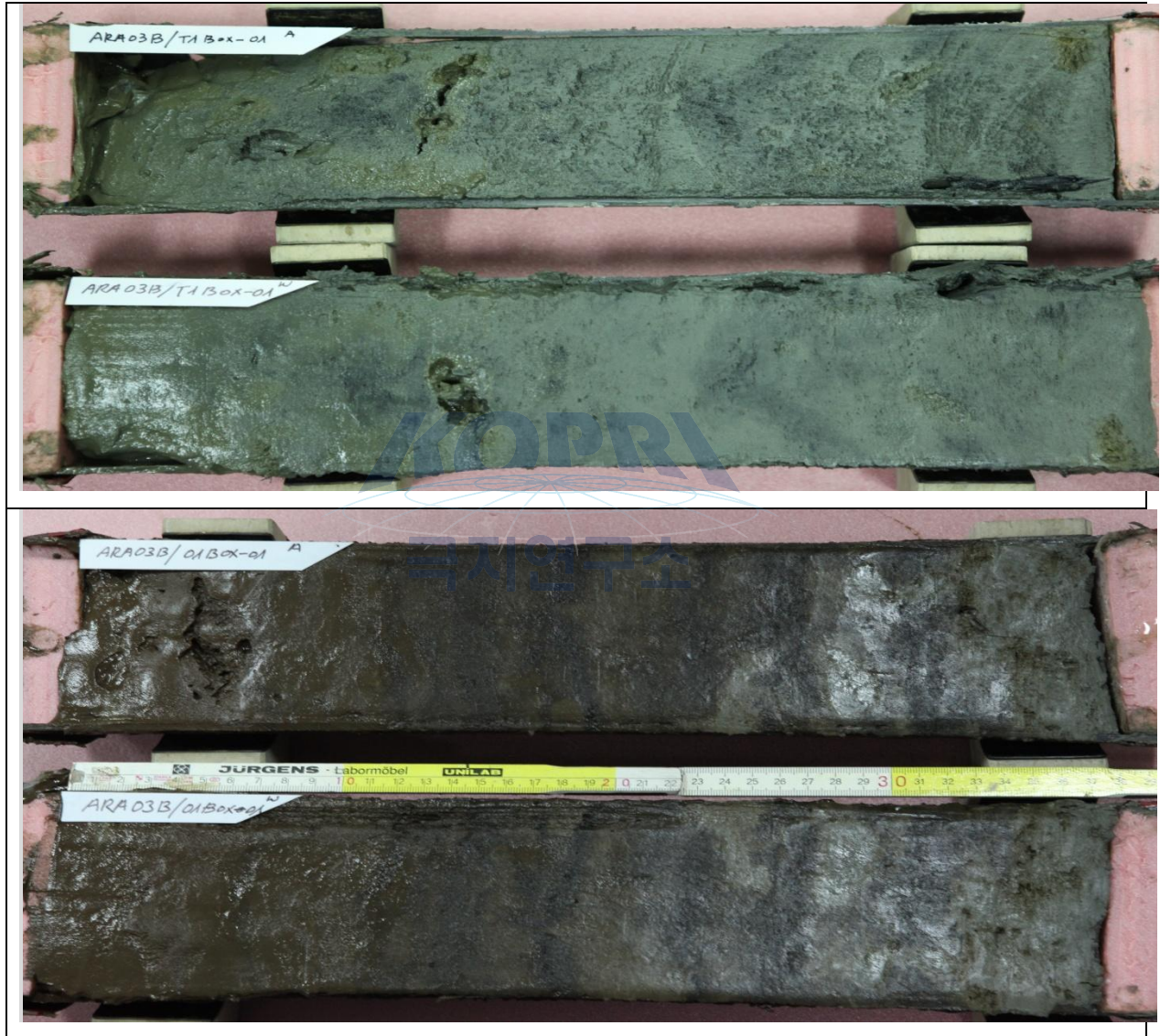

Figure 15. Digital camera (Cannon 5D Mark II) photography of split half part of box cores T01 Box-01 and 01 Box-01 taken on the shelves in the Chuckchi Sea

Figure 16. Split parts (archive and working halves) of sediment core (ARA03B/15AGC-02) recovered with gravity corer from the southeastern flank of the Mendeleev Ridge. White/pink layer is observed at upper part. Pinkish-white layer, which is an important stratigraphic marker for sediment cores from the western Arctic Ocean (Polyak et al., 2009; Stein et al., 2010), were observed in long core sediments recovered from the western Arctic Ocean.

7.2.1.3.6 **Core description**

Sedimentological characteristics will be visually described for all archive half of Box and gravity cores during a post-cruise meeting at KOPRI (Fig. 18). Colors of sediment cores will primarily be described using 'Rock-Color Chart (1991)'. Furthermore, colors of surface sediment cores (opened 8 cores) onboard were scanned by using XRF core scanner, whereas all of the closed cores will be scanned at KOPRI.

7.2.1.3.7 **ITRAX XRF core scanning of sediment cores**

8 box and gravity sediment cores (stations T1, 08, 15A, 19, 24, 28B, 29A, and 30A) were split into halves for ITRAX core scanning. The ITRAX core scanner is a new automated

multi-function core scanning instrument which has been developed that records optical, radiographic and elemental variations from split sediment cores up to 1.8 m in length at a resolution as dense as 200 μm (Croudace et al., 2006). An intense micro-X-ray beam focused through a flat capillary waveguide to irradiate samples to enable both X-radiography and X-ray fluorescence (XRF) analysis.

7.2 Core Physical Properties obtained by Multi-Sensor Core Logging

1.   Introduction

Physical properties provide initial core characterization with a very high vertical resolution. Commonly physical properties are measured on whole cores using automated multi-sensor tracks such as the Multi Sensor Core Logger (MSCL) manufactured by Geotek (UK). Physical properties can be used to define and interpret stratigraphical patterns, including a comparison with lithology and other properties such as data obtained from sediment color or XRF scanning. Physical properties are also useful to link the cores to high-resolution echosounding profiles obtained by Single-Beam-Profiling (SBP) systems, such as the SBP 120 on RV "Araon", thereby aiding the projection of core data from a single spot into larger spatial and temporal scales.

During cruise ARA03B a major goal of MSCL core logging is to provide high-resolution core records of density, sonic velocity and magnetic susceptibility. In the area of investigation, similar data were determined on cores retrieved during previous cruises such as ARA02B and ARK-XXIII/3 (RV "Polarstern", Jokat 2009). In combination with other data, down-core pattern of physical properties provide a powerful tool for lateral core correlation. The overall goal is to improve the stratigraphic framework of the Chukchi Borderland, East Siberian Sea and adjacent basins of the Arctic Ocean for a better understanding of the glacial and paleoceanographic history of the area. In this chapter we mainly describe the acquisition of the data. Apart from a few examples based on preliminary results detailed analysis and core-to-core correlation is beyond the scope of this report and will be carried out after the cruise.

2.   Methods and Data Acquisition

Measurements in the ship laboratory included non-destructive, continuous determinations of wet bulk density (WBD), P-wave velocity (Vp), magnetic susceptibility (MS) and electrical conduction (eventually convertible to non-contact electrical resistivity, NCR) at 10 mm intervals on all cores obtained during the cruise. In addition, four not yet split cores obtained during the 2011 cruise ARA02B were logged (Table xxx-Inka). A standard MSCL track (GEOTEK Ltd., UK) was used to measure temperature, core diameter, P-wave travel time, gamma-ray attenuation, MS and electrical (NCR) sensor response. The technical specifications of the MSCL system are summarized in Table xx-1. The principle of logging cores is described in more detail in the GEOTEK manual "Multi-Sensor Core Logging", which can be downloaded from the web (http://www.geotek.co.uk). The orientation of the P-wave and gamma sensors was horizontal. Gravity cores (GC) were measured in coring liners including end caps. Cores were logged in sections of 1500 mm nominal length. In the following we summarize the data acquisition of the different sensors, data conversion to standard parameters and the calculation of secondary physical properties. Plots of physical properties of all gravity cores measured during the cruise are given in Appendix xx of this report.

- Geometry: In order to convert raw data to density, velocity and volume susceptibility the geometry of the cores must be determined. For the calculation of density and velocity the core thickness along the gamma-ray beam and the direction of sound propagation, respectively, is measured at the position of the Vp transducers. The distance between the Vp transducers were calibrated using plastic cylinders of known geometry. The reference (industrial) outside diameter of the KOPRI GC liner is 115 mm. Core thickness deviation as determined by the MSCL during logging is more likely the result of core deformation between the end caps and the center of the sections rather than fluctuations of core diameters within a section. In other words, the core sections tend to be rounder near the caps and are deformed to slightly oval towards the center. Since this deformation does not change the volume of the core, we have used the reference core diameter in order to calculate volume susceptibility (see MS below) and not the core thickness as determined

between the transducers. In order to calculate core thickness between the transducers, the thickness of the liner wall is subtracted from the reference diameter of the liner plus/minus measured thickness diviation. The Geotek processing software applies the liner wall thickness as a constant. The median wall thickness of KOPRI liners was determined empirically as 2.8 mm (48 data points, maximum 3 mm, minimum 2.7 mm). Fluctuations of total wall thickness of the liners (5.6 +0.4/-0.2 mm) are not detectable by the MSCL system and add to the overall error in the data.

- Density: Wet Bulk Density (WBD) was determined from attenuation of a gamma-ray beam transmitted from a radioactive source (^{137}Cs). A collimator was used to focus the radiation through the core-centre into a gamma detector (Table xx-1). To calculate density from gamma counts, Geotek-MSCL software was used (www.geotek.co.uk), which applies a 2nd order polynomial function to describe the relationship between the natural logarithm of gamma counts per second and the product of density and thickness of the measured material. For calibration the three constants of the equation are determined empirically for each day by logging a standard core consisting of different proportions of aluminum and water as described in Best & Gunn (1999). The data of the standard stair-shaped block of aluminum logged in a liner filled with water are given in Table xx-2.

- Porosity: Fractional Porosity (FP) is the ratio of the total volume over the volume of the pores filled with water. FP determined by MSCL-logging is not an independent data-acquisition parameter but can be calculated from the WBD as follows:

FP = (dg - WBD) / (dg - dw)

where dg = grain density (2.7gcm-3);
dw = pore-water density (1.03gcm-3).

This approach makes the assumption that grain density and pore-water density are constant. In case laboratory data on grain densities of the sediments will become available

at a later stage a re-calculation of porosities may become necessary. In particular this may change the initial porosities of interglacial/interstadial deposits (such as the Holocene) as these deposits contain more organic compounds including silica which can reduce grain densities to as low as 2.4 gcm-3 (e.g. Bryant and Rack 1990).

- Temperature: Temperature (T) was measured as core-surface temperature using a non-contact infrared sensor (Tab. 2) placed 3 cm above the core as an integrated part of the MSCL device. The sensor was calibrated using water samples of known temperatures ranging from 17° to 37°C. Temperature is measured to monitor equilibration of core-temperature with laboratory temperature because some sensors are temperature sensitive.

- Velocity: Sonic Compressional Velocity (Vp) were calculated from the core diameter and travel time after subtraction of the P-wave travel time through the core liner wall (see geometry above), transducer, electronic delay, and detection offset between the first arrival and second zero-crossing of the received waveform (see GEOTEK Manual for details), where the travel time can be best detected. This travel-time offset was determined using a SL-liner filled with freshwater (Vp = 1481 m/s). P-wave velocities (Vp) were normalized to 20°C using the temperature logs. A pore-water salinity of 3.5 % was assumed. The cores were stored in the laboratory for 24 hours prior to logging in order to let the sediments equilibrate with room temperature.

$$Vp = Vpm + 3 * (20 - tm)$$

where Vpm = P-wave velocity at measured temperature;
tm = measured temperature.

- Magnetic Susceptibility (MS): MS on whole cores was measured in terms of SI units, using Bartington MS-2 meter loop sensors (Tab. xx-1). The sensor has been calibrated by Bartington and data output is MS (10^{-5}). The meter was set to zero 100 mm before the core reached the MS sensor. Sensor was checked for possible drift above the top and below the

bottom of the core by logging a 250 mm long liner filled with water as initial and final calibration piece, respectively. Any drift observed was always below 1 and remained uncorrected. In order to calculate volume-specific susceptibility data are corrected for loop-sensor and core diameter as follows:

MS (10^{-6} SI) = measured value (10^{-5} SI) / K-rel * 10

K-rel is a sensor-specific correction calculated from the diameter of the core over the diameter of the loop sensor as outlined in the Geotek MSCL manual (www.geotec.co.uk). We have used the empirical relationship of relative response to varying core and loop diameters outlined in the MSCL-Manual (www.geotec.co.uk):

K-rel = $4.8566(d/D)^2 - 3.0163(d/D) + 0.6448$

D is the diameter of the MS-2 meter core loop (140 mm) and d is the reference diameter of the core (109.4 mm, see geometry above).

- Electrical Resistivity (non-contact, NCR): The NCR technique operates by inducing a high frequency magnetic field in the core, from a transmitter coil, which in turn induces electrical currents in the core, which are inversely proportional to the resistivity. Very small magnetic fields regenerated by the electrical current are measured by a receiver coil. To measure these very small magnetic fields accurately a difference technique has been developed by Geotek, which compares the readings generated from the measuring coils to the readings from an identical set of coils operating in air. For calibration after each core logging run, we logged five 0.15 m long containers with an internal diameter close to that of the core filled with water of eventually known salinities. The recommended range of salinities includes 0.35%, 1.75%, 3.5%, 17.5% and 35%. Unfortunately, the laboratory scale was out of order on RV "Araon" so that quantitatively known salinities were not produced. We have used five different concentration of salt in distilled water of which the accurate salinities remain to be determined in the home laboratory after the cruise with post-processing of the NCR data to

follow.

Data acquisition and processing went through several steps:

1.   MSCL Raw-data acquisition of whole cores using GEOTEK software.

2.   First processing of whole-core data using GEOTEK software. This includes the calculation of core thickness, Vp, and WBD. MS and NRC sensor response remained in raw-data state (10^{-5} SI and mV, respectively).

3.   Second processing of whole-core data using software Kaleidagraph ™. This includes a data quality control on calibration sections logged on top and below the bottom of the core (250 mm liner filled with water) and a removal of these data from the core. It also includes the removal of the liner caps from the depth scale and data cleaning for effects caused by liner caps on Vp, WBD and NCR. In addition, MS is converted to volume MS and the fractional porosity is calculated from the WBD data.

4.   Plotting of core data using PANGAEA Panplot software.

3.   **Preliminary Results and Conclusions**

MS and WBD logs provide nearly complete records in all cores. Thus these parameters offer a good database for core correlation. Minor gaps of data are at or near the end caps of the liner sections. NCR data are largely affected by the end of core sections and were deleted where sensor data drop exponentially to zero.Vp data have gaps of up to 10% mostly because sound propagation was not always possible through the core for reasons not yet known. In most cases, cross-correlations of data pairs of FP and Vp exhibit a negative correlation suggesting a   relationship of a second order polynomial functions (Fig. xx-1). If determined for each individual core these functions can be used to calculate missing Vp data from porosity. Data from cores of Holocene age are an exception as they clearly plot outside the above correlation. The reason and its possible diagnostic use still need to be examined. One likely possibility is that some Holocene deposits contain significant amounts of diatomite frustules. High concentrations of diatoms in sediments can reverse the relationship of FP and Vp so that Vp increase with diatom content despite further increase in porosity (e.g. Weber et al. 1997).

All of the logged cores exhibit distinct fluctuations of physical properties with depth below sea-floor. In the area of investigation, data from the cruise ARK-XXIII/3 indicate a good correlation of WBD with core color. In particular, distinct brown layers are often associated with a significant drop in WBD (increased FP). Pink and pink-white layers function as prominent marker horizons in sediments from the central Arctic Ocean including the Chukchi Borderland and the Mendeleev Ridge (Stein et al. 2010a, 2010b and Matthiessen et al. 2010). These layers are usually marked by increased values of MS and WBD. We have found very similar down-core pattern of physical properties in cores of the expedition ARA03B. Certain pattern of down-core fluctuations become clearer to be correlated if combined plots of MS and WBD are used. Some pattern become distinct diagnostic features for stratigraphic characterization (Fig. xx-2). This includes intervals with strong positive and negative correlations of WBD and MS as well as gradients in one parameter crossing peaks in the other. For example, brown layers labeled as B2 (or B2B, Stein et al. 2010a, 2010b) have a distinct minimum in WBD. This peak correlates with a down-core gradient in MS from higher to lower values. Others, like layer B5 exhibit a clear anti-correlation of WBD and MS with the latter always increased and the former decreased (Fig. xx-2). This suggests a powerful tool for core-correlation not only from one area to the other but also between data obtained during different cruises. The number of cores and the acquired logging data will strongly improve the stratigraphy in the region under investigating thereby constraining the chronology of the glacial and paloceanographic history.

P-wave velocity and core diameter
Plate-transducer diameter: 40 mm
Transmitter pulse frequency: 500 kHz
Pulse repetition rate: 1 kHz
Received pulse resolution: 50 ns
Gate: 5000
Delay: 0 s
Density
Gamma ray source: Cs-137 (1983)
Activity: 356 Mbq (1983)
Energy: 0.662 MeV
Collimator diameter: 5.0 mm
Gamma detector: Gammasearch2, Model SD302D, Ser. Nr. 3043 , John Count Scientific Ltd., 10 s   counting time
Temperature
Infrared Sensor: MICRON M50-1C-06-L
Range: -20° - 300° C
Output Voltage: 10 mV
Electrical Resistivity
Sensor Type: Geotek
Principle: Magnetic Induction
Detection Range: 0.1-10 Ωm
Resolution: approx. 20 mm
Magnetic susceptibility
Loop sensor: BARTINGTON MS-2C
Loop sensor diameter: 14 cm
Alternating field frequency: 565 Hz, counting time 10 s, precision $0.1 * 10^{-5}$ (SI)
Magnetic field intensity: ca.   80 A/m RMS
Counting time: 10 s

Table 1: Technical specifications of the GEOTEK MSCL-25 used during ARA03B

Aluminum Thickness (cm)	Average Density (g/cm^3)	Average Density * Thickness (g/cm^2)
6.58	2.027	22.17
5.76	1.899	20.77
4.93	1.769	19.35
4.12	1.642	17.96
3.29	1.512	16.54
2.48	1.386	15.16
1.65	1.256	13.74
0.93	1.144	12.51
0.00	0.998	10.92

Table 2: Thickness and density of Gamma Attenuation Calibration Liner filled with stair-shaped block of aluminum in water. Density of aluminum: 2.71 g/cm3, density of water: 0.998 g/cm3, internal liner thickness along gamma ray: 104.9 mm
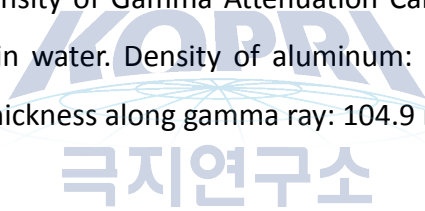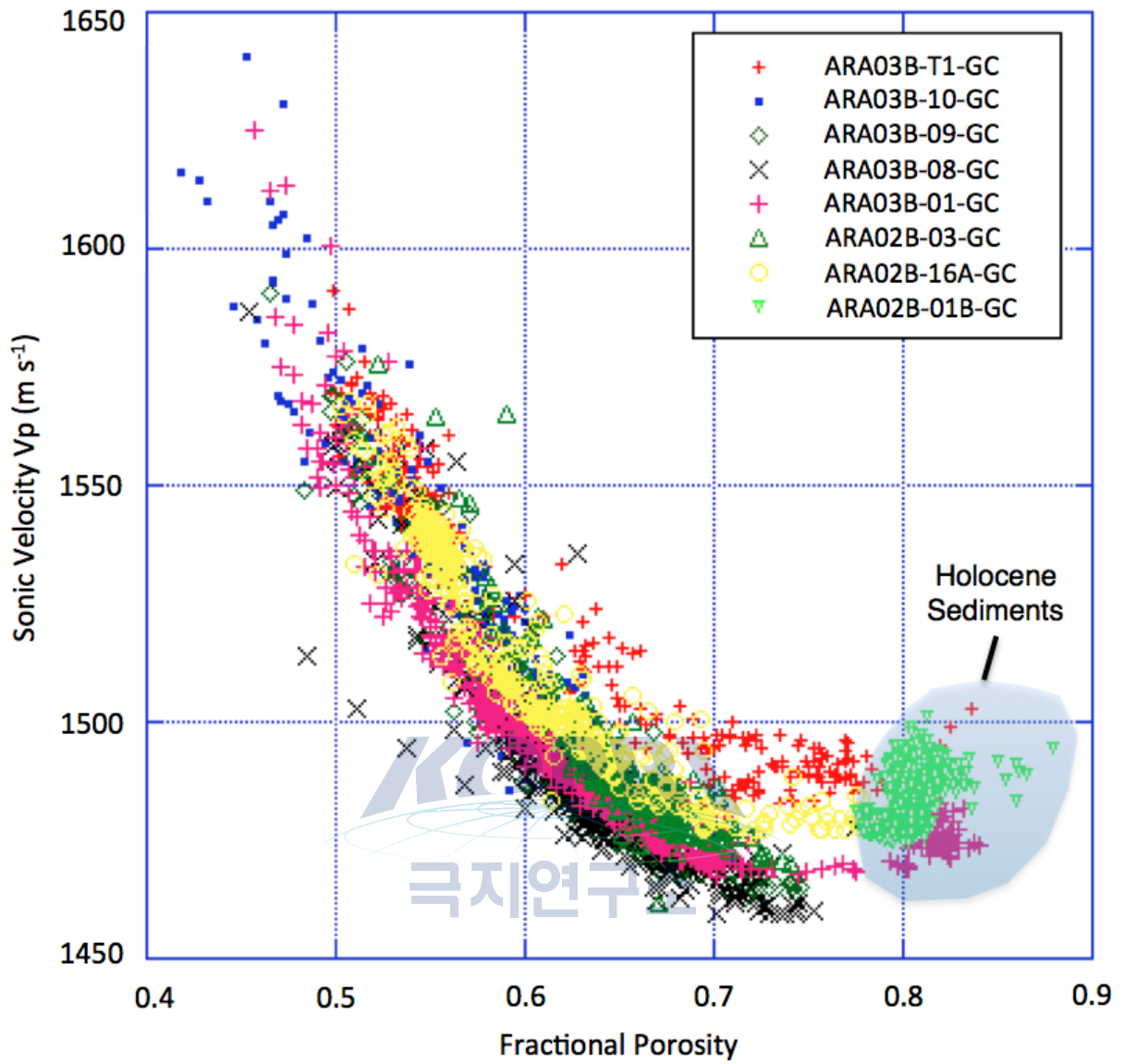
Fig. 7.2.1 Examples of porosity-velocity relationships of selected cores recovered during expeditions ARA02B and ARA03B both logged during ARA03B.
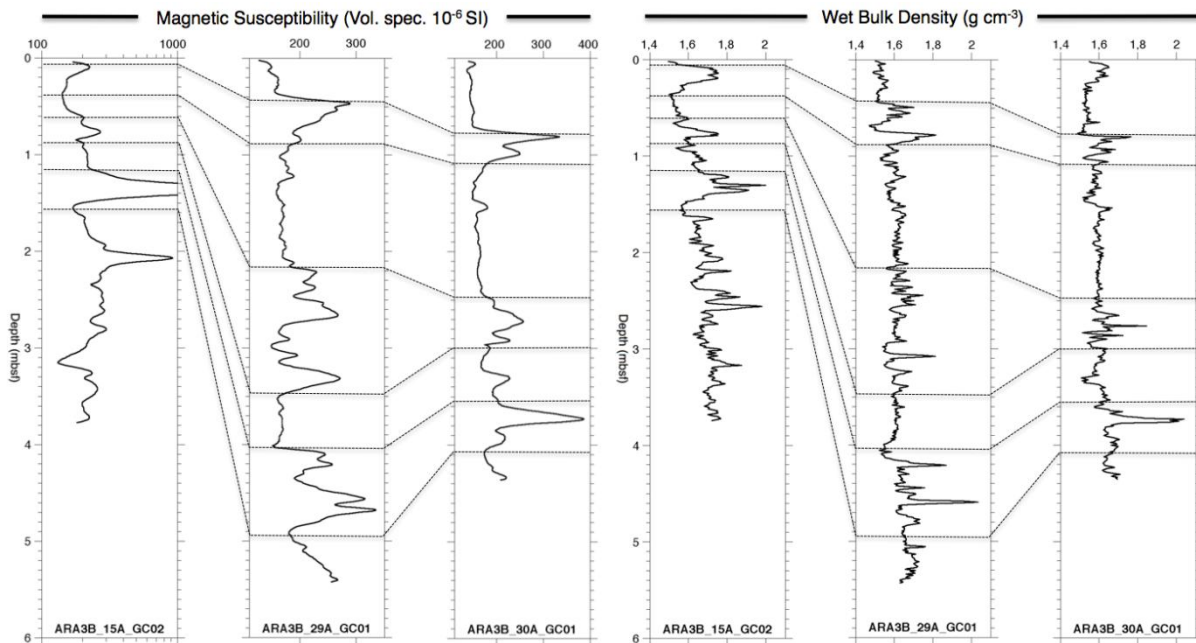
Fig. 7.7.2 Example of core-to-core correlation using magnetic susceptibility and density (preliminary result)

7.3 Biomarker geochemistry

7.3.1 Study for archaeal lipids in particulate and dissolved organic matter

1. Introduction

Glycerol dialkyl glycerol tetraethers (GDGTs) are ubiquitous in marine water and sediments, and are thought to be derived mainly from marine Crenarchaeota Group I, and marine Crenarchaeota Group I was recently classified into a newly-defined archaeal phylum Thaumarchaeota. Thaumarchaeota in marine environments were recognized to be both heterotrophs and chemoautotrophic nitrifiers.

Because isoprenoid GDGTs are specific to Archaea, and creanarchaeol, a major isoprenoid GDGT, is specific to Thaumarchaeota in particular, they are potentially used to understand the temporal and spatial distribution of Achaea and Thaumarchaeota, but little is known about the abundance of GDGTs in the water column.

Schouten et al. (2002, Earth and Planetary Science Letters) proposed a new paleotemperature index, TetraEther index of tetraethers consisting of 86 carbon atoms

(TEX_{86}), based on the distribution of GDGTs by way of an empirical correlation between TEX_{86} values in marine core top sediments and sea surface temperatures (SSTs). Because GDGTs record the water temperature when and where they were produced, the temperatures indicated by the GDGTs in POM provide a key for understanding the season and depth of GDGT production.

Recently, the GDGTs with functional head group (intact-GDGTs) are identified in environmental samples. Because the intact-GDGTs are rapidly degraded to core-GDGTs after the death of archaeal cell, they are thought to be a marker of living Archaea.

The GDGT compositions in sediments and sinking particles corresponded to that in surface water, suggesting that the GDGTs produced in surface water are delivered to sediment surface through the water column. However, the process how the GDGTs in dead archaeal cells sink in the water column is not clear.

In this study, we investigate the spatial distribution of both intact- and core-GDGTs in different particle size fractions in the water column. The aim of this study is to understand the roles of particulate-associated and free-living archaeal community on the production and fate of GDGTs. To reach the goal of this study, we collaborate with KOPRI microbiology group (Dr. Chung Yeon Hwang) to analyze DNA (PCR *amo A*).

2. Materials and methods

During ARA03B cruise, we collected particulate organic matter (POM) and dissolved organic matter (DOM) samples at four different depths at Stations Test-1, 39, 18, 24, 30, and 6 using Niskin bottles. We collected surface water samples (6 m depth) at extra sites.

On Araon, the samples (about 30 l) were passed through Omnipore membrane filters (sequentially through 1.0 μm, and 0.2 μm pore sizes) using a peristaltic pump and Tygon peristaltic tubing. Samples were then acidified to pH 2 with HCl (35%) and passed through Varian Bond Elute PPL cartridge (1g of styrene divinyl benzene polymer, 150Å pore size) with gravity following Dittmar et al. (2008 Limnology and Oceanography). The cartridges were rinsed with 0.01 M HCl for removal of salt, and dried. The cartridges were kept frozen at − 20°C and will send to Hokkaido University.

In the laboratory of the Hokkaido University, DOM will be eluted with methanol. GDGTs will

be extracted from POM samples with organic solvent using a Bligh and Dyer method. Intact-GDGTs in the POM extracts will be analyzed by liquid chromatography-ESI-mass spectrometry. Core-GDGTs in the POM and DOM extract will be separated and further purified according to their polarity by column chromatography and analyzed by liquid chromatography-APCI-mass spectrometry.

3. Expected results

The spatial distribution of intact- and core-GDGTs in POM and DOM in the water column will be interpreted. The abundance ratio of intact- to core-GDGTs (and *amo A* abundance) is an index of the freshness of GDGTs, a key to understand the in-situ production of GDGTs by Thaumarchaeota. Comparison between particle-associated GDGTs (POM > 1.0 µm) and free-living archaeal GDGTs (POM 0.2-1.0 µm) will clarify the role of particle-associated archaeal community in the process of GDGT delivery to the sediment. The results will not only contribute to the better understanding of the ecology of marine Archaea, but also to the better interpretation of GDGT proxies in sediment archives in the context of paleoclimate study of in the western Arctic.
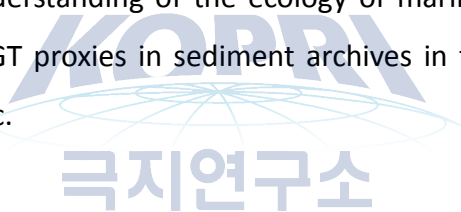
Table 1. List of POM and DOM samples

No	Sample name	Location	Water depth (m)	Volume (L)	method
1	ARA03B Nome test	Norton Sound, Off Nome	6	26.1	Tap
	Station Test 1				
2	ARA03B Test site 10m	Station Test 1	10	27.7	Niskin
3	ARA03B Test site 20m	Station Test 1	20	28.9	Niskin
4	ARA03B Test site 30m	Station Test 1	30	25.2	Niskin
5	ARA03B Test site	Station Test 1	40	27.7	Niskin

	40m				
	Station 39				
6	ARA03B St 39, 65 m	Station 39	65	27.9	Niskin
7	ARA03B St 39, 65 m	Station 39	350	28.0	Niskin
8	ARA03B St 39, 65 m	Station 39	1000	27.4	Niskin
9	ARA03B St 39, 65 m	Station 39	2000	27.4	Niskin
	Station 11				
10	ARA03B St 11 Tap surface	Station 11	6	152.8	Tap
	Station 16				
11	ARA03B St 16 Tap surface	Station 16	6	101.8	Tap
	Station 16B (transit from Station 16 to Ice station)				
12	ARA03B St 16B Tap surface	Station 16B	6	38.6	Tap
	Ice station				
13	ARA03B St 16B Tap surface	Ice station	6	41.5	Tap
	Station 42				
14	ARA03B St 42 20m	Station 42	20	29.1	Niskin
15	ARA03B St 42	Station 42	350	28.9	Niskin

	350m				
16	ARA03B St 42 1000m	Station 42	1000	30.0	Niskin
17	ARA03B St 42 2500m	Station 42	2500	29.7	Niskin
	Station 21				
18	ARA03B St 21 Tap surface	Station 21	6	125.1	Tap
	Station 25				
19	ARA03B St 25 10m	Station 25	10	29.4	Niskin
20	ARA03B St 25 38m	Station 25	38	29.3	Niskin
21	ARA03B St 25 70m	Station 25	70	28.3	Niskin
22	ARA03B St 25 155m	Station 25	155	29.8	Niskin
	Station 30				
23	ARA03B St 30 50m	Station 30	50	29.7	Niskin
24	ARA03B St 30 350m	Station 30	350	29.8	Niskin
25	ARA03B St 30 1000m	Station 30	1000	29.8	Niskin
26	ARA03B St 30 2000m	Station 30	2000	30.1	Niskin
	Station 36				
27	ARA03B St 36 Tap surface	Station 36	6	82.5	Tap

	Station 44				
28	ARA03B St 44 65m	Station 44	65	29.4	Niskin
29	ARA03B St 44 500m	Station 44	500	29.4	Niskin
30	ARA03B St 44 1000m	Station 44	1000	29.7	Niskin
31	ARA03B St 44 3500m	Station 44	3500	30.0	Niskin
32	ARA03B St 44 3820m	Station 44	3820	7.3	Niskin
	Station 2				
33	ARA03B St 36 Tap surface	Station 2	6	68.8	Tap

7.3.2 Biomarker geochemistry, grain size and clay mineral analysis

1.   Introduction

Biomarkers, organisms-derived organic compounds, are useful for understanding paleoenvironments as well as modern process of organic matter production and sedimentation. Grain size is a fundamental item in the description of sediments and is useful for stratigraphic correlation as well as understanding depositional process and the provenance of sediments. Clay mineral assemblage provides means of assessing the provenance of sediments.

In this study, we plan to examine the spatial and temporal distribution of biomarkers, grain size distribution and clay mineral assemblage, in the sediments of multiple cores retrieved from the Chukchi Abyssal Plain, the Arlis Plateau, the Wrangel Abyssal Plain, and the continental slope of the East Siberian Sea to reconstruct paleoenvironmental changes in those area. Special attention will be paid for glycerol dialkyl glycerol tetraethers (GDGTs)

useful for paleotemperature estimate (TEX_{86} SST proxy), and lignin of vascular plants origin. In the analytical process, we also analyze sterols, phytols, fatty acids, and other compounds to evaluate the feasibility of these compounds as paleoenvironmental markers.

2. Materials and methods

2.1. Samples

During this cruise, we collected multiple cores at Stations 16, 18, 19, 27, 28, 29, 30, and 41 (Tables 1). The samples are frozen and will be sent to Hokkaido University. A couple of gravity cores will be selected afterward, sub-sampled and sent to Hokkaido University.

2.2. Methods

In Hokkaido University, lipids will be extracted with organic solvent under high pressure and temperature and separated into four fractions according to their polarity by column chromatography. Biomarkers in apolar and polar fractions will be analyzed by gas chromatography. GDGTs in polar fraction will be analyzed by liquid chromatography-mass spectrometry after further purification. Lignin in sediment will be analyzed by pyrolysis-gas chromatography-mass spectrometry after chemical treatments.

Sediments will be wet sieved after dispersal by ultra-sonication and separated into >250 μm, 250-63 μm, <63 μm size fractions. The grain size distribution of <63 μm size fraction will be determined using a laser particle size analyzer. The <63 μm size fraction was further analyzed by X-ray diffraction for the determination of clay mineral assemblages.

Table 1. List of multiple cores to be analyzed

Name	Length (cm)	Number of samples
ARA03B 16 MUC-01	53	53
ARA03B 18 MUC-01	52	52
ARA03B 19 MUC-02	23	23
ARA03B 27 MUC-02	33	33
ARA03B 28 MUC-02	47	47

ARA03B 29 MUC-02	61	61
ARA03B 30 MUC-01	55	55
ARA03B 41 MUC-03	51	51

Samples were split every 1 cm onboard.

3. Expected results

The spatial and temporal distribution of biomarkers in sediments will be interpreted. Analysis of GDGTs for multiple cores will show the changes of water temperatures. Spatial distribution of GDGTs in the water column will be useful when we consider the depth at which temperature is reflected in GDGT composition. Analysis of lignin for multiple cores will show spatial and temporal changes in terrestrial organic matter since the last glacial period. Correlation of biomarker composition with grain size and mineral composition will be useful to identify the provenance of biomarkers.

The spatial and temporal changes of grain size distribution and clay mineral assemblages in sediments will be interpreted for stratigraphic correlation. The provenance and transportation process will be discussed based on mean grain size, sorting and provenance-specific clay minerals.

7.4 Spatial distribution of benthic bacterial assemblages in the Arctic Ocean

7.4.1. Introduction

The Arctic Ocean is globally important as a key indicator and driver of climate change. However, assessment of impacts of climate change on Arctic ecosystems has typically focused on terrestrial ecosystems (Fischlin, Midgley et al. 2007; Post, Forchhammer et al. 2009) although vulnerability of Arctic marine biota to climate change is well established (Gradinger 1995). Moreover, most reports of documented changes in Arctic marine biota in response to climate change concerned marine mammals, particularly polar bears, and fish (Wassmann, Duarte et al. 2011) rather than microbes although the polar regions contain

diverse microbes and microbial habitats (Vincent and Laybourn-Parry 2008; Thomas, Fogg et al. 2009) and allow microbes to keep activities (Deming 2002). It is important to determine what effects on bacterial diversity in the Arctic Ocean and if the changed bacterial diversity will affect rates of carbon cycling and the elemental cycling pathways with consequences for the pelagic and benthic food webs in the future as the concerns (Carmack and Macdonald 2002; Grebmeier, Overland et al. 2006; Arrigo, van Dijken et al. 2008; Bates and Mathis 2009; Cai, Chen et al. 2010). It is assumed that the bacterial communities of seawaters in the North Pacific sector would be affected by the environmental change from the sea-ice melting because the extent of sea-ice was dramatically reduced in this area during summer. Thus, it was concerned about how bacterial communities in the Arctic marine ecosystems are influenced by climate change. The aim of this study is to understand the effects of environmental factors on the spatial distribution of marine bacteria by monitoring distributions of major phylotypes in bacterial communities in the Arctic Ocean.

The bacterial community concept in benthic ecology should consider whether assemblages are described on the basis of the substratum that they occupied, i.e. the biotope (the region of a habitat associated with a particular ecological community). The expedition for the R/V *ARAON* to the Arctic Ocean was progressed from August to September in 2012. Total ten sampling sites were selected to monitor benthic bacterial assemblages in the Arctic Ocean related to the global warming issue.

7.4.2. Materials and methods

Sampling site description, Sample collection and DNA extraction

Total 13 sediment cores were collected by the box corer or multicorer equipped in the *ARAON* (Table 1.1). The sediment cores were cut into a centimeter unit along the vertical length after peeling off a thin layer from the surface of whole core by a sterile knife for decontamination, and then respectively transferred into sterile tubes. These tubes containing sectioned sediments were stored in a freezer (− 10°C) equipped in the ARAON and transport back to our laboratory on ice for DNA extraction. Total DNA is extracted according to a conventional phenol/chloroform DNA isolation method (http://openwetware.org/wiki/ Phenol /chloroform_extraction) and purified by a

commercial kit (QIAGEN).

Table 1.1.   The list of sampled sediment cores

No.	Core ID	Date	Location (GPS)		Core Length (cm)	Maximum Depth (m)
			Latitude	Logitude		
1	ARAO3B/01BOX	12.8.4	74° 37.0500'N	166° 23.7700'W	34.5	379
2	ARA03B/08BOX	12.8.6	76° 36.5598'N	161° 12.7302'W	41.5	2165
3	ARAO3B/10BOX	12.8.6	76° 42.7548'N	161°51.8950'W	21	1051
4	ARAO3B/12BOX	12.8.9	77° 45.0119'N	165° 22.4914'W	31.5	429
5	ARA03B/15(B)MUC	12.8.10	78° 06.5982'N	175° 14.0130'W	46	1149
6	ARA03B/41BOX	12.8.15	82° 19.2284'N	171° 33.3245'E	38	2710
7	ARA03B/24BOX	12.8.20	74° 30.0090'N	174° 00.0316'E	32	57
8	ARA03B/26BOX	12.8.21	75° 22.2743'N	177° 17.4846'E	25	354
9	ARA03B/28MUC	12.8.22	76° 13.1156'N	179° 50.1574'W	42	1179
10	ARA03B/29MUC	12.8.24	77° 00.3825'N	177° 21.6930'W	46	1394
11	ARA03B/30BOX	12.8.25	77° 04.5363'N	172° 19.6133'W	43	2013
12	ARA03B/31BOX	12.8.26	76° 08.6613'N	174° 54.8039'W	26	2180
13	ARA03B/35(A)BOX	12.8.28	75° 26.3542'N	172° 37.8704'W	34	1079

Amplification of 16S rRNA gene and sequencing

Prokaryotic 16S rRNA gene sequences are amplified from the extracted gDNA using primers targeting the V1 to V3 hyper variable regions. The primers are used for bacteria for V1-21F (5'-*CCTATCCCCTGTGTGCCTTGGCAGTC-TCAG*-AC-GAGTTTGATCMTGGCTCAG-3';the italic font indicates the sequences of adaptor and key, followed by a common linker AC) and V3-537R (5' *CCTATCCCCTGTGTGCCTTGGCAGTC-TCAG*-[*X*]-AC-WTTACCGCGGCTGCTGG-3'; the [*X*] denotes an 7-9 nucleotide long barcode uniquely designed for each water sample, and underlining indicates the gene specific section). PCR reactions are carried out by using the DreamTaq^{Tm} Green PCR Master Mix (Fermentas, EU) under the following conditions: initial

denaturation at 94°C for 5 min; followed by 30 cycles of denaturation at 94°C for 30 sec,annealing at 55°C for 30 sec, and elongation at 72°C for 1 min 20 sec; and a final extension at 72°C for 10 min. PCR amplicons are purified using the Qiaquick PCR purification kit (QIAGEN), and that concentrations are measured using a spectrometry (NanoDrop Technologies, USA). The purified amplicons are mixed and subjected to pyrosequencing. The DNA sequencing is performed by Macrogen Incorporation (Seoul, Korea) using a 454 GS FLX Titanium Sequencing System (Roche).

Pre-processing, bacterial diversity and taxonomic classification of sequencing data sets

Analysis of pyrosequencing data is performed by the MOTHUR program Ver. 1.23 (Schloss, Westcott et al. 2009), basically according to the protocol suggested by Schloss et al (http://www.mothur.org/_wiki/Schloss_SOP) (Schloss, Gevers et al. 2011). In brief, sequencing reads from the different samples are separated by unique barcodes. Then, barcode, linker, and PCR primer sequences are removed from the original sequencing reads. The resultant sequencing reads are subjected to a filtering process including quality trimming and chimera removal. After being aligned against pre-aligned SILVA reference database, sequencing reads are used for the calculation of distance matrix. Clustering of operational taxonomy units (OTUs) is conducted by the furthest neighbor algorithm with each similarity cutoff of 99%, 97%, 95% and 90%, the results of which are subsequently used for the comparison of bacterial communities of samples based on alpha diversity in various similarity cutoff thresholds. In the alpha diversity analysis, species richness is estimated by ACE and Chao1 indices, while species evenness is calculated by Shannon and Simpson indices (Shaw, Halpern et al. 2008). For the analysis of beta diversity, the principal coordinates analysis (PCoA) is used with a similarity cutoff threshold of 99%.

Taxonomic and phylogenetic analyses

Taxonomic classification of the individual reads are carried out using the NAST algorithm in the Greengenes database (http://greengenes.lbl.gov) (DeSantis, Hugenholtz et al. 2006). Detailed phylogenetic analyses of sequencing reads are performed for representative sequences retrieved from major OTUs, which have a frequency over 1% in

each sample, after OTU clustering at a cutoff level of 99%. Retrieved sequences are aligned by SINA aligner against SILVA seed reference sequences. Aligned sequences are imported into the ARB database (SSURef_108) and used for the determination of phylogenetic affiliation. For construction of a phylogenetic tree, aligned sequences are exported into MEGA 5.05 together with other related sequences (Tamura, Peterson et al. 2011). A phylogenetic tree is constructed by neighbor-joining method with 100 bootstrap tests. Additionally, BlastN analyses are performed against non-redundant database of GenBank and ARB database, when need for more accurate phylogenetic assignments.

Statistical analyses

To verify the link between physiochemical parameters or major phylotypes among the samples, a nonparametric correlation analysis was performed by the spearman's rho test using SPSS Ver. 16.0 (SPSS Institute, USA). To infer a tendency for relations between the major phylotypes and each physiochemical parameter, the spearman test and a linear regression analysis were performed in the SPSS.

7.4.3. Expected result

7.4.3.1. Sediment property

To estimates the physiochemical properties of sediment samples the XRF and X-ray analysis proceed by the ITRAX core scanner equipped in the ARAON and sedimentary structure, particle size, pH, and salinity are measured in further analysis at Gwangju Institute of Science and Technology (GIST). The data of sedimentary properties in samples is used for statistical analysis to confirm the correlation with bacterial properties in sediments.

7.4.3.2. Bacterial diversity and taxonomic classification

All sequencing reads obtained from samples are analyzed for alpha and beta diversity. In analysis of alpha diversity, species richness and evenness of bacterial diversity are estimated in samples. The beta diversity analysis using PCoA (Principal Coordinates Analysis) is useful to measure species richness relate to line transects along one or more environmental gradients. To more characterize differences among bacterial communities suggested by

above analyses, taxonomic assignments of all sequencing reads are performed by comparison to the Greengenes database at the class level. To gain information about the phylogenetic composition of bacterial communities at finer levels, a detailed analysis is performed for representative sequencing reads, each of which were retrieved from major OTUs clustered at the similarity level of 99%.

7.4.3.3. Correlation analysis between major phylotypes (class level) and physiochemical parameters

A statistical analysis between major phylotypes and physiochemical parameters proceed to confirm the biological-environmental link.

7.4.4. Summary and conclusions

The aim of this study is to understand the effects of environmental factors on the spatial distribution of marine bacteria by monitoring distributions of major phylotypes in bacterial communities in the Arctic Ocean. Our expected data from the 2012 Arctic cruise can provide valuable insights into monitoring of key bacterial groups that account for environmental change in the Arctic Ocean.

References

Arrigo, K. R., G. van Dijken, et al. (2008). "Impact of a shrinking Arctic ice cover on marine primary production." Geophys. Res. Lett **35**(19): L19603.

Bates, N. R. and J. T. Mathis (2009). "The Arctic Ocean marine carbon cycle: evaluation of air-sea CO2 exchanges, ocean acidification impacts and potential feedbacks." Biogeosciences **6**(11): 2433-2459.

Best, A. I., Gunn, D.E. (1999) Calibration of marine sediment core loggers for quantitative acoustic impedance studies. Marine Geology, 160, 137-146

Bryant, W.R., and Rack, F.R., 1990, Consolidation characteristics of Weddell Sea sediments: results of ODP Leg 113, in Barker, P.F., Kennett, J.P., et al. (eds.): Proceedings of the Ocean Drilling Program Scientific Results, v. 113, College Station, TX (Ocean Drilling Program), p. 211–223

Cai, W. J., L. Chen, et al. (2010). "Decrease in the CO2 uptake capacity in an ice-free Arctic Ocean basin." Science **329**(5991): 556-559.

Carmack, E. C. and R. W. Macdonald (2002). "Oceanography of the Canadian Shelf of the Beaufort Sea: a setting for marine life." Arctic: 29-45.

Croudace, I.W., Rindby, A., Rothwell, R.G., 2006. ITRAX: description and evaluation of a new multi-function X-ray core scanner. In Rothwell, R.G. (Edi.), New techniques in sediment core analysis. Geological Society, London, Special Publications, 267, 51-63.

Deming, J. W. (2002). "Psychrophiles and polar regions." Current Opinion in Microbiology **5**(3): 301-309.

DeSantis, T. Z., P. Hugenholtz, et al. (2006). "Greengenes, a chimera-checked 16S rRNA gene database and workbench compatible with ARB." Applied and environmental microbiology **72**(7): 5069.

Fischlin, A., G. F. Midgley, et al. (2007). "Ecosystems, their properties, goods, and services." Notes.

Gradinger, R. (1995). "Climate change and biological oceanography of the Arctic Ocean." Philosophical Transactions of the Royal Society of London. Series A: Physical and Engineering Sciences **352**(1699): 277.

Grebmeier, J. M., J. E. Overland, et al. (2006). "A major ecosystem shift in the northern Bering Sea." Science **311**(5766): 1461-1464.

Jokat, W. (ed) (2009): The Expedition of the Research Vessel "Polarstern" to the Arctic in 2008 (ARK-XXIII/3).- Rep. Polar Mar. Res. 597: 1-221.

Matthiessen, J., Niessen, F., Stein, R., Naafs, B. D. (2010). Pleistocene glacial marine sedimentary environments at the eastern Mendeleev Ridge, Arctic Ocean, Polarforschung, 79(2), 123-137.

Post, E., M. C. Forchhammer, et al. (2009). "Ecological dynamics across the Arctic associated with recent climate change." Science **325**(5946): 1355.

Schloss, P. D., D. Gevers, et al. (2011). "Reducing the Effects of PCR Amplification and Sequencing Artifacts on 16S rRNA-Based Studies." PloS one **6**(12): e27310.

Schloss, P. D., S. L. Westcott, et al. (2009). "Introducing mothur: open-source, platform-independent, community-supported software for describing and comparing microbial

communities." Appl Environ Microbiol **75**(23): 7537-41.

Shaw, A. K., A. L. Halpern, et al. (2008). "It's all relative: ranking the diversity of aquatic bacterial communities." Environ Microbiol **10**(9): 2200-10.

Stein, R., Matthiessen, J., Niessen, F. (2010a). Re-coring at Ice Island T3 site of key core FL-224 (Nautilus Basin, Amerasian Arctic): sediment characteristics and stratigraphic framework, Polarforschung, 79(2), 81-96.

Stein, R., Matthiessen, J., Niessen, F., Krylov, A., Nam, S., Bazhenova, E.(2010b). Towards a better (litho-) stratigraphy and reconstruction of Quaternary paleoenvironment in the Amerasian Basin (Arctic Ocean), Polarforschung, 79(2), 97-121.

Tamura, K., D. Peterson, et al. (2011). "MEGA5: molecular evolutionary genetics analysis using maximum likelihood, evolutionary distance, and maximum parsimony methods." Molecular biology and evolution.

Thomas, D. N., G. Fogg, et al. (2009). "The biology of polar regions." Antarctic Science **21**(3): 313-314.

Vincent, W. F. and J. Laybourn-Parry (2008). Polar lakes and rivers: limnology of Arctic and Antarctic aquatic ecosystems, Oxford University Press, USA.

Wassmann, P., C. M. Duarte, et al. (2011). "Footprints of climate change in the Arctic marine ecosystem." Global Change Biology.

Weber, M.E., Niessen, F., Kuhn, G., Wiedecke, M. (1979). Calibration and application of marine sedimentary physical properties using a multi-sensor core logger, Mar. Geol. 136: 151- 172

Yamamoto, M., Okino, T., Sugisaki, S., Sakamoto, T., Late Pleistocene changes in terrestrial biomarkers in sediments from the central Arctic Ocean. Organic Geochemistry, 2008. **39**, p. 754-763.

Yamamoto , M., Polyak, L., Changes in terrestrial organic matter input to the Mendeleev Ridge, western Arctic Ocean, during the Late Quaternary. Global and Planetary Change, 2009. **68**, 30–37.